

# POLITECNICO DI TORINO



**Corso di Laurea Magistrale  
in  
Ingegneria per l'Ambiente e il Territorio**

**Tesi di Laurea**

*Different constructive solutions against explosions  
and blast load characterization*

**Relatore:**  
Ing. Claudio Oggeri

**Relatore esterno:**  
Ing. Lina Maria Lopéz

**Correlatore esterno:**  
Ing. Maria Chiquito

**Candidato:**  
Elena Ercules  
Matricola: s231076

**Anno Accademico 2017-2018**

---

---

---

## Acknowledgments

The people to thank are many and each one for a distinctive reason. First of all, I thank my supervisors; the Professor Claudio Oggeri for helping me from the first year of masterful with his advice and his experience, the teachers Lina Maria Lopez and Maria Chiquito for having guided me in the last months and for the time they have dedicated to helping me in the realization of this final project. I must also recognize the professor Riccardo Castedo who helped me to participate in the project and has always been present, and to the guys in the UPM group.

A special recognition goes to my family; to my parents who allowed me to take a course of study and who believed in me from the beginning, to my sister Elisa and Jacopo who were able to spur me even in the most difficult moments. Thanks to my friends Marci, Dino, Mari, Fede, Chia and Anna who have always been close to me even in the distant months. I would like to thank Michela, Cava, Gio, Andre, Ivana and Sonia who have always help me with the preparation of the exams and which have made the study hours sweeter. In addition, thanks to the support of Lilli and Debby, in the event of bad news, they raised my spirits with nutella spoons.

Finally, last but not least, thanks to Cesar and Marco who helped me with the Spanish and the technical terms that I often confused. Also thanks to my roommates, but especially to Vera and Ila who have endured me in the last months before the last exam and in the writing of the thesis and that helped me to compose the sentences that at eleven o'clock at night seem perfect but that in reality they no made sense.

Moreover, thank all the people who in their heart know they have helped me to reach this first goal but I have not mentioned.

*Thank you very much.*

---

---

---

---

## Abstract

Terrorist attacks are increasingly widespread and dangerous for our communities. For this reason, in order to protect buildings from these threats, the structures behavior subject to explosion is evaluated.

In particular, this master thesis analyzes the effects on performances of four masonry walls exposed to an explosive charge placed at a distance of 5 m from each of them.

Before the field tests, several scientific articles were considered to asses the explosive charge had such to generate an intermediate damage to the walls with dimensions 2.5x2.5x0.24 m. These analyze were made taking into account the charge in kilograms of equivalent TNT and subsequently converting the values found in kilograms of Dynamite.

In each test performed there is a wall, called the *control wall*, without any reinforcement and three in which there is a reinforcement on the facade directly exposed to the explosive charge or on the opposite facade. The reinforcements, supplied by the same company, are of three distinct types: a premixed and fiber-reinforced mortar, a high resistance carbon fiber net applied by an adhesive and a bi-directional fiberglass fabric fixed to the wall face by an adhesive.

The tests were carried out in the *La Marañosa* field, a military camp 14 km away from the center of Madrid. The masonry walls were fixed on metal auxiliary structures which are in turn fixed on a slab of concrete already present on site. The amount of Dynamite used were of 22.8 kg or 31.6 kg, sizes studied to guarantee intermediate damage. For the evaluation of the explosive performance, the pressure gauges were positioned at a distance of 5 m, equal to the distance of the explosive charge with respect to the walls. In addition, on the outer face of the wall, were posicioned the accelerometers that allowed to measure one of the three components of the vibrations, and the high-speed camera, that allowed to calculate the speed of the shock wave in the tests and to have a video of the progress of the phenomenon. The damage were measured using the electrical Schmidt Hammer in 20 points for each wall facade. This examination on the quality of the walls was evaluated by measuring the real rebound coefficient, the so-called Q value. Furthermore, the areas of the walls, in which the fragmentation occurred, were calculated using the AutoCad software.

---

---

From the three tests carried out, it is observed that the charge of 31.6 kg of Dynamite, placed at a distance of  $1.71 \text{ m/kg}^{1/3}$  from the walls and at a height of 0.70 m above the ground, makes it possible to obtain an intermediate damage with greater effect respect to the charge of 22.8 kg.

The parameters obtained from the three tests are similar to the data determined by the theoretical analysis. From the experimental tests it was found that the analysis of the behavior of the walls is more visible in the two tests where the 31.6 kg explosive is used. In these two cases it is found that the most suitable solution to avoid fragmentation is the presence of reinforcement in the facade in direct contact with the explosive charge. In particular, the reinforcement that has the best anti-fragmentation capabilities is that made of carbon fibers.

In the following months, more specific analyzes will be carried out on the results obtained by the three tests and will be increased with other tests that present different boundary conditions compared to those treated in this final thesis.

---

---

# Table of contents

<b>Introduction .....</b>	<b>3</b>
<b>1 - Explosives.....</b>	<b>7</b>
1.1 - Classification of explosives .....	7
1.1.1 - Classification of explosives on the basis of the reaction speed....	7
1.1.2 - Classification of explosives based on chemical composition.....	10
1.2 - Use of explosives .....	11
1.3 - Main types of explosives .....	12
1.3.1 - Simple explosives .....	13
1.3.2 - Composite explosives .....	16
1.4 - TNT equivalent.....	19
1.5 - Detonation process.....	21
1.6 - Blast-loading categories.....	26
1.6.1 - Unconfined explosion .....	26
1.7 - Explosion of a spherical charge in the air .....	32
1.8 - Fragmentation.....	34
1.9 - Trajectory of the fragments.....	41
<b>2 - Project PICAEX.....</b>	<b>43</b>
2.1 - Geographical framework .....	44
2.2 - Test procedures .....	47
2.3 - Masonry test wall .....	50
2.3.1 - Support structure.....	53
2.3.2 - Method of transport .....	54
2.3.3 - Reinforcement additives.....	57
2.4 - Characterization of the explosive charge.....	62
2.4.1 - Definition of the scaled distance .....	63
2.4.2 - Determination of the triple point .....	70
2.4.3 - Parameters of shock wave .....	72
2.4.4 - Determination of the charge used in the test.....	77
2.5 - Fragmentation analyses.....	80
2.6 - Tools used.....	81
2.6.1 - Schmidt's hammer (sclerometer).....	81
2.6.2 - Accelerometer .....	87

---

2.6.3 – Pressure gauge .....	88
2.6.4 – High speed camera .....	89
2.6.5 – Data acquisition system .....	90
2.6.6 – Scanner .....	91
2.7 – Tests.....	93
2.8 – Results.....	100
<b>3 – Conclusions.....</b>	<b>119</b>
<b>References .....</b>	<b>123</b>
<b>Attachments .....</b>	<b>127</b>
Attachment A: Main characteristics of bricks .....	127
Attachment B: Mapei products .....	128
Attachment B1: Product 1 called PLANITOP INTONACO ARMATO .....	128
Attachment B2.1: Product 2.1 called MAPEGRID C170 .....	130
Attachment B2.2: Product 2.2 called MAPEWRAP 31 T.....	131
Attachment B3.1: Product 3.1 called MAPEWRAP EQ NET .....	132
Attachment B3.2: Product 3.2 called MAPEWRAP EQ ADHESIVE..	133
Attachment C: Accelerometer mounting instructions.....	134
Attachment D: High-speed camera specifications .....	135

## Introduction

Modern States are forced to face different challenges that threaten the national security of different Countries. Among these challenges include international terrorism and high diffusion weapons of mass destruction in all over the World, one of the most important threat that has to be faced today. In fact, it should be considered that in a total of 4.4% of global accidents worldwide [Centro para el desarrollo Tecnológico Industrial, 2017] there are roughly 2.6% of human losses caused by terrorist attacks in the last 15 years. The deaths occurred have been many and damages to the infrastructure systems have been so relevant between the Countries that Cities Security have become now days an actual issue.

One of the strength's points of the infrastructure system consists in the level of development reached by from technology and manufacturing point of view; according to this it is possible to assure certain security standards. Unfortunately modern society is increasingly dependent on the infrastructure system from the economic and social perspective; hence, a certain security requirements must be realized in phase of construction and during the operational one. According to these reasons, the security task is carried on by the Sistema Nacional de Gestion de situaciones de crisis. In particular, "Sistema Nacional de Gestion de situaciones de crisis" evaluates the critical infrastructures protections trying to find new arrangements, aim to reduce the vulnerability of the system as is the case with the PICAEX project.

Project PICAEX (*Protección de Infraestructuras Críticas Frente a Explosiones*) has the purpose of developing a general methodology in order to analyze the damages into reinforced concrete structures and the wall built with different materials following different design concepts. The evaluation method is focused on simulations supported by a huge amount of data from real-scale tests. The main result is that it allows to reduce critical infrastructure vulnerability from terrorist attacks leaded with the use of the IED explosive (*Improvised Explosive Device*).

This project, still active today, is made up of a consortium of three private companies that accept to work together to develop this project. These companies are: TAPUSA, FHECOR, and MAPEI.

TAPUSA is a company specialized in the construction of bridges and structures. One of its main objectives is the implementation of the I+D+i (Investigación, desarrollo y innovación, that is research, development and innovation in the new construction technology, new production process and the use of recyclable materials) in order to improve global security in public buildings.

In particular this company deals with:

1. Defining the actions that affect the structure and their measurements;
2. Structural analysis after the explosions, numerical analysis and design of the elements to be tested, numerical interpretation of the results;
3. Definition of the methodology analysis and project of the structure.

FHECOR is one of the most important Spanish consultants specialized in structures, covering a wide range of types and structural materials, being present in all the phases of the infrastructures life cycle. This company has a department of I+D+i where this project and the associated calculations are realized.

The general purpose of FHECOR is to be able to offer solutions to its customers in defending the IED.

In order to carry out its aim, it is fundamental to:

1. To Compute numerical analysis models with the appropriate simplifications;
2. Interpret the results obtained by testing with explosive;
3. Define the type of structure analysis and design considering the higher number of explosion cases.

MAPEI is the world leader in the manufacture of innovative adhesives and chemical products for buildings. It has a particular interest in the PICAEX project for the development of new products and improvement of existing ones. It owns two factories for the assembly of materials that are certificated in accordance with the international standards required for the realization of the specimens. The company's technical objectives in the project are:

1. The investigation and validation of the product developed before for another purpose;

2. To make improvements to its product;
3. To optimize the choice of material to increase safety.

Besides these companies the Explosive Group of Departamento de Ingeniería Geológica y Minera de la Escuela Técnica Superior de Ingenieros de Minas y Energía, de la UPM collaborates in the project; specifically they are involved in explosive tests, with the main task of define the test charge and the map of damages determined by numerical methods.

In this project, the explosive in analysis is an explosive IED (*Improvised Explosive Device*), an easy-to-manufacture explosive that can be built through the use of cheap materials with a high guarantee of effect considering its potential effect on the infrastructures in general. For these reasons it is studied how to improve the resistance to the explosion in reinforced concrete, the most used material in critical constructions and infrastructures. This material is extremely diffused in civil infrastructures because it has good resistance to wear or fire. Moreover, it is available on low-priced and it is easy-to-operate thanks to its good mechanical properties. The main drawback in using this material is the high vulnerability of the structures to explosives. Hence, three different reinforcement possibilities to improve the resistance against explosion have been studied. The first method consists of adding fibers (glass, steel, carbon or polypropylene) as internal reinforcement, or proceeding in coating the cement with aluminum foam, steel foil as external reinforcement or both methods. For this very reason, it is mandatory to define the right reinforcements to limit the damage of the attacks and work on different levels to define the technical objectives of the PICAEX project. Through this project it will be defined a real risk scenario, in other words a test with a real-time IED explosive, by the use of the Schmidt hammer to elaborate the damage map produced by the explosion. Furthermore several numerical forecasting tools that will model the behavior of reinforced concrete will be calculated. Through this calculation it will be possible to validate the coating as an element that increases resistance to the explosive and finally obtain a geometry that allows a better dissipation of the energy that produces the explosion.

To allow a comprehensible reading of the elaborate, it was decided to divide the discussion into two chapters. The first chapter will mainly deal with the theoretical concepts and notions of existing articles. The second chapter will

be addressed to the PICAEX project with the analyzes and design choices made during the entire work plan.

# 1 - Explosives

An explosion is a phenomenon of chemical-physical transformation that happens in a very rapid time, generating a large amount of energy and gas. It is considered usable when the explosive substance is subjected to a suitable energy (electrical, thermic or shock) that is a correct primer. It is important that the reaction does not stop but continues until the total decomposition of the charge.

A substance to be considered explosive must meet the basic criteria. First, it must have a *high energy content*. Furthermore explosives must have *chemical stability* which allows them to keep in time and to be activated and finally triggering the decomposition reaction is necessary. In addition, they must have a very *high reaction speed* that allows the release of energy in a very short time.

## 1.1 - Classification of explosives

Explosives are various and they can be divided into different categories according to different parameters. They can be divided into families according to their decomposition speed or according to their chemical composition as we will see below [Mancini Renato & Marilena Cardu, 2001].

### 1.1.1 - Classification of explosives on the basis of the reaction speed

The explosives, as mentioned above, are the decomposition of the charge that takes place very quickly. These explosive reactions can be divided into two distinct classes based on the speed of the reactions of individual charges. The classification distinguishes the phenomena of: explosion and detonation. The speed taken into account as a reference for the classification of explosives is the sonic speed, that is the speed with which a sound propagates in means. This reference speed allows us to distinguish the deflagrations, characterized by a low propagation speed of the reaction, up to 300 m/s, that is a subsonic velocity and detonation characterized by a higher reaction rate of about 1000-8000 m/s, namely one supersonic speed.

Deflagrating explosive (non-confined) is a combustion phenomenon of a substance due to the presence of oxygen, consisting of a low reaction speed ( $< 300$  m/s) that is dependent on the conformance and on the granulometry of the charge. The decomposition reaction of explosive particles develops hot gases that allow to reach high temperatures until the charge is exhausted as can be seen in Figure 1-3. Detonation is a phenomenon that occurs with an instantaneous decomposition of the charge. It is an exothermic chemical reaction that propagates in the material by generating a shock wave. This shock wave compresses the material by generating heat and intermolecular fractures, producing the release of fuel and oxidant that recombine by generating gases. The formation of these gaseous products releases large amounts of energy (in the form of light, noise, etc.) allowing the shock wave to self-fuel. As can be seen clearly from Figure 2-3, detonation is propagated by sudden increase in pressure and temperature, bringing the substance under reaction conditions, and the generated energy serves to press the adjacent state and allow the propagation of the charge. There is an "ideal detonation" where the reaction zone is very thin and the reaction complete at the detonation front with detonation speed. The explosions are classified as either deflagrations or detonations.

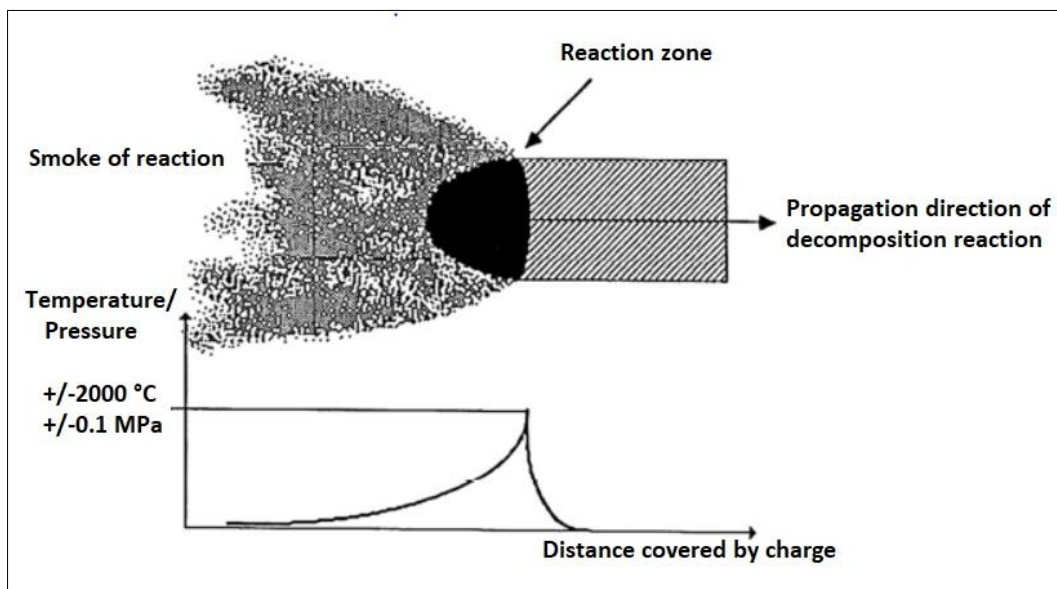


Figure 1. Deflagrazione of explosives, chemical decomposition by thermal transfer of oxygen

# 1 - Explosives

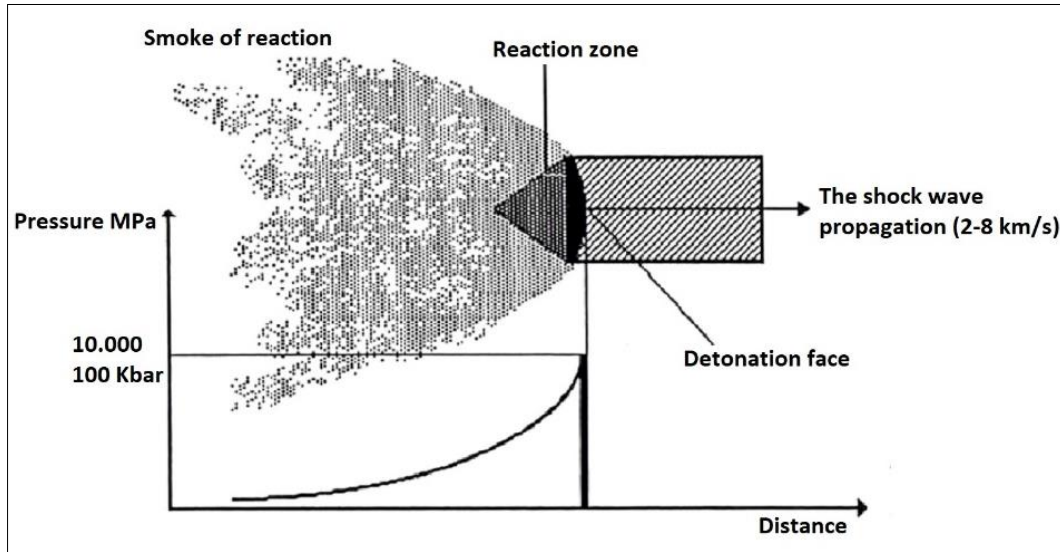


Figure 2. Detonation, propagation of decomposition under the effect of a shock wave



Figura 3. On the left an example of deflagration and on the right an example of detonation

In addition, detonating explosives are divided into:

- a) *Primary or primer explosives*
- b) *Secondary Explosives*

*Primary explosives* are highly susceptible to impact, friction and heat, and the released energy and detonation speed are low. For this reason, they are used as a component in detonators in combination with other compounds with the explosive trigger function that cannot detonate by a single stimulus: these explosives are the secondary ones. Among the main primary explosives most commonly used are Mercury Fulminate, Lead Acidate Azotidrato di Piombo and Lead Styphnate.

*Secondary explosives*, as previously mentioned, need a primary one to start their decomposition reaction. They are compounds or mixtures that contain high amounts of energy, great stability and are subdivided into military or industrial explosives.

### **1.1.2 - Classification of explosives based on chemical composition**

Another type of classification can be defined on the chemical composition of the explosive. Three different explosives can be found:

- a) *Chemical compounds*
- b) *Explosive mixtures*
- c) *Explosive mix*

The *chemical compounds* contain both an oxidant, that is oxygen, and a combustive agent, generally consisting of hydrogen and carbon. When triggered, they combine to produce gaseous products. An example of an explosive belonging to this explosive family is Tritol, Trinitrotoluene, quoted with the acronym TNT.

*Explosive mixtures* are substances produced by the combination of two or more compounds, each of them is not an explosive if taken individually. This can be beneficial in case of safe transport and handling. In explosive mixtures, oxygen is never in a free state but is provided by one of the two explosive compounds. An example of this family of explosives is the mixture of ammonium nitrate (oxidative substance containing a large amount of oxygen) and combustible oil, known more commonly as ANFO.

Finally *explosive mix* consisting of the composition of two or more compounds of which, at least one, is an explosive. Usually these non-explosive substances are added to mitigate the sensitivity to external actions and the power of the explosive. Explosive blends are distinguished by physical mixtures obtained by fusion of the ingredients and chemical mixtures obtained by gelatinization. These explosive mixtures are very satisfying from the energetic point of view; some blends if they were used with only the components that generated the explosion would be of low power and with various drawbacks. An example of this group of explosives is Dynamite and Blasting Gelatin and Plastic Explosives.

## 1.2 - Use of explosives

Depending on the characteristics of the different explosives, it is possible to define the different use for each substance.

Their use is manifold and spans into three large groups, which are military, civilian, and improvised explosives that will be exposed later on.

*Military explosives* such as Pentrite (PENT), Tetrile (CE), Exogenous (eg Cyclonite, C6) and Trinitrotoluene (TNT) can be used alone or by adding substances that allow improve performance, such as aluminum powder. These types of explosives can also be added in plastic materials such as synthetic polymers. In this case plastic explosives are obtained, gelatinized and are between the most powerful exhibitors. One of the most used plastic explosives in recent years is the explosive C4 (where C stands for "Compound", "Composition"), an explosive produced by the RDX (Cyclotrimethylentrinitroamine) composition. These explosives have features that allow them to be resistant to moisture and extreme temperatures and it is possible to find them in different shapes and colors. Due to their humidity tolerance they can be hidden in liquids by avoiding organic solvents to prevent the explosive substance from dissolving.

*Civil explosives* are substances that differ from color, granulometry and solidity between solid and gelatinous. They are mainly used for geotechnical works, underground excavations and demolition works. In mining field, the most used explosives are those based on Nitrate, Potassium or Ammonium, also there is the Blasting Gelatin, consisting of 92% by Nigrlyceria and for the remainder, that is 8% by Cotton Collodius, Dynamite based on Nitroglycerin and other inert substances. However, these explosives are dangerous because they are sensitive to shocks, which makes transportation very difficult. For this reason, many countries have adopted the combination of explosive substances once they have reached the workplace in order to avoid explosive cartridges already fragmented (as it is still adopted in Italy) that are more dangerous and sensitive. In addition, explosives for civil use have a variable density but very similar to that of water. This allows good tolerance to the environments in the presence of water, but some of them do not detonate if they are immersed in water. These explosives are also susceptible to high temperatures, as explosives or other substances in the interior can decompose and come out.

*Improvised explosive* devices are devices called “Improvised Explosive Devices” (IEDs) and are generally secretly designed to carry out terrorist and guerrilla warfare operations. These types of explosives can be of different shapes and sizes, and they can contain different quantities of explosives or other material, always capable of causing damage. Precisely for this reason it is very difficult to define the power of such a weapon. Detonators can also be of various types, can be taken from military equipment or can be crafted in the home. Precisely because of the poor ability to possess the materials suitable for the correct manufacture of a device or for the low professionalism of the manufacturer. In fact, these devices can encounter various problems: premature or incomplete detonation may occur, or gas outflow can corrode the metallic container that might decompose.

### **1.3 - Main types of explosives**

The most widely used explosives, in general, are chemical explosives that possess a high speed of charge decomposition, which is a rapid oxidation reaction that generates a sudden increase in temperature and the formation of large quantities of gas. Usually the explosives are found in the form of white or black powder, which before being inserted into the container are wet, giving the powder a pasty consistency to avoid premature explosions. Among the most used explosives we can remember: TNT (Trinitrotoluene), Ottogene (HMX), RDX and Nitroglycerine and compound explosives such as Dynamite, Black Powder, plastic explosives (C-4), and the ANFO, a combination of Ammonium Nitrate and Fuel Oil. The physical and chemical characteristics of the various explosive materials affect their use. Among the possible uses one has to be taken into account: in addition to the civil and the military one there is also the terrorist one. The IED device is made up of the most suitable explosive substances to overcome normal safety checks. Following are the main explosives that are commonly used with the main technical characteristics.

### 1.3.1 - Simple explosives

#### Trinitrotoluene (TNT)

Trinitrotoluene, commonly known with the acronym *TNT* and in Italy with the name of *Tritolo*, is an aromatic nitrocompound obtained by the nectarization of toluene. At room temperature it is in a crystalline solid light yellow form as can be seen in Figure 4. It is an explosive insoluble in water but soluble in organic solvents such as for example in ethylic ether and in benzene. The Tritol is one of the most widespread explosives thanks to its characteristics that allow it to be very stable and insensitive to shocks and stress. It is one of the best explosives used in the military field, but it is not very suitable in the mine because during its combustion it releases the Carbon Monoxide, a poisonous gas, in odor and taste, that would pollute the tunnel air. Its triggering takes place by means of a detonator. Moreover it is a little hygroscopic explosive and does not react with metals; this allows it to be stored for many years. But it must be protected from the exposure of alcohols, which combined together generate an unstable compound, very sensitive to shocks and heat. As in most nitrocompounds, it is used for the composition of explosive mixtures such as Amatol, mixed with Ammonium Nitrate.

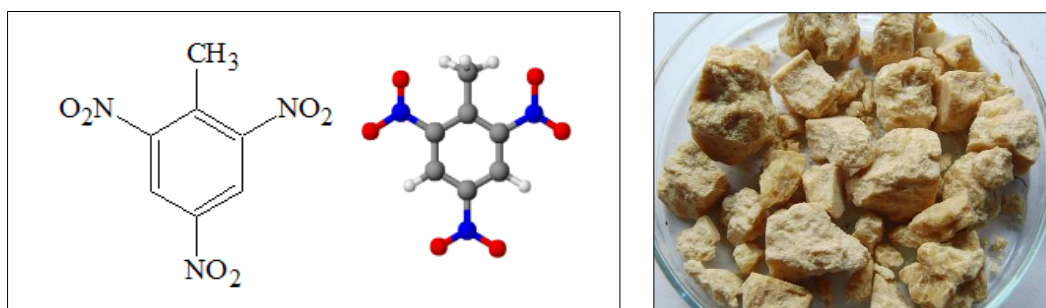


Figure 4. On the left, the chemical layer of Trinitrotoluene is shown; on the right, an image of the TNT at room temperature

#### Nitroglycerin

Nitroglycerine, also known as trinitrine, is an explosive substance sintered in 1847 by Asciano Sobrero. It is a substance with a high reaction speed (7000-7400 m/s) but extremely sensitive and unstable. In 1867, Alfred Nobel stabilized nitroglycerine, generating an explosive mixture consisting of 75% of Nitrogligerin and 25% of Diatomaceous powder, giving rise to Dynamite. Nitroglycerin is a powerful detonating explosive, which at room temperature is a colorless to yellow oily liquid (Figure 5) when it is not very

pure. Decomposes easily exploding at impact and for heating above 50°C, detonating at about 200°C. However, it can detonate even at ambient temperatures. Precisely because of its instability and for safety reasons, it is never used pure but always used mixed with other stabilizing substances and forms the basis for the formation of various types of Dynamites.

Nitroglycerin is formed by glycerine gelling process in a nitrating mixture, that is a mixture of concentrated nitric acid (70%) and concentrated sulfuric acid (98%), all carried out at a temperature of 15°C.

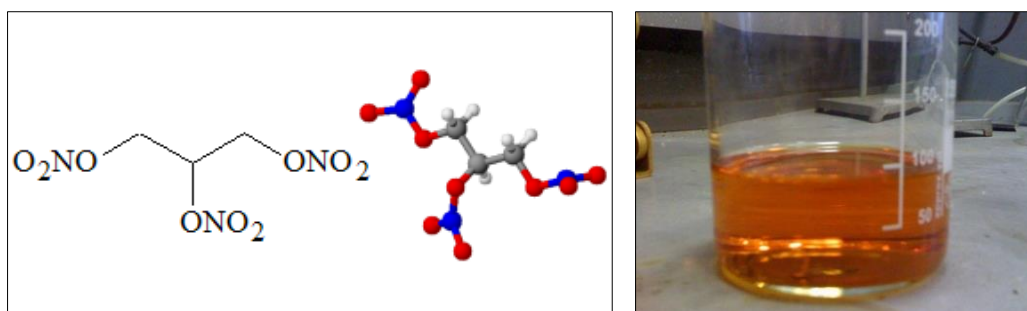


Figure 5. Chemical formula of Nitroglycerine and example of explosive at room temperature in poor conditions

### Ciclotrimetilentrinitroammina (RDX)

Ciclotrimetilentrinitroammina (Figure 6), commonly called RDX, is a nitroamine which is one of the most used explosives in the military field. It is one of the new explosives invented and in fact the first two letters, Research and Development, have the same meaning of the brand new explosives and as a third digit they are made up of an identification number. In the case of this explosive the third digit is identified with the letter "X", which stands for unknown. It was not possible to enter a number for this explosive due to reaching the maximum number in the archives. Subsequently, an identifying number was attributed to the Cyclohexymethylenetrinitroamine, by now, has been memorized with the starting name, then it was always called RDX, by the military.

RDX is an explosive generated by reacting concentrated nitric acid on hexamine. When it is freshly prepared and is pure it is encountered as a white crystalline solid. It begins to decompose at a temperature of 170 degrees centigrade and detonates at a higher temperature, around 250 degrees centigrade. If conserved in ambient temperatures it is very stable but unstable to water, with a fair sensitivity to impact that can increase if it is crystallized at a temperature of -4 degrees. To detonate this explosive needs a detonator. It is usually used in mixtures with other explosives, for example RDX is the basic component for some military explosives such as

C-4.

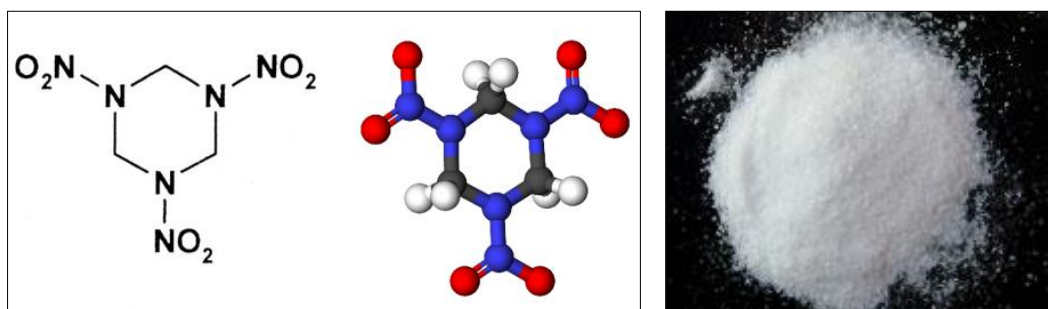


Figure 6. Chemical formula of RDX and example of explosive in poor conditions

### Ciclotetrametilentetranitroamina (HMX)

Ciclotetrametilentetranitroamina (Figure 7), commonly called HMX or Ottogene, is a very powerful and unstable shock explosive. It is a nitroamine very similar to RDX. It is an explosive used in the military field: in detonators, as an explosive to plastic, in nuclear weapons and as solid fuel for rockets. The acronym of this explosive means "High Molecular weight" and the third letter is like the RDX.

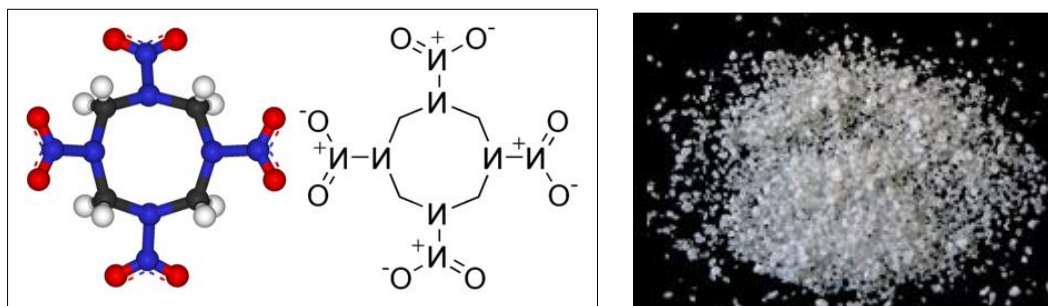


Figure 7. Chemical formula of HMX and example of explosive in poor conditions

### Pentrite (Pentaerythritol tetranitrate)

Pentrite, also known as PETN (Figure 8), is one of the most powerful explosives so far produced and it is comparable to the RDX and HMX. The PETN is a more sensitive explosive than TNT, in fact it is never used as a secondary charge, but always as a primary charge in detonators and to constitute the slow-burning fuses and as a reinforcing of the ammunition of small arms. It is shown that PETN is not quickly biodegradable and if thrown into watercourses it causes pollution of the layer and can continue to pollution of the aquifer.

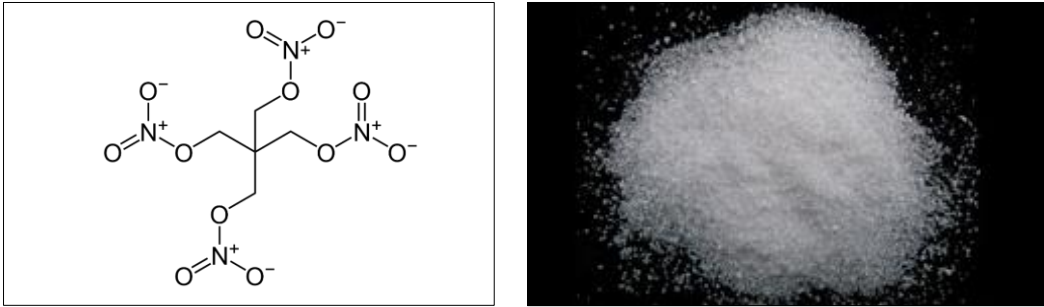


Figure 8. Chemical formula of PETN and example of explosive in poor conditions

### 1.3.2 - Composite explosives

#### Dynamite

Dynamite is an explosive invented by Alfred Nobel in 1866, in the attempt to stabilize the nitroglycerine, by Antonio Sobrero, by adding silicon-based absorbing substances. It was a great discovery because it was considered the safest (and most stable) explosive of the time. However, at low temperatures, the nitroglycerine escapes from the dynamite sticks (which can be seen in Figure 9) putting in serious danger the workers who have to handle it. In these conditions there was a probability of release of nitroglycerine and safety problems previously found. After highlighting this problem, the studies focused on the search for new materials.



Figure 9. Examples of Dynamite sticks

### ANFO

ANFO (Figure 10) is the acronym of "Ammonium Nitrate Fuel Oil" is a highly safe explosive mixture consisting of Ammonium Nitrate, Diesel and other minor additives, used in general for civil uses in quarries and mines, given their low cost and low sensitivity. This explosive need an optimal fuel-combustive ratio that ensures perfect detonation. Also, since its sensitivity is very low, it requires a repeater to make sure that the detonation occurred. It is very important that in the detonation of the ANFO there is a proper percentage of ammonium nitrite (95.5%) and hydrocarbon (heavy oil, 5.5%). In the opposite case, harmful toxic gases such as carbon monoxide and carbon dioxide are generated, just for this reason it is an explosive not allowed underground. Furthermore, the ANFO is hygroscopic, so its storage must be done carefully and away from humid environments, since water interferes with its explosive function.

This explosive is very popular due to its great stability and low cost. For this last reason, terrorists, such as ETA and Palestinian extremists, have adopted this explosive among those they used.



*Figure 10. Example of ANFO*

## **Black powder**

Black Powder (Figure 11) is one of the first explosives used in history. It is a deflagrating explosive with a decomposition rate of the subsonic charge. This reduces the pressure peaks on the firing chamber of the weapons and makes this explosive less suitable for the use of abatement of rock masses. It is a mixture of wood carbon, sulfur and potassium nitrate and is used for the realization of a slow combustion fuse.



*Figure 11. Example of black powder in nature*

## **C-4**

The C-4 (Figure 12) is a plastic explosive used both in the military field and in the field of demolitions. Plastic explosives are generally semi-solid with high potential insensitive to impact and by its characteristics are easy to handle, durable and safe. The C-4 is an explosive consisting of the explosive RDX enriched with additives that make it similar to an easy-to-mold filler. Thanks to a high percentage of paraffin we can always find the C-4 as a paste of various colors (from opaque white to gray).

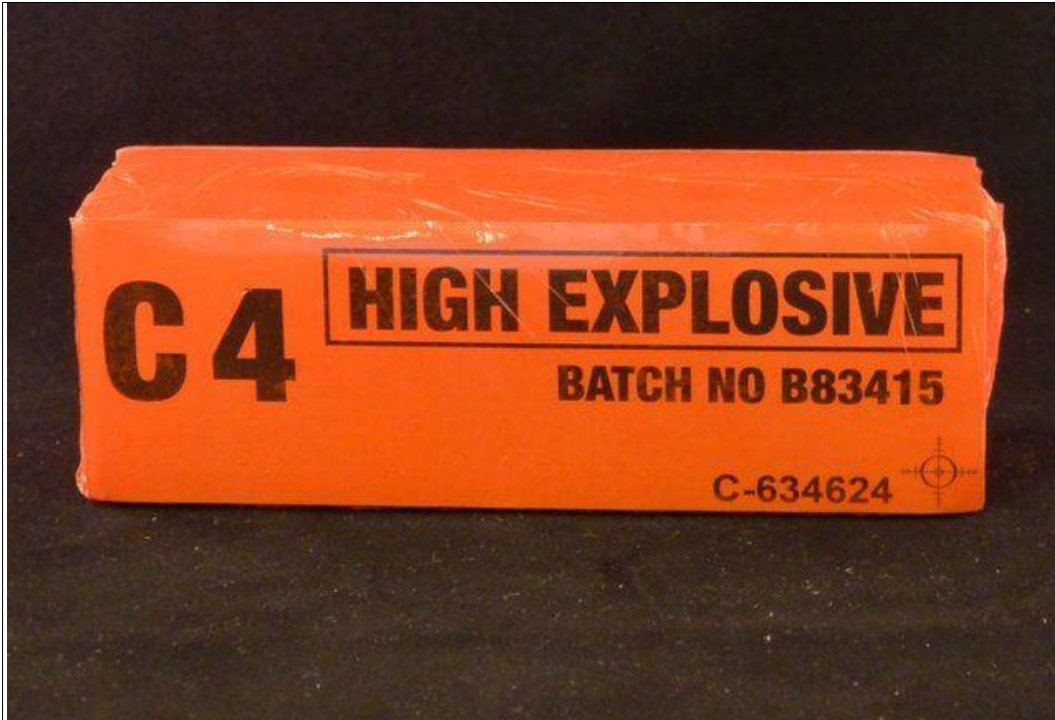


Figure 12. Example of high explosive C-4

## 1.4 - TNT equivalent

The differences in the characteristics and behavior of the different explosives as described in the previous chapter allows us to understand that the explosion generated by two charges of equal weight but of different materials placed at the same distance produce different shock fronts.

In fact, the explosion resulting from a charge A can not be compared to the burst of charge B. The two bursts can be compared using a conversion factor that, depending on some properties, makes the effect of the charge B destructive as that of the charge A. For this reason, the idea arises to refer only to a curve for the characterization of the parametric of the wave front generated by any explosive material. The material has been always plotted by condoning a reference explosive: TNT equivalent.

An equivalent TNT charge is taken, and it represents the charge weight of TNT which produces the same effects as the charge under test.

The first step in quantifying the explosive wave generated by an explosion caused by a different explosive of the TNT, is to convert the considered charge mass into an equivalent mass of TNT. This type of explosive was used as the reference one only because there were many experimental data related to the characteristics of the shock waves [UFC 3-340-02,].

The TNT can be measured by different relationships depending on the maximum pressure, the impulse, specific energy and many others [Sochet I., 2010]. However, the values obtained by the different criteria give distinct numerical results. This is due to the fact that the explosion depends on several factors and not just one. The value of equivalent TNT depends on many factors, for example the range of output and the shape of the material. Usually, the criterion used to estimate the equivalent TNT is the one based on the specific energy.

## 1.5 - Detonation process

Most of the structural damage due to an explosion on the surface or at low altitude in the air is caused by the shock wave that accompanies the phenomenon. In fact, the material damage is produced by overpressure of the shock wave, ie generated by a pressure drop of 3-5 bar or more compared to atmospheric pressure consisting of a value of 1 bar considering the standard conditions at sea level. The distance at which the shock wave propagates depends on several factors, mainly the type of explosives and the energy it has, subsequently from the medium in which it expands, the presence of water and air, and finally from the height where the explosion occurs. One aspect to take into account because it has a slight effect on the shock wave is afterburning. By using this process in high-energy explosives, only a third of the total chemical energy is released, the remainder being released into the air more slowly.

The detonation wave has a very high speed, ranging from 7000 m/s to 9000 m/s. During detonation, the solid or liquid explosive rapidly transforms into very hot, dense and very high pressure gases. Gas expansion occurs very rapidly in all directions producing a displacement of the air surrounding said shock wave. The shockwave can be associated with a wall generated by very compressed air that has a strong overpressure and moves at a high speed. The wave front as it moves away from the source point undergoes the dissipation of the air producing a lowering of the pressure peak as the distance increases, as we can see in Figure 13.

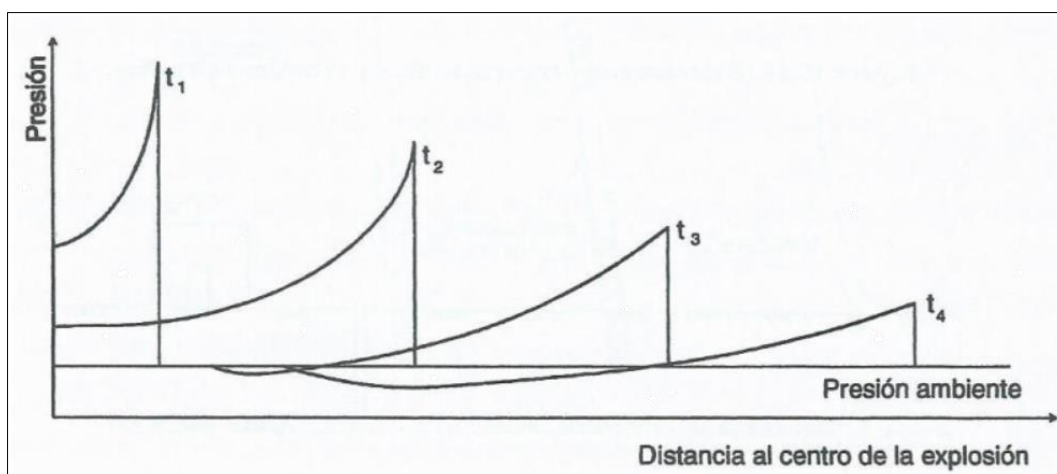


Figure 13. Decay of the pressure peak as the distance to the explosion point increase

The speed of the shock wave is very high and, this subsequently generates a *depression zone*.

During the explosion three different zones are generated. The gas due to the decomposition reaction of the explosive charge generates a thrust on the surrounding air, which is obliged to move leaving the volume occupied generating a zone of rarefaction where the pressure assumes a value lower than the atmospheric pressure. This area of rarefaction, which we can clearly see from Figure 15, is also called the *negative phase of the shockwave*. It generates an air suction to fill the voids formed by the initial displacement of the air surrounding the explosive. After the gas has finished expanding and the pressure has reached atmospheric pressure, the displacement of air that followed the wavefront changes direction come back way the point of explosion.

The inversion of the flow is caused by a small difference in pressure between the atmospheric conditions and the gas pressure (lower than atmospheric pressure). When the inversion of the flow occurs, the pressure can again overcome the atmospheric pressure and define a secondary peak returning to the conditions of expansion of the gas. This phenomenon defines a free oscillation and is defined as the *pulsation of the explosive gas system*.

In Figure 15 it is possible to see the ideal trend of pressure at a point at a certain distance from the explosion to a high energy content recorded over time. It is possible to notice that there are two phases in the graph: a positive and a negative phase. The positive part is the most significant part because there are small buildings and framed structures in which the damage depends on the drag force associated with the air flow that accompanies the shock wave and the pressure is called *dynamic pressure*.

Most of the damage directly caused is due to the incident pressure or even the peak pressure and the dynamic pressure, which both work in a positive phase. The dynamic pressure has a longer life, but the amplitudes during this time are very low, in fact the damage generated is negligible compared to the incident shock wave, which has a very high altitude.

Structural damage is also caused by the negative phase, such as windows or brick or gypsum walls that are not designed to withstand loads facing out.

The Figure 14 shows the compression and rarefaction phases and the behavior of the affected structure. The effects of the phenomenon of the backwash are the reason why many times the structures are inclined in the

opposite direction to the wavefront propagation direction. Furthermore, it is noted that the duration of the negative phase is greater than the positive one but with a smaller peak than the positive face. Precisely for this reason the analyzes will be made not where the effects are negligible, ie in the negative phase, but where the peak is higher and where the highest damage values will be obtained, ie in the positive phase.

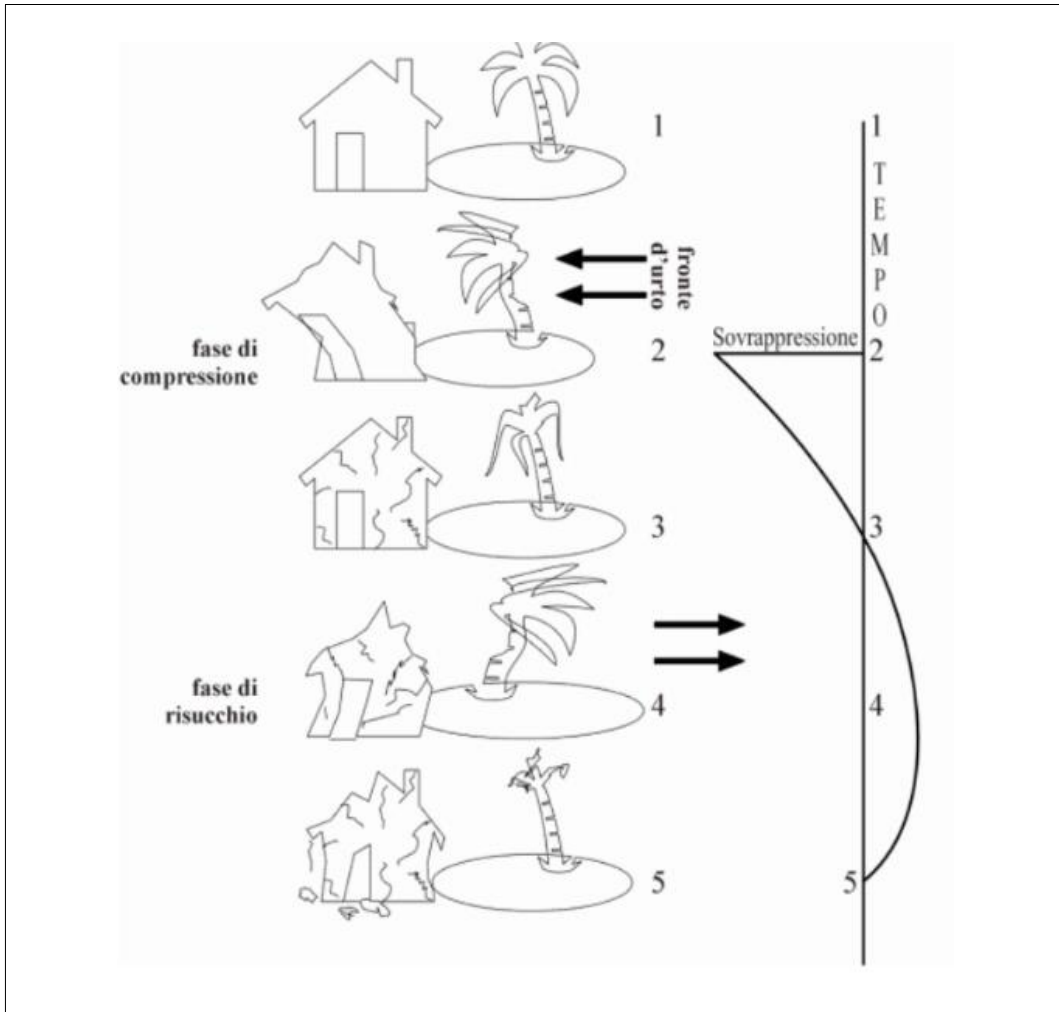


Figure 14. Behavior of a structure subjected to a shock wave

From Figure 15 above it is possible to see the different parameters that constitute the pressure wave. Analysing them with greater attention it is possible to notice:

- First arrival time ( $t_A$ )

It is the time that the shock wave takes to go to the considered measurement point. It includes both the triggering time of the charge and the time it takes the wave to arrive at the point of study.

- *Overpressure peak ( $P_{so}$ )*

It is the maximum pressure value obtained at the time of first arrival.

*Duration of the positive phase ( $t_0$ )*

It is the time that pressure takes to reach atmospheric pressure.

- *Pressure peak ( $P_{so^-}$ )*

It is the minimum value reached in the rarefaction zone

- *Duration of the negative phase ( $t_0^-$ )*

Corresponds to the duration of the negative phase (greater than the positive phase)

- *Pulse of the positive phase ( $i_s$ ) and pulse of the negative phase ( $i_s^-$ )*

These parameters allow us to define qualitatively the energy transmitted by the explosion, represented by the curve shown in the Figure 15.

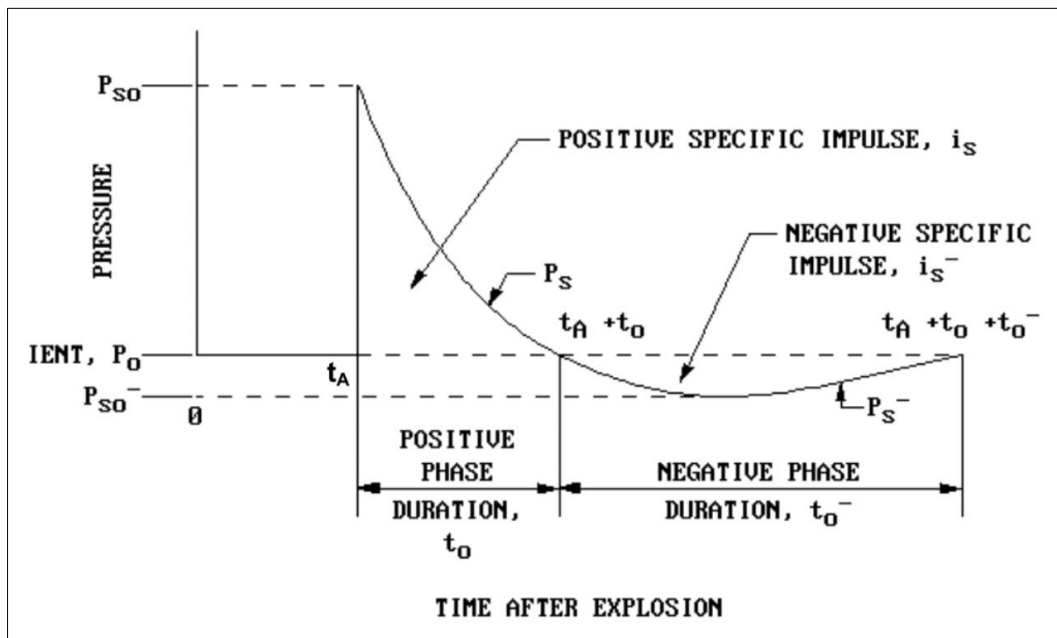


Figure 15. Pressure variation with respect to the passage of time

Then the positive phase impulse is defined by the following relation:

$$i_s = \int_{t_A}^{t_A+t_0} [P(t) - p_0] dt \quad (1)$$

$$i_s^- = \int_{t_A}^{t_A+t_0+t_0^-} [p_0 - P(t)] dt \quad (2)$$

Where  $P(t)$  is the pressure as a function of the pressure with respect to time and  $p_0$  represents the atmospheric pressure (value equal to 101325 Pa).

The pressure function during the history was calculated in different ways, generally considering only the positive phase [S. Ahmad, 2014].

For the determination of the pressure as a function of time we proceed with the calculation of the *decay coefficient*, also called the *shape coefficient*. To define this coefficient three different equations are used:

1. The equation extracted from the approximation and interpolation of the curve obtained from the Friedlander equation using the pulse of the positive phase we obtain the formula of the decay coefficient as a function of the scaled distance:

$$b = 5.2777 \cdot z^{-1.1975} \quad (3)$$

2. Obtained from the modeling of the previous Friedlander equation; the coefficient is obtained as a function of the ratio in absolute value between the minimum and the maximum pressure value from which the interpolation returns the following formula [Lam Nelson, 2004]:

$$b = z^2 - 3.7 \cdot z + 4.2 \quad (4)$$

3. Finally, following the modified equation of Friedlander, the formula of Wei and Dharani is found in literature [Florek Jason R., 2007]:

$$b = -0.0697 \cdot z - \frac{9.63}{z} + \frac{15.9}{z^2} - \frac{5.65}{z^3} + 2.735 \quad (5)$$

Through these equations of the decay coefficient we could calculate the pressure as a function of time, going to see the behavior that it assumes depending on the coefficient considered [Karlos Vasilis, 2016].

$$p(t) = P_s \cdot \left(1 - \frac{t}{t_0}\right) \cdot e^{-\left(b \cdot \frac{t}{t_0}\right)} \quad (6)$$

## 1.6 - Blast-loading categories

The wave loads on the walls of the structures are divided into two large families [UFC 3-340-02], based on the confinement of the explosive charge. The confined explosions and the unbounded explosions are distinguished, each of which is divided into three types of load as we can see in Table 1. In this document we will analyze the case of the explosion not confined in free air and from a height above the ground: these two characteristics that are of interest in the PICAEX project.

Table 1. Blast loading categories

Categories of explosive loads	
Confinement	Categories
<i>Unconfined explosion</i>	Free air burst explosion
	Air burst explosion
	Surface burst explosion
<i>Confined explosion</i>	Fully vented explosion
	Partially confined explosion
	Fully confined explosion

### 1.6.1 - Unconfined explosion

#### Free air burst explosion

The explosion in free air is a type of explosion in which the shock wave spreads from the center of the detonation, striking the protective structure or the structure without there being any kind of amplification (therefore the loads on the structure are in the open air). In this case the incident wave front moves radially from the center of the explosive, as can clearly be seen from Figure 16, and at the moment of impact with the hypothesized rigid structure, it will be reflected and reinforced.

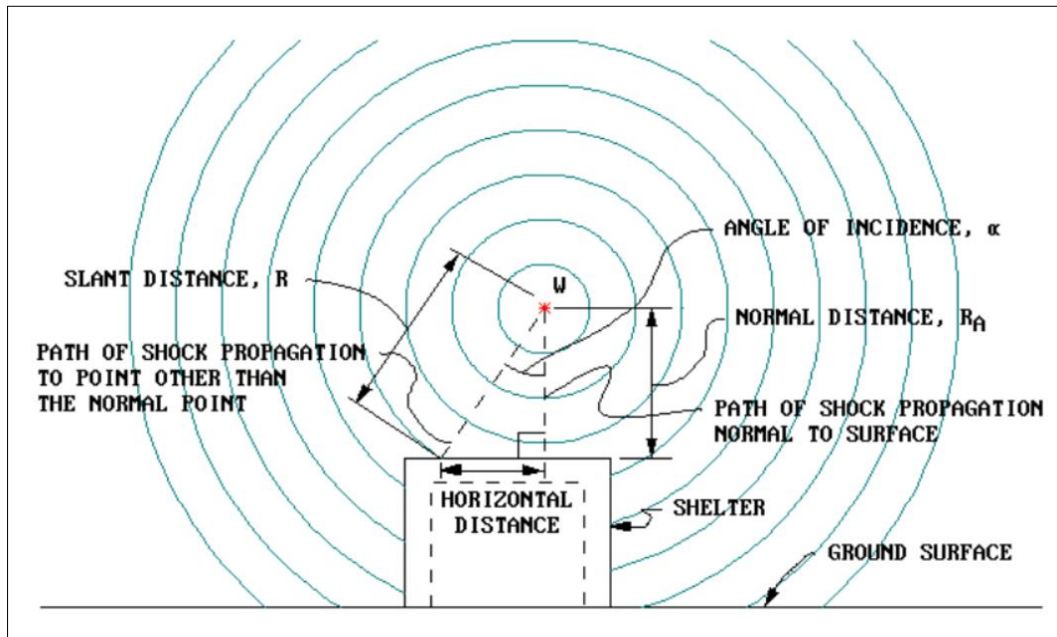


Figure 16. Free-Air burst blast environment

The parameters characterizing the positive phase (peak pressure, impulse, duration and time of first arrive, detected on the target before the reflection occurs) are determined by Figure 18 that depends on the distance scaled, ie the real distance between the bursting point and the structure under examination and the weight under the cubic root of the equivalent explosive charge that will be treated later.

The curves that are represented in Figure 18 have been developed through polynomial interpolation [Michael M. & Swisdak Jr., of data 1984] of experimental data, obtained by defining real conditions and therefore influenced by meteorological effects, from Kingery and Bulmash [Kingery C.N. & Bulmash G., 1984].

In the Engineering field these curves are widely used for the prediction of pressures in free field and to define the loads acting on the structure considering the actual conditions present. It is emphasized that for the use of this graph all units of measurement must be reported to conventional US units. Furthermore, it can be noted that in this figure there are parameters that are scaled with respect to others, this allows to give conservative limits for the project.

To define blast loads at different times and on different structural surfaces, the parameters of the negative phase can be defined by the following figure (Figure 17).

In general, the parameters of the negative phase, as mentioned above, can be ignored because of the greater interest in the analysis of the positive phase (in rigid structures such as in reinforced concrete), but in the flexible structures it may be useful to analyze the negative phase and define the parameters that characterize it through this graph shown above.

These curves contain an important limit within them. They can be represented up to a scaled distance ( $z$ ) equal to  $100 \text{ ft/lb}^{1/3}$ , because once this value has been exceeded, the properties of the shock wave start to suffer the effect of environmental conditions.

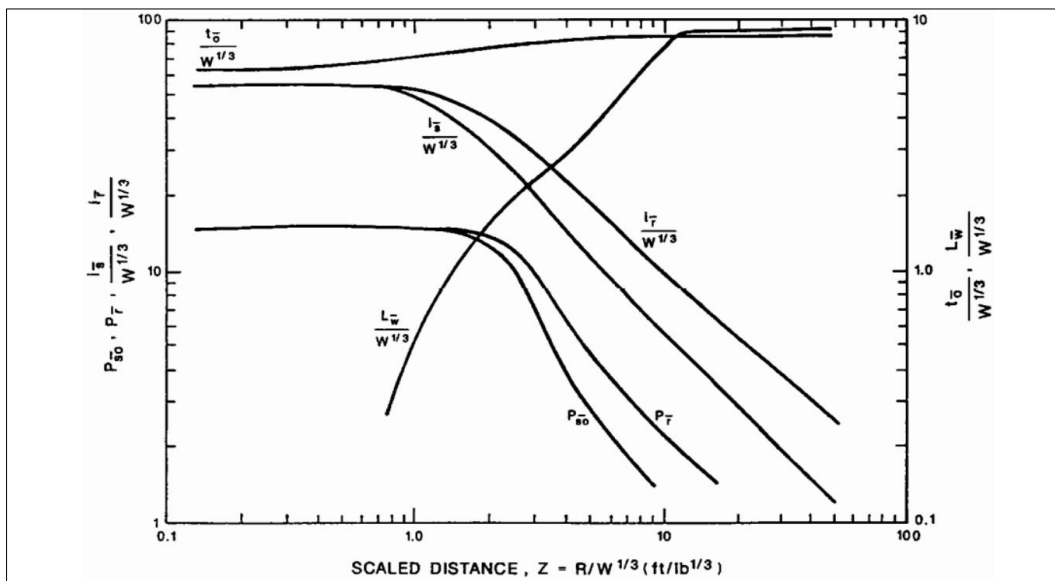


Figure 17. Free air burst explosion. Negative phase shock parameters for a spherical TNT

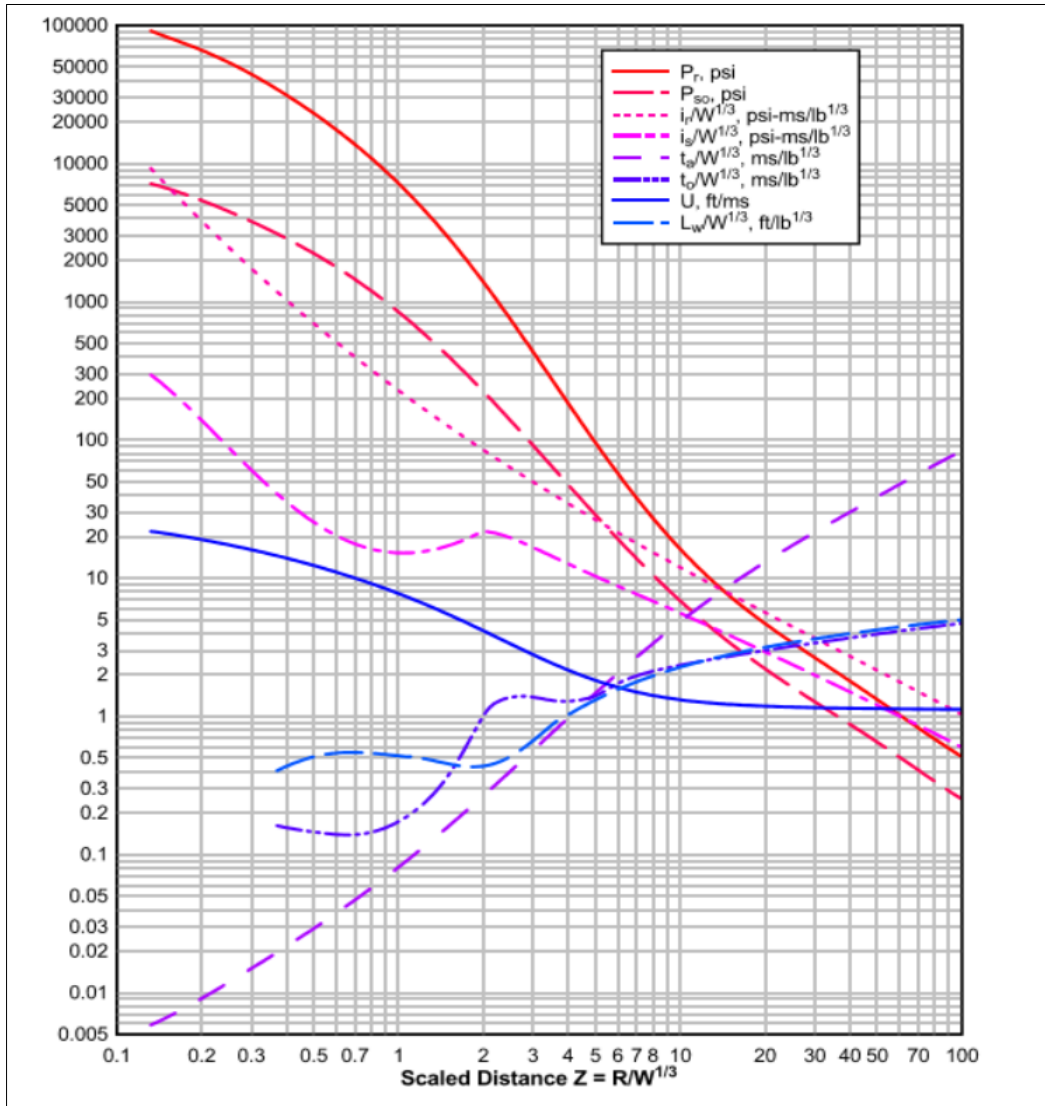


Figure 18. Free air burst explosion. Positive phase shock parameters for a spherical TNT

### Air burst explosion

The Air burst explosion is characterized by the charge that is raised from the ground to a certain height and a distinct distance from the protective structure. The shock wave at the burst moment radially propagates from the center of the explosive and affects the surface of the ground before reaching the structure. The shock wave continues to propagate, but wave interaction with the ground generates a front face called *front of the Mach*, which increases the destructive effects of the explosion itself. This type of front is generated by the interaction of the incident wave and the reflected wave of the earth's surface (Figure 19).

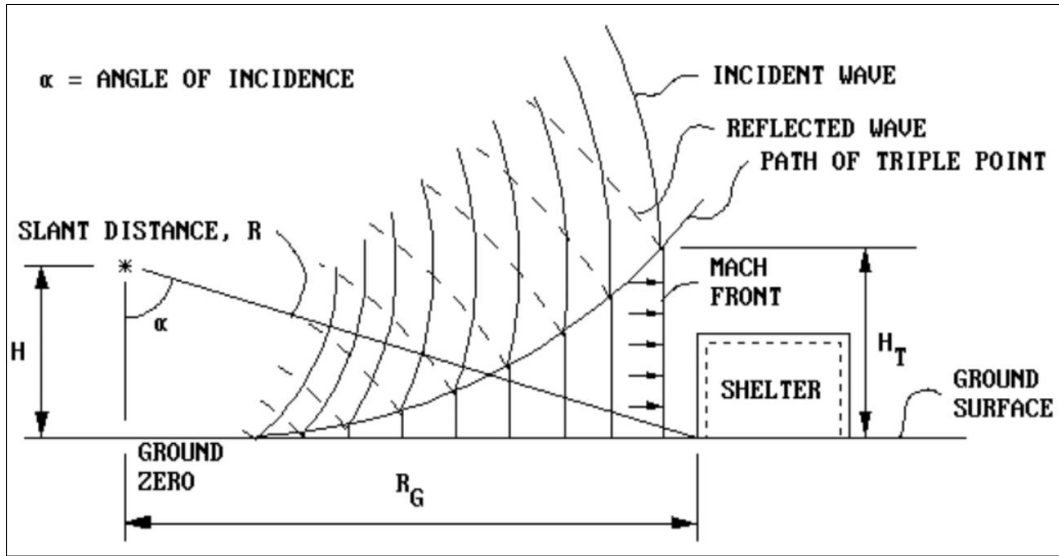


Figure 19. Air burst blast environment

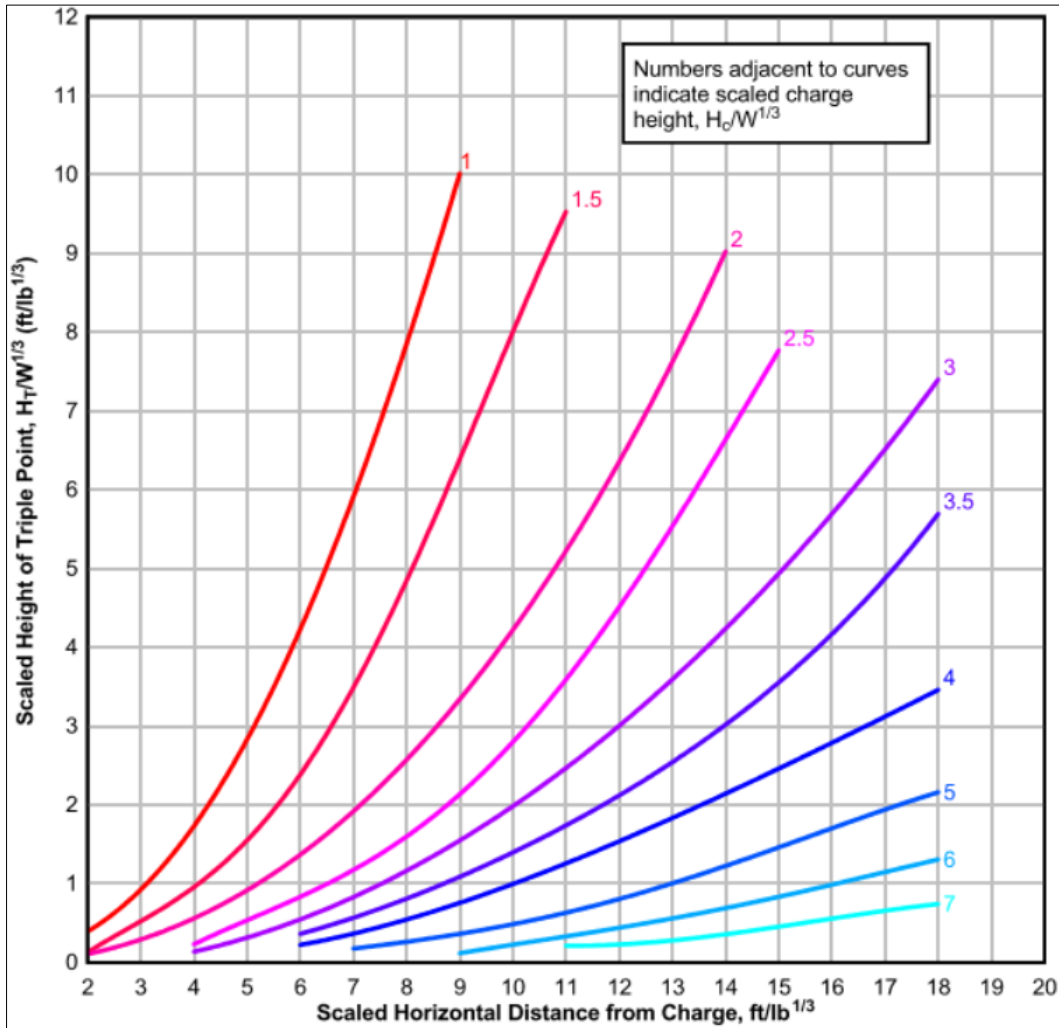


Figure 20. Scaled height of triple point

Pressure variations occur above the height of the front of the Mach, so we look for a charge and a distance that is scaled in such a way that the *triple point* (point where the incident wave, the reflected wave and the Mach wave meet) is greater than the height of the structure under examination. By defining this initial hypothesis, the phenomenon is perceived as a plane wave over the entire height of the front. Mach's front increases in height as the distance from the burst point increases, and the union of the triple points in the different moments of time and in the different distances allows to define the *trajectory of the triple point*. Structures with a lower height than the triple point are subject to a flat wave, ie a uniform pressure. The height of the triple point is defined by Figure 20, which is obtained from [UFC 3-340-02], where, as a function of the horizontal distance scaled by the charge and the height of the charge from the ground, we obtain the height of the triple point.

If the triple point does not extend above the structure, then the loads applied to the structure will vary according to the point considered on the wall, ie the structure is no longer subjected to uniform pressure. Above the triple point the pressure amplitudes are smaller than those found on the Mach's front.

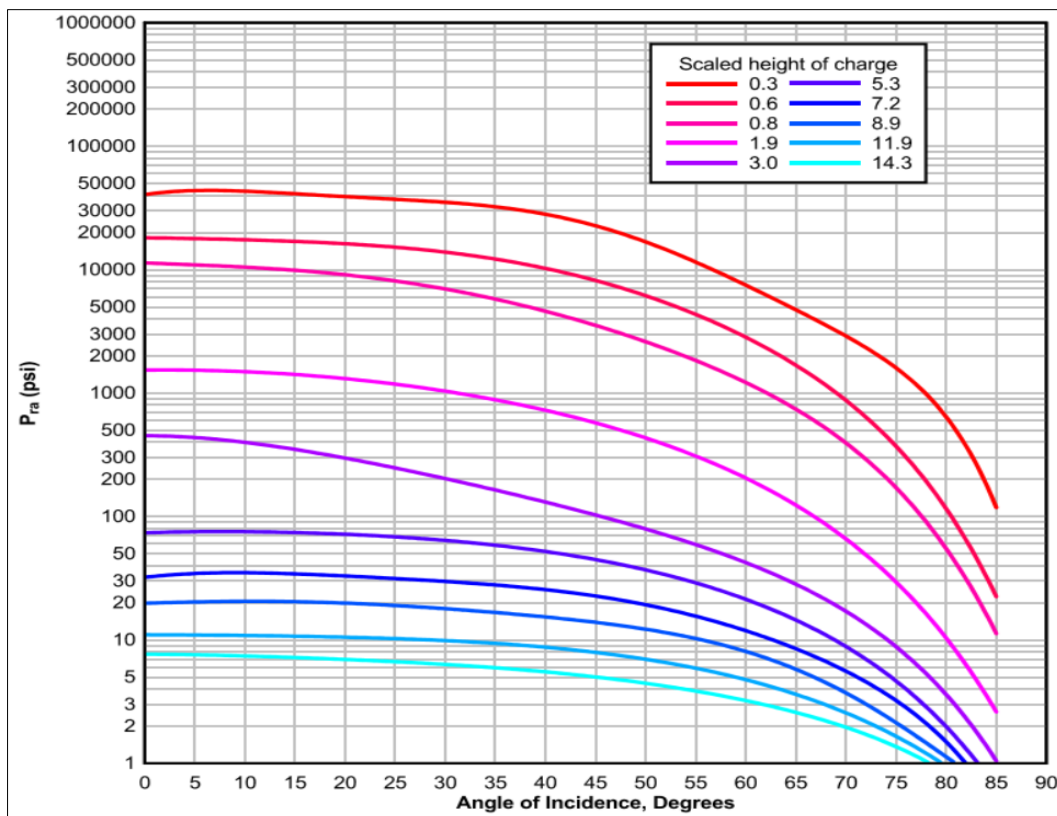


Figure 21. Variation of reflected pressure as a function of angle of incidence

To define the amplitude of the explosive loads acting on the considered structure, considering a charge placed at a certain height of the ground, one considers the incident pressure peak  $P_{ra}$  determined by the Figure 21 [UFC 3-340-02] below. This diagram can be used knowing the height of the charge from the ground and the angle of incidence. Moreover, with the same procedure used for the determination of incident pressure, the value of the  $i_{ra}$  pulse can be obtained, as shown in Figure 22.

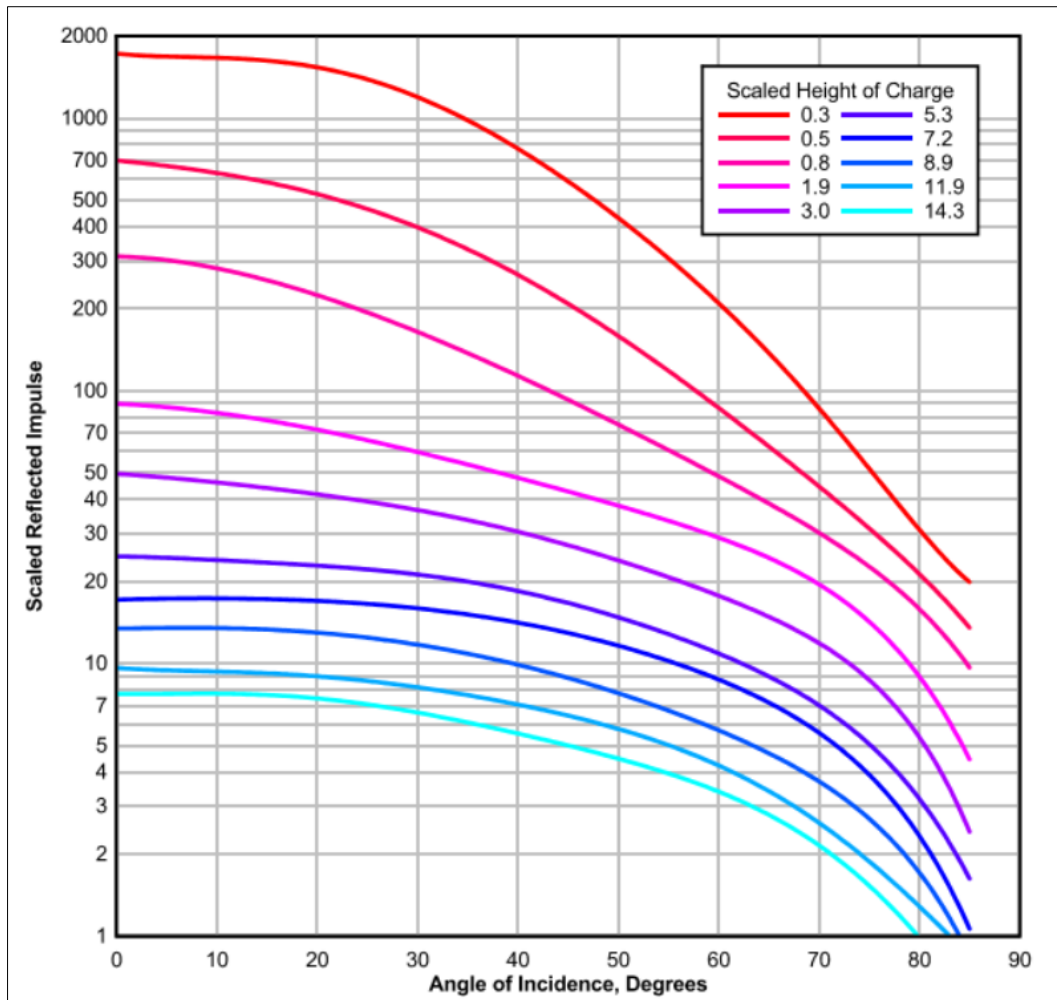


Figure 22. Variation of scaled reflected impulse as a function of angle of incidence

### 1.7 - Explosion of a spherical charge in the air

When the ignition and bursting of a uniform explosive material occurs, due to the abrupt variation in pressure and temperature, the shock wave expands into the surrounding air, without encountering obstacles, such as a spherical surface. The explosive forms can generate a direction of propagation of the preferential shock wave, but the spherical explosives

generate an equal propagation in all directions and allow the verification of asymmetric shocks. Precisely for this reason, the spherical explosive charges are usually the forms chosen in the experimental tests and the numerical analyzes to predict the explosive loads at a point at a certain distance from the source of the explosion.

The parameters that characterize an explosion are determined on the basis of the energy deriving from the explosion and the distance between the charge and the structural element that we consider. One of the simplest approaches to the scaled waveform calculation is Hopkinson [Swisdak Jr & Michael M, 1994] and Cranz [Hopkinson B, 1915]. The scaled law is commonly described as *cube rule scaling* [López L M, 2015] in which it is used in many design experiments. It is stated that similar shockwaves are produced by charges with the same geometry, consisting of the same explosive material, distance scaled, but of different diameters, and detonated at the same environmental conditions.

Precisely for this reason if two charges of the same explosive material have a mass equal to  $W_1$  and  $W_2$  and a diameter equal to  $d_1$  and  $d_2$  it can be said that the charge mass is proportional to the diameter elevated to the third of each respective explosive. So we can write:

$$\frac{d_1}{d_2} = \left(\frac{W_1}{W_2}\right)^{1/3} \quad (7)$$

If we want to have the same overpressure in the burst of the two charges we can rewrite the equation as:

$$\frac{R_1}{R_2} = \left(\frac{W_1}{W_2}\right)^{1/3} \quad (8)$$

Where  $R_1$  and  $R_2$  are two distances in which the overpressure produced by the respective charge takes place.

From here comes the definition of the scaled distance introduced in the previous chapter defined by the equation:

$$z = \frac{R}{W^{1/3}} \quad (9)$$

The use of this variable allowed, by means of combinations of different quantities of explosives and different distances, to refer to a wide range of

situations to the experimental data on shock waves in a compact and efficient way.

## 1.8 - Fragmentation

The explosion can cause serious damage due to the impact of fragments. The objects generated by the explosion will have an impact on civil structures and can generate human victims. The fragmentations are divided into two large families:

- a) *Primary fragmentation*
- b) *Secondary fragmentation*

The *primary fragmentation* identifies the fragments generated by the device itself, ie the fragments generated by the explosive cover and by the objects placed near it. From the explosion a large number of the small fragments are generated, these fragments are characterized by a very high initial speed that will be analyzed taking into account the secondary fragments.

The *secondary fragmentation* is generated by the intersection of the shock wave with objects or structures placed near at the explosive device. Objects near the shock wave with a certain pressure will be damaged, generating fragments or even explosion debris that, at great speed and small size, can be compared to bullets that travel a determinate trajectory threatening human lives and structures, and in the most extreme cases can be achieved the collapse.

In this analysis only secondary fragmentations will be examined, since these are the most important and useful debris in this project. It is very interesting to define how the fragments of the wall under test are propagated and to examine the maximum distance of the fragment for the design of the tests.

### Secondary fragmentation

To define the secondary fragmentation, which interests us, we first have to define the type of High explosive and the detonation that will be used in the test, then its configuration, for example if the charge is spherical or cylindrical. Furthermore, it is necessary to define the position of the charge with respect to the test wall and the type of propagation after switching on.

In order to define the fragments generated by the explosive HE, it will be necessary to define in detail: shape, weight and speed. To do this you will have to follow the following steps:

1. Define the distance  $R$  from the center of the explosive to the point of interest ie the test wall;
2. Determine the shape and size of the fragments according to the structure being considered;
3. Calculation of the speed of the fragments.

Per lo svolgimento del punto tre, per prima cosa si deve andare a distinguere di quale famiglia fa parte la velocità che vogliamo calcolare:

- Velocity of Unconstrained Secondary Fragments;
- Velocity of Constrained Secondary Fragments.

In our case study we will define the Velocity of Unconstrained that reflects our design choices

To determine the Velocity of Unconstrained Secondary Fragments [UFC 3-340-02] we must take into account the interaction between the shock wave and the affected object as we can see in Figure 23. We can observe the three phases that stand out as the wave passes over the object. When the wave hits the wall in the first interaction phase, one part is reflected from the front and the other is developed around the object. In the second phase diffraction it generates a local weakening of the wall and are formed of the vortices behind the object. Finally, there is the phase of the rarefaction wave in which it passes through the object, attenuating the reflected pressure. The pressure varies over time and the maximum that can be found on the front face during this "dragging" phase of the load is the *stagnation pressure*. As we said in the previous section, the pressure varies over time and at the instant  $t_a$  the net transverse pressure rises suddenly up to a maximum peak of reflected pressure  $P_r$ . For a flat surface this jump instantly takes place as shown in Figure 15 but, generally for an irregular surface there is a time equal to  $(T_1 - t_a)$  to reach the peak of pressure as we can see better in Figure 24. Then as we can observe the pressure decays linearly.

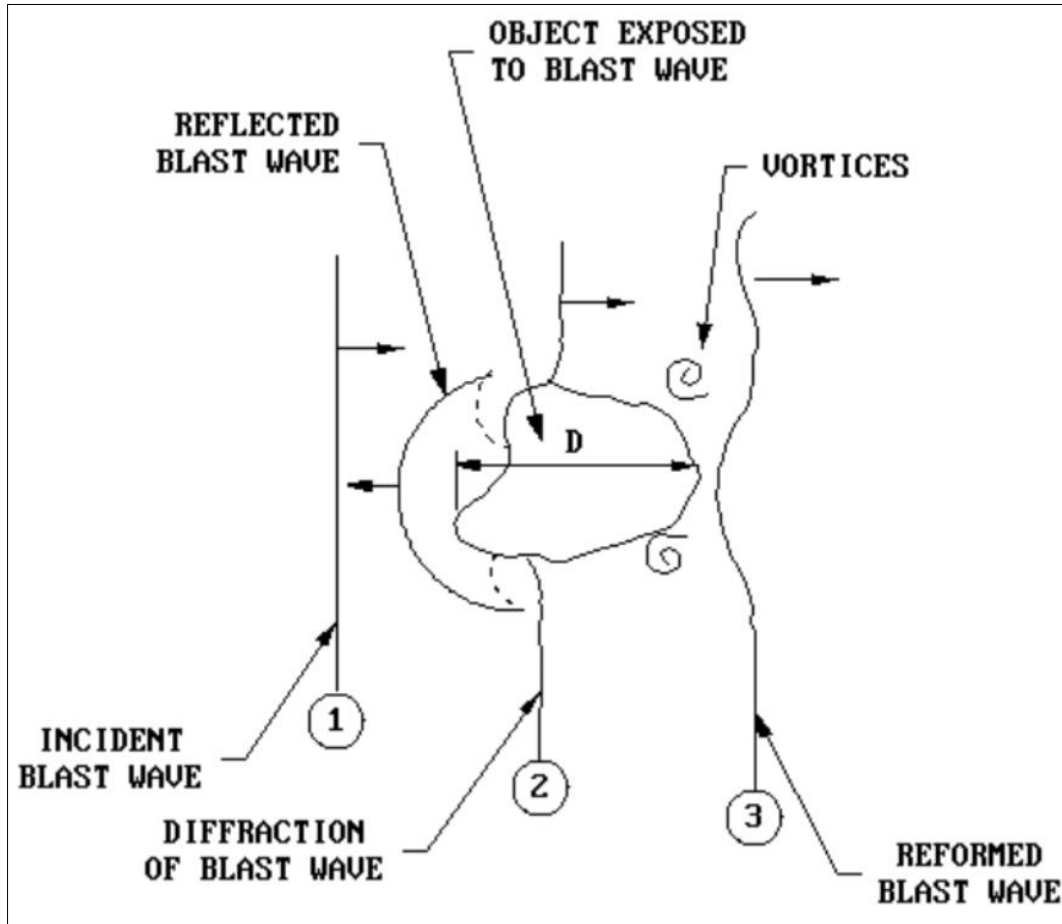


Figure 23. The interaction of a blast wave with an irregular object

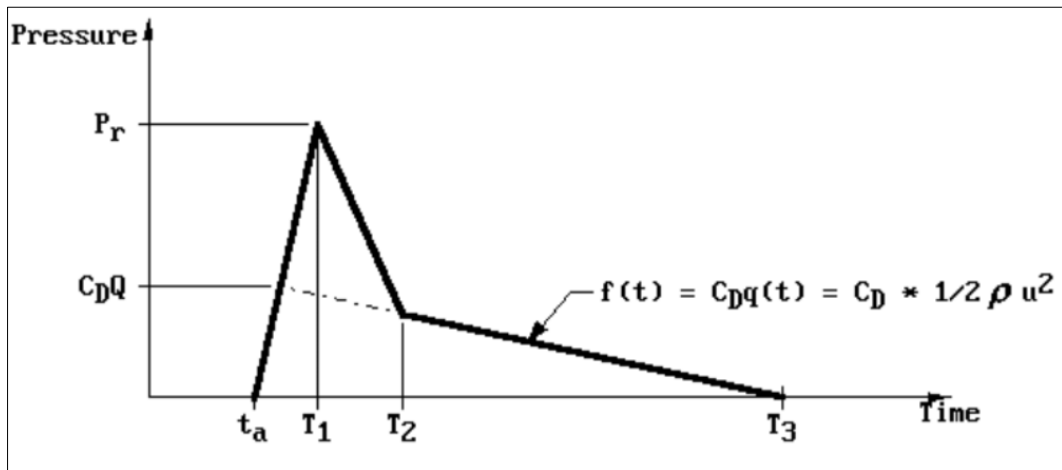


Figure 24. Idealized Pressure-Time Loading on an irregular Fragmentation

The initial hypotheses must be made for the non-constrained secondary fragments:

- a) The object of the examination behaves like a rigid body;

- b) No type of energy is absorbed to break the object and deform it elastically and plastically;
- c) Gravity effects are neglected during the acceleration phase of the movement.

The equation of motion for the object is:

$$A \cdot p(t) = M \cdot a \quad (10)$$

Where  $A$  represents the area exposed to the explosion front,  $p(t)$  is the pressure as a function of the time,  $M$  is the mass of the object and  $a$  is its acceleration.

The initial velocity of the fragments can be obtained by means of mathematical functions or in the case in which it can not be described in the form of a function, it can be defined by an integration:

$$v(T_3) = \int \left( T_3/t_a \right) \cdot a \cdot dt = \frac{A}{M} \cdot \int \left( T_3/t_a \right) \cdot p(t) \cdot dt = \frac{A}{M} \cdot i_d \quad (11)$$

Where  $v(T_3)$  is the initial velocity of the object and  $i_d$  represents the diffraction impulse.

In the case of intermediate force shocks, the solution of the previous equation can be represented by Figure 25 where there are:

- $P_{so}$ , is the peak of incident overpressure that can be defined through Figure 17 by knowing the value of the scaled distance;
- $p_0$ , is the atmospheric pressure;
- $C_D$ , is the drag coefficient, a value known for the most common forms of the charge obtained from Figure 26;
- $i_s$ , is the incident specific impulse that can be defined by Figure 17, knowing the value of the distance scaled;
- $a_0$ , is the velocity of sound in the air;
- $K$ , is the constant with a value of 2 in the case of charge in air;
- $H$ , is the minimum transverse dimension of the mean presented area of object;
- $X$ , is the distance from the front of the object to the largest cross-section;
- $M$ , is the mass of object;
- $A$ , is the mean presented area of object;
- $v_0$ , is the initial velocity of object.

This analysis, however, is suitable for the case of objects placed far away from the explosive charge, where the object is not subjected to a high-speed flow and the  $C_D$  is a constant. Figure 25 can be used in the majority of cases, when the distance between the center of explosion and affected object is greater than 20 rays of the charge.

Instead, in the case where the explosive charge is positioned near the object under examination, the initial speed is a function of the impulse and the variation of pressure is not important. In this last case, the impulse ( $i$ ) acting on the wall in question is equal to the applied momentum:

$$i = \frac{M \cdot V}{A} \quad (12)$$

In this case the initial velocity of the secondary fragments is calculated using the formula:

$$v_0 = \frac{1000 \cdot i \cdot \beta \cdot A}{12 \cdot M} \quad (13)$$

Where  $v_0$  the initial velocity of the secondary fragment,  $A$  represents the area and  $M$  the mass of the object hit by the wave,  $\beta$  is the form factor of the fragment that is obtained from Figure 27 and  $i$  is the specific impulse acquired.

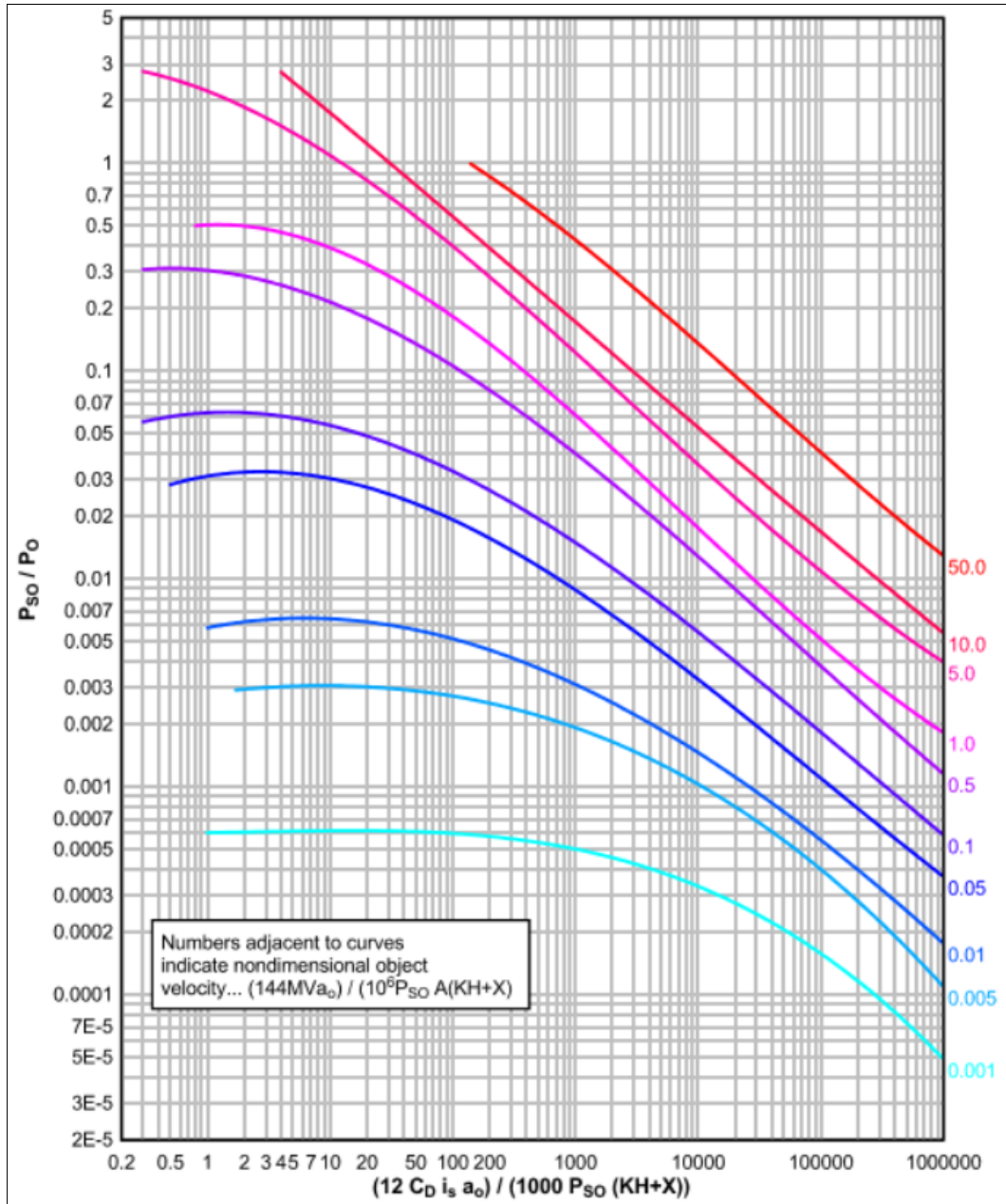


Figure 25. Definition of object velocity as a function of pressure and impulse for charges placed away from the object under examination

# 1 - Explosives

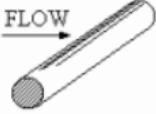
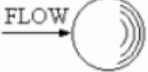
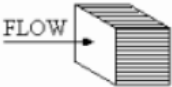
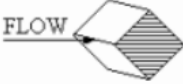
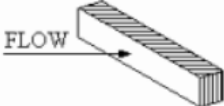
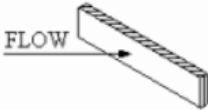
SHAPE	SKETCH	$C_D$
CIRCULAR CYLINDER (LONG ROD), SIDE-ON		1.20
SPHERE		0.47
ROD, END-ON		0.82
DISC, FACE-ON		1.17
CUBE, FACE-ON		1.05
CUBE, EDGE-ON		0.80
LONG RECTANGULAR MEMBER, FACE-ON		2.05
LONG RECTANGULAR MEMBER, EDGE-ON		1.55
NARROW STRIP, FACE-ON		1.98

Figure 26. Definition of the drag coefficient

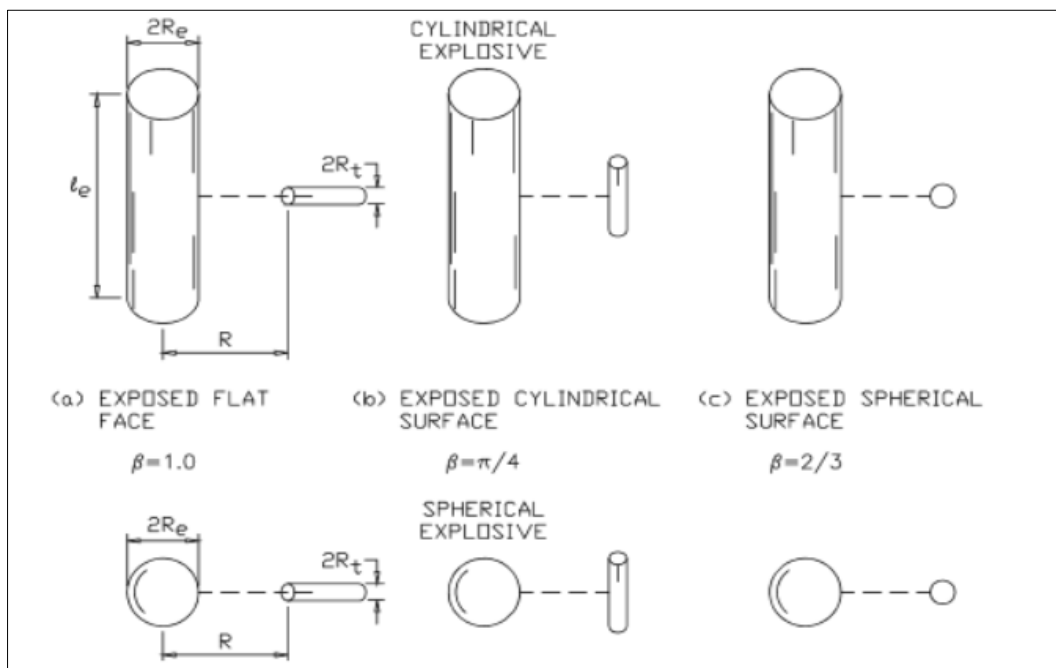


Figure 27. Determination of the fragment shape factor

## 1.9 – Trajectory of the fragments

After the formation of the primary and secondary fragments that can be considered as small projectiles moving on a specific trajectory up to the interaction with a target or the ground. For the determination of the trajectory of the fragments we will have to consider the inertia, the gravity and the fluid dynamic forces, definable by the velocity at each instant of the fragments [UFC 3-340-02].

The analysis of the trajectory of the fragments is performed by simplifying the fluid-dynamic forces using the concepts of aerodynamics. The force is defeated in two forces called resistance, ie the long component to the trajectory or normal to the force of gravity, and the lifting, that is the normal component to the trajectory:

$$F_L = C_L \cdot A_L \cdot \frac{1}{2} \cdot \rho \cdot V^2 \quad (14)$$

$$F_D = C_D \cdot A_D \cdot \frac{1}{2} \cdot \rho \cdot V^2 \quad (15)$$

Where

- $F_L$ , is the lift force;
- $F_D$ , is the drag force;
- $C_L$ , is the lift coefficient that it is defined empirically;
- $C_D$ , is the drag coefficient that it is defined empirically;
- $A_L$ , is the lift area;
- $A_D$ , is the drag area;
- $\rho$ , is the density of the medium through which the fragment is traveling;
- $v$ , is the velocity of the fragment.

In general the fragments are heavy, so  $C_D \gg C_L$  for any orientation of flight and for this reason, in this case, the lift force can be neglected because much less than the drag force.

Considering a simplified hypothesis in which it is considered that the fragment moves on a plane, the equation of acceleration can be written in the X and Y direction in the case of dragging only:

$$a_x = A_D \cdot C_D \cdot \ddot{a}_0 \cdot [V_x^2 + V_y^2] \cdot \frac{\cos \alpha}{2M} \quad (16)$$

$$a_y = -1.2 \cdot 10^{-5} \cdot g - A_D \cdot C_D \cdot \rho_0 \cdot [V_x^2 + V_y^2] \cdot \frac{\sin \alpha}{2M} \quad (17)$$

Where:

- $a_x, a_y$  are the acceleration in the X and Y directions, respectively;
- $\rho_0$ , the mass density of the medium through which the fragment travels;
- $V_x, V_y$  are velocity in the X and Y directions, respectively;
- $g$ , the gravity force (32.2 ft/sec<sup>2</sup>);
- $M$ , the mass of the fragment;
- $\alpha$ , the trajectory angle.

At the initial time ( $t = 0$ ) we will have that:

$$V_x = v_0 \cdot \cos \alpha_0 \quad (18)$$

$$V_y = v_0 \cdot \sin \alpha_0 \quad (19)$$

Where  $v_0$  is the initial velocity and  $\alpha_0$  is the starting angle of the trajectory. These equations can be solved simultaneously to determine the distance traveled by the fragment. In the Figure 28 are shown a summary of the different results of R interval for the respective fragments. In addition it should be noted that for the use of Figure 28 is not required the initial value of the angle of the trajectory.

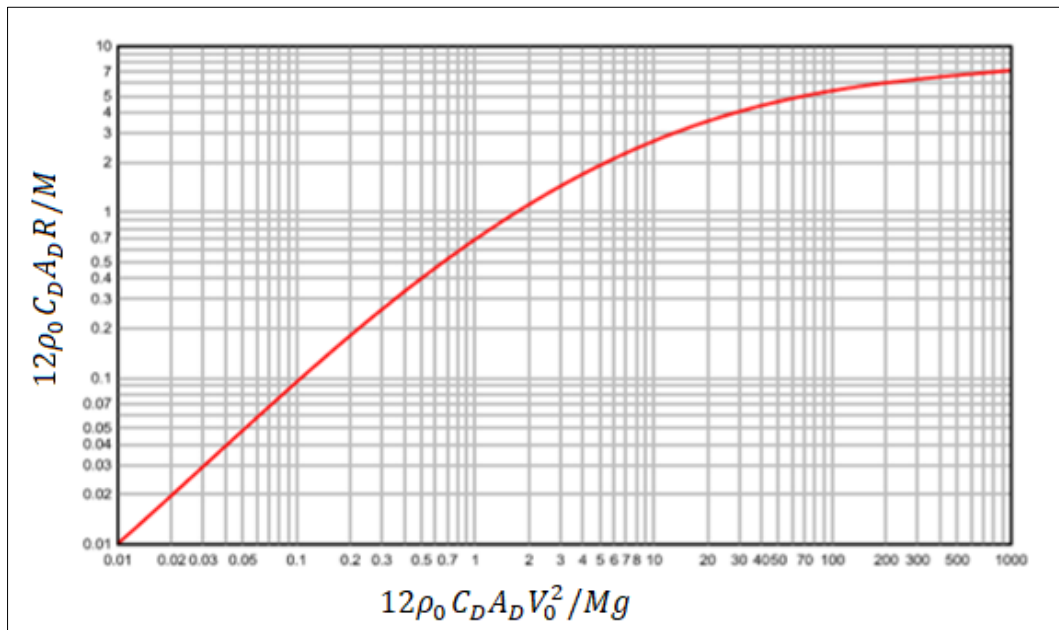


Figure 28. Fragment range prediction

## 2-Project PICAEX

In recent years, the terrorist attacks have increasingly increased, affecting above all the Europe. We can remember some episodes of recent years, for example in 2006 in the covered parking lot of the Terminal 4 of the Madrid airport of Barajas, where a car bomb destroys four floors of the airport parking structure, killing 2 people and injuring many. Or we can remember the attack on the May 22, 2017 in Manchester (Great Britain) where a bomb explodes at the end of the concert of the pop star beloved by teen Ariana Grande inside the Manchester Arena concert hall. The Isis claims the attack, causing the death of at least 22 people and injuring about 120. We can see in Figure 29 the structural effects and the discomfort and fear of the people present at the time of the attack.



*Figure 29. Effects of the terrorist attacks mentioned. On the left, the 2006 attack in Madrid and on the right in 2017 in Manchester*

Because of these numerous attacks, the number of security checks in airports, stations, places of major events and public places increased, trying to limit unpleasant events. Even with security checks, terrorists are increasingly looking for ways to overcome these controls by hiding explosive materials in objects or substances that can overcome vigilance without problems.

We want to underline that the explosion of a bomb can cause damage to the structures and in worse conditions the collapse. These damages can cause injuries and deaths due to the fall of foundation, pillars and walls but also

by the fragmentation of the walls which, due to the effect of the shock wave, are transformed into small projectiles that threaten human life.

Just as mentioned in the introduction, the protection of the critical infrastructures must be one of the priority actions in a security manner and a product is sought to reduce the vulnerability of the structures as it is carried out in the PICAEX project, acronym of *Protección de Infraestructuras Críticas frente a Explosiones*. For the realization of the project was generated by the consortium of three companies: *Tapusa*, *Fechor* and *Mapei*, each of which has a specific role within the project. The addition to the project of the *Explosive Group of Departamento de Ingeniería Geológica and Minera de la Escuela Técnica Superior de Ingenieros de Minas y Energía*, of the UPM allowed the characterization of the explosive charge that represented the IED really used in the terrorist attacks and the analysis and management of the field test.

This project is a work plan lasting about a year. Precisely for this reason it is divided into two phases. The first phase is based on the analysis of the available data, the search for similar experiences and the design of the data obtained from the elements that will constitute the test, and the second phase which mainly focuses on the field tests and the analysis of the results of the tests.

## 2.1 - Geographical framework

The construction of the samples, ie the walls being studied, and the tests that make up the project take place within the *La Marañosa Technical Institute*, a body of investigation, technological development and innovation (I+D+i), in the field of Defense and Security in the military and civil sectors. This technical plant is located in the community of Madrid in San Martín de la Vega, 14 km from the center of the capital. The institute consists of eleven buildings spread over 44,000 square meters of land. There are seven specialized areas with a total of 138 laboratories and a staff of 800 civilian and military workers and investigators. Here in the previous image, taken from Google maps (Figure 30) we can observe the technical institute La Marañosa through a top view.

The objective of the La Marañosa technical institute is to promote the technological capabilities of interest for the defense of dual use (civil and military) also by working closely with other national centers and companies

on research and development projects that strengthen the capacity of innovation.



Figure 30. Top view of the La Marañosa Technological Institute, located south-west of Madrid

The test takes place in an area of the Marañosa called *barranco del toro* [Figure 31] where there is a concrete slab on the ground (5m X 5m in size) in which it performs the basic task of the test.

Before the tests, the area will be cleaned from each material obtaining the base plate without any obstacle material so as to allow the assembly of the auxiliary walls and load support structures and an analysis of the fragments accurate and easy to carry out.



*Figure 31. Service area for tests, barranco del toro*

Instead, for the manufacture of the walls, ie the constituent specimens tests, we have chosen an establishment, always inside the field La Marañososa. This structure is a prefabricated disused, only 200 m from the barranco de toro (place where the test will take place) and is constituted by access roads not too steep, easily passable by heavy means of transport. As can be seen from Figure 32, the plant is characterized by a large internal space, sufficient for the construction of the 16 walls, and by numerous access doors along one side of the building (Figure 33).



*Figure 32. Internal view of the prefabricated building*



*Figure 33. External view of the prefabricated building on the side of the entry ways*

These access routes consist of a height of 2.75 m, but there are two different widths, some doors are about 4m others of about 3 m. This structure is not supplied by the current and the running water, for this reason the supply must be through a current generator and a water storage tank.

The use of this structure for the prefabrication of the test walls is an excellent solution because in this way it avoids the problem of unfavorable weather conditions that can negatively affect the execution of the test. Furthermore, by adopting this solution, it is possible to lengthen the curing times of the products supplied by Mapei.

## **2.2 – Test procedures**

The tests characterizing the PICAEX project are carried out in the area of the La Marañososa away from downtown Madrid about 14 km as explicated in the previous section.

For the realization of the work plan it is proposed the realization of four tests which is characterized by four walls and an explosive.

In the different tests the same charge is always used [as for example in the López L.M., 2015] and it is positioned at a distance of 5 m and at a height of 1m from the ground.

In the test field the walls will be anchored to fixed metal auxiliary structures in the place. Once the test and the analyzes have been completed, the wall

will be demolished and removed leaving the metal structures in place which will be reused as supports for the walls of the subsequent tests.

The test walls are made inside a prefabricated building located in La Marañososa. Each single test is characterized by four walls which three of them are reinforced by products supplied by Mapei with the purpose of evaluating also the best type of additives that can be placed for the protection of the critical structures. The fourth wall without reinforcement plays a very important role, they are considered as the control wall, that is the wall which reference is made for the comparison of the four distinct tests

First, we hypothesized six different reinforcement options, provided by the Mapei which differ from each other from the product used, from the location of the aforesaid reinforcement and from the type of material of which the wall in question is constituted. Later we can see (in Table 2) the nomenclature of the different elements that will constitute the wall and (in Table 3) the different combinations and options that are evaluated for the project. In addition to the reinforcements applied to the walls under examination, for each option an interior wall plaster coating is applied in order to analyze the fragmentation caused by the explosion, which we will deal with more accurately in the following sections.

After the initial analyzes carried out by the concurrent companies, option five was chosen as the best combination of materials (as seen in red in the Table 3) to be used in the four tests.

The Figure 34 shows a technical diagram of how the elements constituting the test are arranged. For each test the four walls are organized at a distance of 5 m from the charge which is raised from the ground, so as to consider that the wall is subjected to a uniform pressure.

Table 2. The nomenclature of the products that will constitute the test wall

Wall nomenclature		MAPEI product		Location reinforcement		Type of material	
Control wall	C O	Product A	A	Exteriore	E	Brick	L
Solution 1	S1	Product B	B	Inside	I	Concrete block	H
Solution 2	S2	Product C	C	Both faces	T		
Solution 3	S3						

Project PICAEX

Table 3. The different combinations that are considered as possible choices

Option 1		Option 2		Option 3		Option 4		<b>Option 5</b>		Option 6	
T 1	CO - L	T 1	CO-H	T 1	CO-L	T 1	CO-L	T 1	<b>CO-L</b>	T 1	CO-H
T 1	S1-A-E- L	T 1	S1-A-E- H	T 1	S1-A-E- L	T 1	S1-A-I- L	T 1	<b>S1-A-E- L</b>	T 1	S1-A-E- L
T 1	S2-A-I- L	T 1	S2-A-I-H	T 1	S2-B-E- L	T 1	S2-B-I- L	T 1	<b>S2-B-E- L</b>	T 1	S2-B-E- L
T 1	S3-A-T- L	T 1	S3-A-T- H	T 1	S3-C-E- L	T 1	S3-C-I- L	T 1	<b>S3-C-E- L</b>	T 1	S3-C-E- H
T 2	CO - L	T 2	CO-H	T 2	CO-H	T 2	CO-H	T 2	<b>CO - L</b>	T 2	CO-H
T 2	S1-B-E- L	T 2	S1-B-E- H	T 2	S1-A-E- H	T 2	S1-A-I- H	T 2	<b>S1-A-I- L</b>	T 2	S1-A-I- H
T 2	S2-B-I- L	T 2	S2-B-I-H	T 2	S2-B-E- H	T 2	S2-B-I- L	T 2	<b>S2-B-I- L</b>	T 2	S2-B-I- H
T 2	S3-BT-L	T 2	S3-B-T- H	T 2	S3-C-E- H	T 2	S3-C-I- L	T 2	<b>S3-C-E- L</b>	T 2	S3-C-I- H
T 3	CO - L	T 3	CO-H	T 3	CO - L	T 3	CO - L	T 3	<b>CO - L</b>	T 3	CO-H
T 3	S1-A-E- L	T 3	S1-A-E- H	T 3	S1-A-E- L	T 3	S1-A-I- L	T 3	<b>S1-A-E- L</b>	T 3	S1-A-E- H
T 3	S2-A-I- L	T 3	S2-A-I-H	T 3	S2-B-E- L	T 3	S2-B-I- L	T 3	<b>S2-B-E- L</b>	T 3	S2-B-E- H
T 3	S3-A-T- L	T 3	S3-A-T- H	T 3	S3-C-E- L	T 3	S3-C-I- L	T 3	<b>S3-C-E- L</b>	T 3	S3-C-E- H
T 4	CO-L	T 4	CO-H	T 4	CO-H	T 4	CO-H	T 4	<b>CO-L</b>	T 4	CO-H
T 4	S1-B-E- L	T 4	S1-B-E- H	T 4	S1-A-E- H	T 4	S1-A-I- H	T 4	<b>S1-A-I- L</b>	T 4	S1-A-I- H
T 4	S2-B-I- L	T 4	S2-B-I-H	T 4	S2-B-E- H	T 4	S2-B-I- H	T 4	<b>S2-B-I- L</b>	T 4	S2-B-I- H
T 4	S3-B-T- L	T 4	S3-B-T- H	T 4	S3-C-E- H	T 4	S3-C-I- H	T 4	<b>S3-C-I- L</b>	T 4	S3-C-I- H

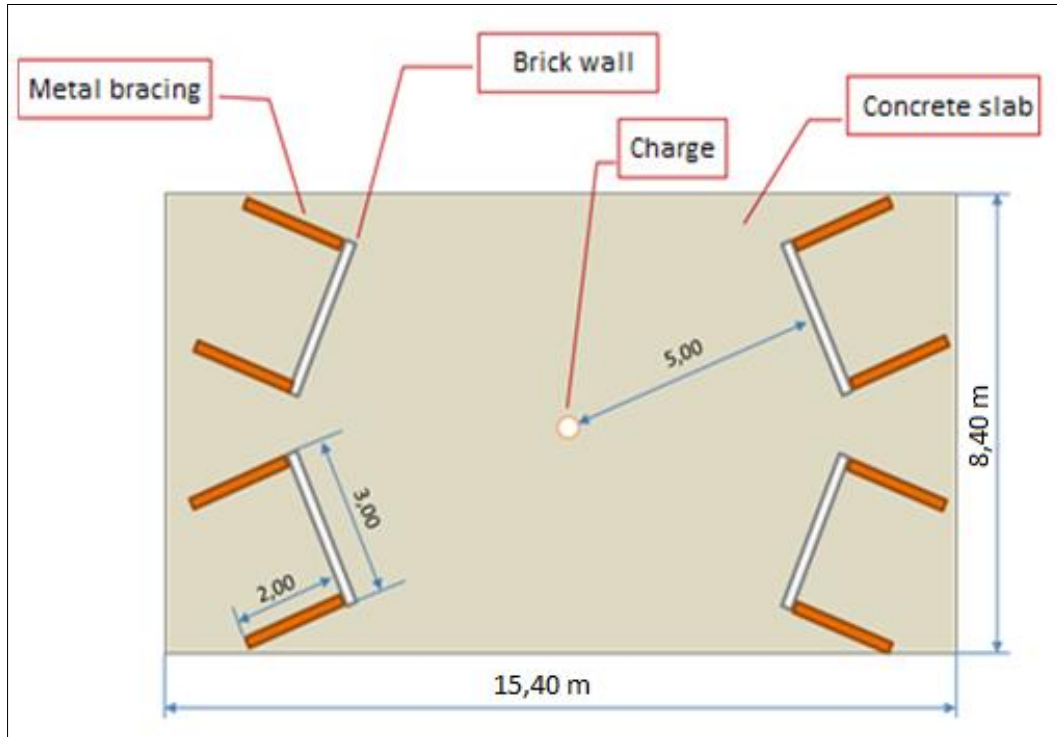


Figure 34. The technical diagram of the test's realization

At the end of each single test, the analysis will be made of how the wave invests the specimens and how the walls react to the stress induced by the bursting of the charge. The analyzes that will be carried out will be implemented through an advanced finite element calculation code of general application specifically developed for the resolution of complex nonlinear dynamic problems typical of real phenomena called LS-DYNA. This software is characterized by a wide range of possibilities of use, allowing the simulation of complex problems, characterized by large deformations and is widely accepted as the main analysis software for the most advanced engineering applications.

## 2.3 – Masonry test wall

As previously mentioned, the walls that are needed for the project are sixteen (four for each test). Each wall is mades in the same way and in the same week in a prefabricated area inside the La Marañosá field.

All the walls that characterize the project tests are made of masonry (an example of a test wall is shown in Figure 35). The bricks constituting the walls are brick elements for masonry that are laid on a layer of mortar with vertical holes. Each brick used in the project is characterized by dimensions

equal to 237x107x68 mm and requirements comply with the European Standard UNE-EN 771-1: 2011. The specific properties that distinguish these elements for buildings are shown in Attachment A which is present at the end of the discussion.

The bricks are held together by a Portland Composite Cement (EN 197-1CEM II/B-M (V-L) 32.5 N) which shows the most important features in Table 4.

Table 4. Table 4. General characteristics of the Portland Cement

Essential characteristics	Compliance with the provision	Technical specifications
Common cements: components and composition	CEM II/B-M (V-L)	EN 197-1:2011
Compression resistance (initial and nominal)	32,5 N	
Setting time	Complies	
Volume stability: Expansion	Complies	
Content of SO <sub>3</sub>	Complies	
Content of Cl <sup>-</sup>	Complies	

The walls of the project are characterized by 2.5 m in height and width and 0.24 m in thickness. Each wall reaches a weight of about 27 KN which equates to 2.7 tons assuming a specific weight of the mortar of about 18 KN/m<sup>3</sup>.

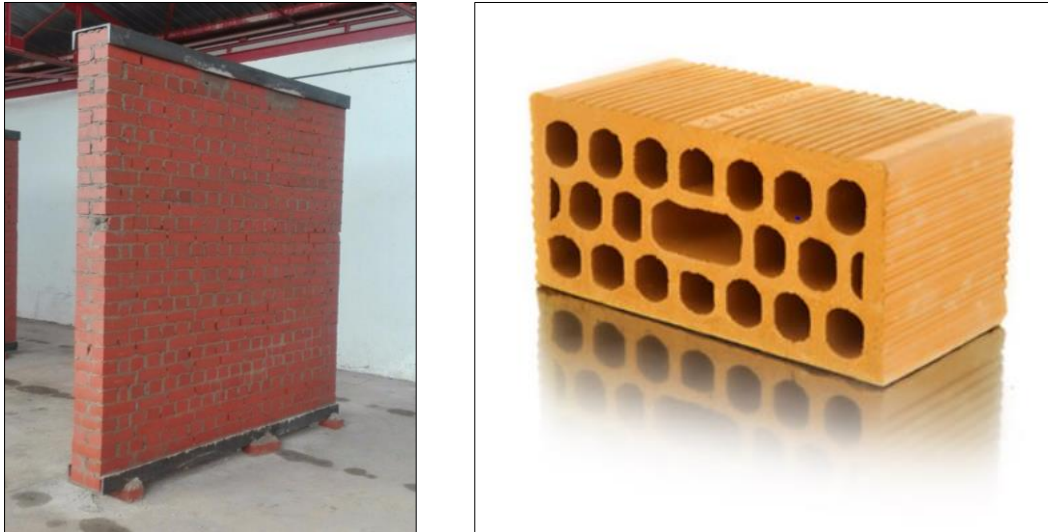


Figure 35. On the left one of the walls used in the project and on the right a brick brickwork for masonry

At the lower and upper ends of the masonry wall are positioned U-shaped steel profiles called UPE. The UPE 300 have been chosen as profiles to be used in the project in which the dimension values are shown in Table 5. In general, these steel sections are used in constructions but in this case they act as protective elements of the masonry when installing the wall in the auxiliary structures that allow the wall to be held steady for the duration of the test and during transport. To facilitate the transfer of the walls from the building to the site where the test will take place, steel plates are welded to the UPE profiles present in the ends of the walls. For each wall there are four steel plates each of which is characterized by the dimensions of 2500X200X15 mm. In each slab there is a hook that allows you to attach to the ropes of the crane.

Table 5. Characteristics of the UPE 300

UPE 300	Normal dimension					Cross section (A)	1m Nominal weight (G)
	h	b	s	t	R		
	mm	mm	mm	mm	mm	cm <sup>2</sup>	kg/m
	300	100	9.5	15.0	15	56.6	44.4
Size of details					Surface		
	h1	d	φ	e <sub>min</sub>	e <sub>max</sub>	AL	AG
	mm	mm	-	mm	mm	m <sup>2</sup> /m	m <sup>2</sup> /m
	270	240	M27	50	55	0.968	21.78

This system allows the wall to be moved from the seat where it was manufactured to the truck that will transport it to the test site and subsequently be mounted on the auxiliary structure without much difficulty. Next (in Figure 36) shows a diagram created using AutoCad software that explains the dimensions of the wall, of its components and of the steel plates welded to the UPM.



Figure 36. Metal elements and dimensions characterizing the wall

### 2.3.1 - Support structure

As previously described, each test is characterized by four masonry walls and each of them will be mounted on a support structure before the test takes place. The supporting structures are steel elements that are attached to the concrete slab, which forms the basis of the field in which the test will take place. These steel elements are joined to the walls when they are already fixed to the ground. When the walls are mounted in the supporting metal structures, the four plates welded to the UPE profiles, used to facilitate movement, are removed leaving the face of the wall free from any constraint. Once the test and the analyzes have been completed, the wall which is integral with the auxiliary structure will be demolished without replacing the steel structure which will then be used throughout the project.

Following are reported in the Table 6 the dimensions and the number of all the elements constituting the support structure, with the respective weight and type of material and the number of the different components.

Table 6. Characteristics of the element that constitutes the support structure of the wall

Element	Number	Weight	Materials
<b>Metal-Steel-275 Mpa</b>			
Stiffener 10mm	96	21.79 kg	Metal - Steel- 275 Mpa
Stiffener 15mm	144	538.70 KG	Metal - Steel- 275 Mpa
Plate 25mm	32	94.20 KG	Metal - Steel- 275 Mpa
HEB200	16	2290.08 kg	Metal - Steel- 275 Mpa
HEB300	12	3301.89 kg	Metal - Steel- 275 Mpa
UPE80	32	127.60 kg	Metal - Steel- 275 Mpa
<b>Steel Rebar - B500C</b>			
Anchorage fi 25mm	32	108.74 kg	Steel Rebar - B500C
Anchorage fi 32mm	16	50.66 kg	Steel Rebar - B500C

In the Figure 37 you can see how the test wall is assembled with the steel auxiliary structure [Wang Junguo, 2016].

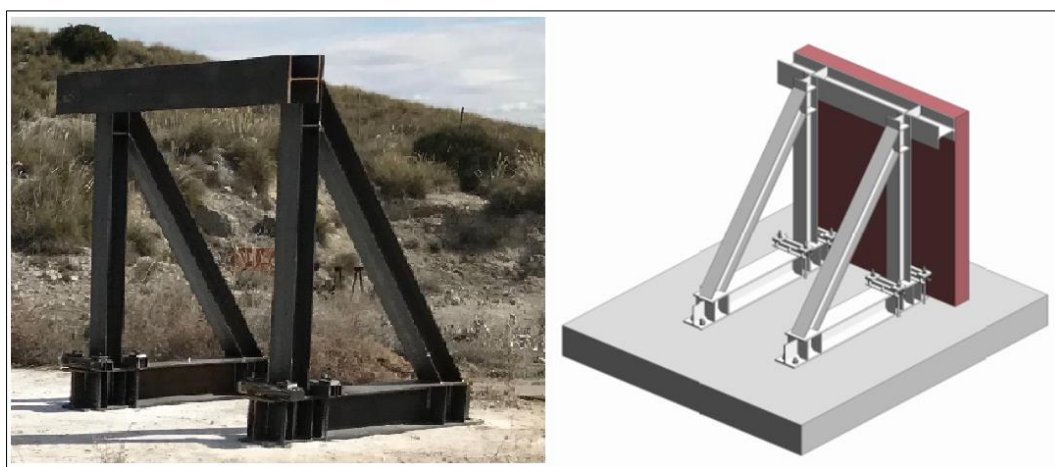


Figure 37. Mounting the wall on the support structure

### 2.3.2 – Method of transport

As explained previously, the place of manufacture and the test field are both located within the field of research and development The Marañosa at a distance of approximately 200 m from each other.

The choice of the appropriate transport methodology for the test walls is very difficult. Consider that the test walls were built inside a building

(Figure 33) to avoid that the samples are subject to climatic events which alter the characteristics of the material. The manufacturing building is characterized by wide access routes only on one side of the building. These access routes consist of doors with a width of about 3 m and some of about 4m but all with a height of about 2.8 m. This is a first problem encountered for the transport of walls because the masonry elements are characterized by a height of 2.5 m so there is only 0.30 m of difference between the two heights. Furthermore, the wall can not be transported by rotating it 90 degrees in that this element is a masonry wall and there is no need to generate torsional stresses on it and damage the construction before the test. To cope with problems of volume and fragility of the wall, it was decided to move the wall vertically above a forklift that allows it to be lifted. The forklift is a vehicle equipped with wheels driven by electric motors, diesel and gas, which is used for lifting and moving goods from logistics depots or for loading and unloading goods from transport means as in our case.

In order not to drop the structure and at the same time transport it vertically, it was decided to insert a polyester plate over the forklift at the point of contact of the wall and of the metal structure of the vehicle. The polyester is an aromatic thermoplastic polymer with a linear structure that at room temperature is a glassy solid but, above the glass transition temperature (about 100°C), acquires plasticity and is able to flow, it starts to decompose up to a temperature of 270°C. The expanded polystyrene comes in the form of light white foam thickened in the form of heel and used as packaging and as an insulator. In our case, the layer of polystyrene allows the wall not to be damaged in transport in contact with the metal structure of the forklift.

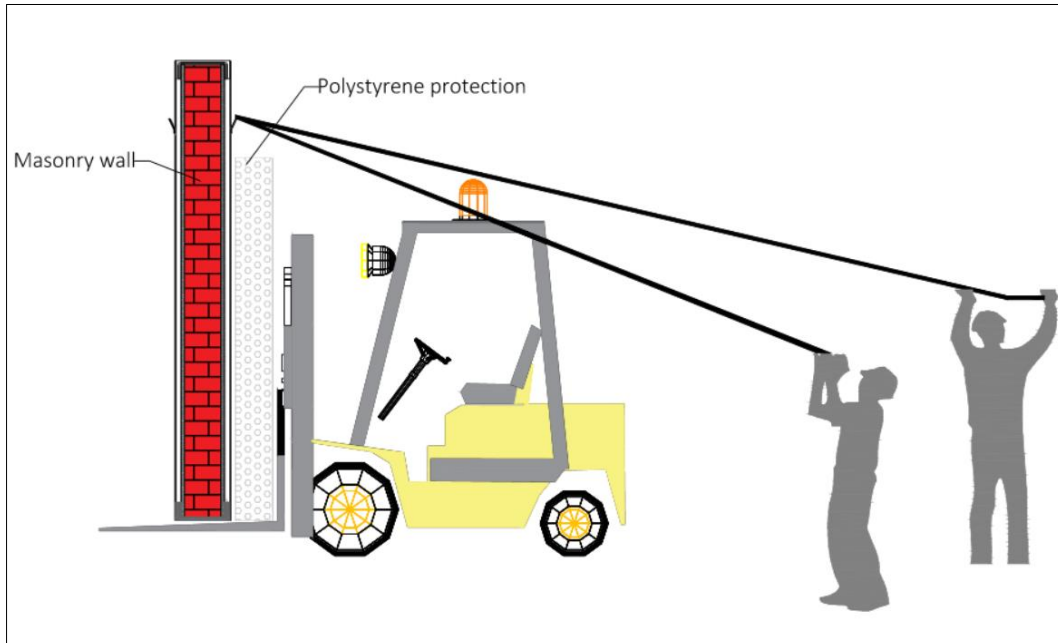


Figure 38. Transportation of the wall from the building to the truck

Moreover, to ensure that the wall in the transport does not fall backwards, it has been thought to hook the rope to the hooks welded to the steel plates of the wall and during the entire maneuvers two operators will have the task of keeping the ropes taut to keep the wall supported to the polystyrene layer. In Figure 38 it is possible to understand more clearly the transport phase by means of a forklift truck.

Once the first obstacle has been overcome, the wall outside the building must be transported to the test site by a truck. The path to be covered by the truck is about 200 m and is a very winding dirt road with steep slopes. Precisely for this reason, the walls will be loaded on the crane truck using the forklift and will be surrounded by sandbags to eliminate the probability of damage during transport. At the extreme ends of the wall there will be two larger sacks of about 1 m<sup>2</sup> and along the long sides of sandbags smaller than 20-25 kg tall up to 1 meter in height, as can be seen in Figure 39. Subsequently through this crane truck the wall is lifted by means of the ends attached and mounted in the fixed auxiliary structure to the concrete pavement which plays the basic role of the test field.

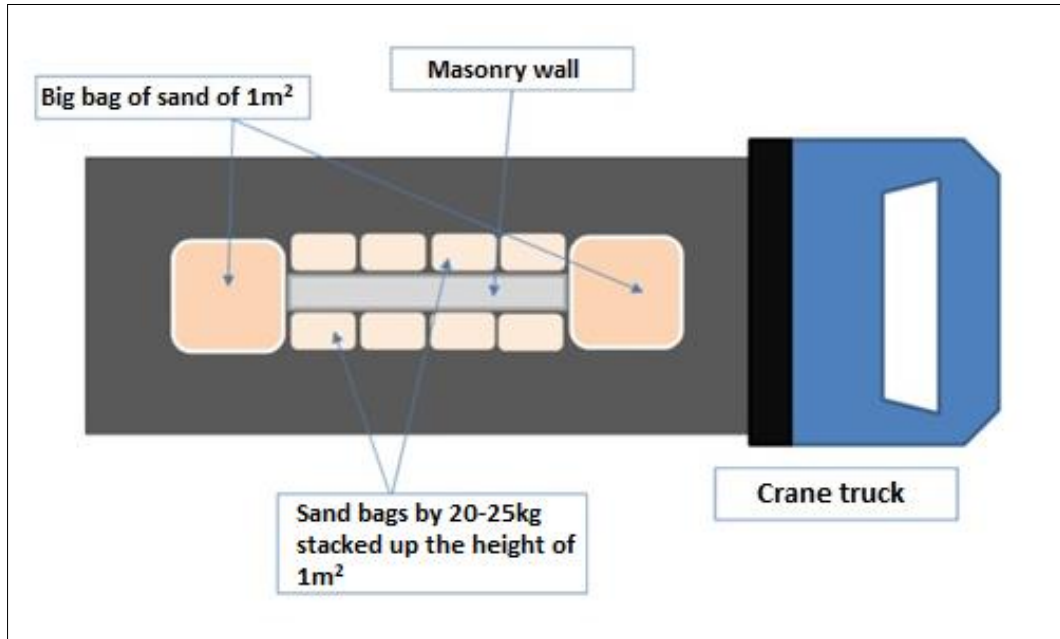


Figure 39. Arrangement of the wall inside the transport truck

### 2.3.3 – Reinforcement additives

As mentioned earlier in every single test there is a control wall, without reinforcement that serves for the comparison between a test and the other, and the three remaining walls are characterized by a reinforcing layer

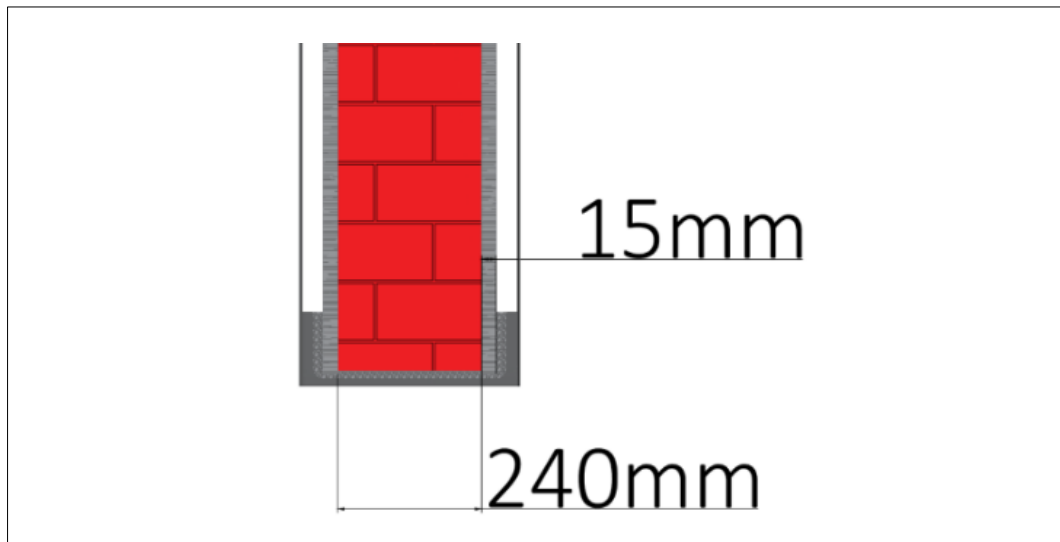


Figure 40. Reinforcement applied to the masonry wall

consisting of the combination of three products supplied by the company MAPEI (Table 3). Reinforcement is a substance that is placed on a façade or

both, depending on the combination chosen, with a thickness of 15 mm (Figure 40).

The following compounds were selected as reinforcing products:

### 1. PLANITOP INTONACO ARMATO

The Planitop Intonaco Armato [Mapei, web] is a two-component, premixed fiber-reinforced mortar with high ductility based on natural hydraulic lime (NHL) and Eco-Pozzolana, natural sands, special additives and synthetic polymers in water dispersion according to a formula developed in the MAPEI research. This product is an applicator in different fields, it is particularly suitable for the repopulation of irregularity of stone, brick and tuff surfaces and reinforcements of elements, vaults and masonry. It has a high adhesion value thanks to the presence of synthetic resins in water dispersion and subsequently hardening results in a compact layer, tough and impermeable to water and aggressive gases present in the atmosphere. The product has been classified by the European technical standards EN 998-2 as mortar type M15 and according to the EN 998-1 standard as plaster of type GP category CS IV because it is characterized by a mechanical resistance to compression greater than 15 N/mm<sup>2</sup> (in Table 7).

Table 7. Characteristics of the Planitop Intonaco Armato

Material characteristics	
Density of the mixture (UNI EN 1015-6) (kg/m <sup>3</sup> )	1.900
Application thickness (mm)	3-10mm
Application temperature allowed	from +5°C to +35°C
Duration of the mixture	1h
Compressive strength 28 days (UNI EN 1015-11) (N/mm <sup>2</sup> )	>15
Initial shear strength (N/mm <sup>2</sup> )	0,15
Elastic compression module (UNI EN 13412) (GPa)	8
Adhesion to the masonry support 28 days (UNI EN 1015-12) (N/mm <sup>2</sup> )	≥0,8

The preparation of the product depends on the type of application chosen. In our case where the surface and application is small, a manual application will be used, whereby the preparation of the material will take place by means of an agitator or a glass mixer. The application of Planitop Intonaco Armato takes place using a flat metal spatula with a uniform layer of 7-8 mm per coat. There are some limitations on the use of the product. In fact it

can not be applied with temperatures below + 5°C and does not maintain the same characteristics if additives or aggregates are added. The Figure 41 shows one of the walls covered with Planitop Intonaco Armato.



Figure 41. Example of the Planitop Intonaco Armato of the Mapei in the test walls

## 2. MAPEGRID C170 with MAPEWRAP 31T

The second product supplied is a combination of a Mapegrid C170 recycled grid impregnated with Mapewrap 31T semi-fluid epoxy adhesive.

The Mapegrid C170 (shown in Figure 42) brings significant advantages when used in structures of historical or artistic interest. Instead of replacing the existing structure with another, this type of system offers the possibility of improving the mechanical characteristics and overall ductility without altering the way in which the masses and the rigidity inside the structures are distributed.



Figure 42. Example of the Mapegrid C170 with the Mapewrap 31T in the test walls

The latter is a very important aspect also in the field of anti-seismic design because it allows a more uniform distribution of the stresses of the phenomenon.

This system is a special fabric characterized by a square mesh made of high-strength carbon fibers. Its structure allows to increase the tensile strength and increases their general ductility, so that stress is distributed in a more uniform way, of the work to be reinforced. If Mapegrid C170 is used for greater strength of walls and masonry vaulted elements, it is necessary to remove all the deteriorated or detached part up to a solid and solid substrate, so that the reinforcement packet does not come off [Mapei, web]. We recommend water-repellent surfaces with low-pressure water jets. Allow the surface water to evaporate so that the masonry is saturated and the surface is dry.

After applying the first layer of mortar, place Mapegrid C170 and press so that it adheres well. Impregnate the mesh with the component B of the mortar so that it touches better in the mortar. Overlap adjacent pieces of

Mapegrid C 170 of at least 15 cm in both length and width. Next, apply another layer of uniform mortar.

The Mapewrap 31T is used for the impregnation of Mapei fabrics used to reinforce concrete or masonry elements. This product is an adhesive solvent-free epoxy resin with a thixotropic consistency that has been specifically developed in the research and development of Mapei. The MapeWrap 31 T consists of two pre-dosed components, component A which is a resin and component B which is a catalyst. They must be mixed together before use. After mixing the product it remains workable for about 50 minutes at + 23°C, but once hardened it becomes very strong and has excellent dielectric properties.

### **3. MAPEWRAP EQ ADHESIVE with MAPEWRAP EQ NET**

The third product is the combination of a MapeWrap EQ Net, the glass fibre reinforcement used in combination with MapeWrap EQ Adhesive.

MapeWrap EQ Net (as can be seen in the Figure 43) is a reinforcing fabric, characterized by glass fibers with a special surface treatment based on polyurethane. This type of reinforcement allows to uniformly distribute the stress applied to the wall. This system can be used in solid and compact materials.

The MapeWrap EQ Adhesive is applied in the clean and dry wall. The adhesive is applied by means of a short-haired roller. Subsequently, the MapeWrap EQ reinforcement mesh is placed on the adhesive and another layer of MapeWrap EQ Adesivo is extended and, by means of a metal roller, the adhesive adheres well to the fibers of the fabric. In addition we have to pass the MapeWrap Roller over the adhesive to eliminate the air bubbles trapped in the fabric. The most suitable application for the adhesive takes place at a temperature between +5°C and +30°C. In the case where the temperature is lower than +5°C, the substrate must be strengthened by means of an insulating system to avoid the risk of freezing.

For more information on the technical characteristics provided by the product, the Attachments B1-2-3 are available at the bottom of the report, which show all the tables relating to the characteristics of each single product treated.



*Figure 43. Example of the MapeWrap EQ Net with the MapeWrap EQ Adhesive in the test walls*

## **2.4 – Characterization of the explosive charge**

In this section we will analyze all the procedures made for the realization of the charge used in the PICAEX project.

First off, we must consider that the explosive charge chosen is raised from the ground because if positioned on the ground, a crater is generated and part of the energy is transmitted to the ground. This part of energy is transformed into seismic waves that propagate in the ground at high speeds

causing an oscillation of the ground itself in which the intensity depends on the quantity of explosive used and the characteristics of the soil itself. These vibrations as a real seismic event can go to generate damage to the structures. Moreover, in this case the amplitude of the vibrations would depend on the transmissivity of the ground, the degree of confinement of the charge and the distance of the charge from the point of interest. In our project we only want to consider the effects of explosives that considers the arrival of the incident wave on the wall as mentioned in numerous articles that have been consulted, as in the treatment of Wang J. [2016] and that of Alsayed SH [2016].

### **2.4.1 - Definition of the scaled distance**

The concept of reduced distance as mentioned in the first section is introduced to identify the distance from the explosion center at which two explosive charges, with the same specific energy of explosion but with different weight, generate the same effect in terms of pressure. As previously stated in the first chapter, the formula for determining the scaled distance is determined using Formula 9 in the first chapter.

In order to define the most suitable scaled distance for the project experiment, a first phase of research was carried out of pre-existing articles with experiments similar to the one to be carried out in the PICAEX project. This factor has been used previously in many research experiments, such as in the López LM [of 2015] discussion where the charge was placed at a distance scaled from the test walls of  $2.9 \text{ m/kg}^{1/3}$  and raised from the soil just as in our treatment, however, using a charge of 5 kg of TNT equivalent. In addition we went to study the results reported by other authors in case the walls or structures in question are always made of masonry. For example, in the discussion of Junguo Wang [of 2016], six tests were done on clay brick masonry walls and ventilated cement walls, in which three of them were reinforced by polyurea coat. The polyurea coating can occur partially that is only in the front part of the wall or a total reinforcement in which it is both on the front face and on the back face of the wall.

The general characteristics of the Juenuo Wang experiment are shown in Table 8, which shows the type of reinforcement (Type of R), the thickness of the polyurea (R), the distance (d) of the charge with respect to the test wall, the weight (Weq) in kg of TNT equivalent, the distance scaled (z), the height of the charge (h), pressure at the center of the wall (P1) and finally the

results obtained from the tests (Result) in which the symbology of the effects produced by the explosion are shown in Table 9.

Table 8. Characteristics of the tests performed by Junguo Wang, 2016

Test	Type of R	R	d	Weq	z	h	P <sub>1</sub>	Result
-	-	mm	m	kg	m/kg <sup>1/3</sup>	m	MPa	-
1	clay brick unreinforced	0	1	2	0,79	1,4	10,5	A
2	clay brick reinforced partially	3	1	5	0,58	1,4	36,3	B
3	clay brick reinforced fully	3	1	8	0,5	1,4	54,7	C
4	clay brick reinforced fully	3	1	20	0,37	1,4	155	A
5	Aerated brick wall unreinforced	0	10	5	5,85	1,4	0,05	C
6	Aerated brick wall reinforced fully	3	3	5	1,75	1,4	0,82	D

Table 9. Results of the effects produced by the explosion of the charge to the structures under examination

Type of damage in the wall	
A	Total collapse of the masonry wall
B	Medium damage (irreparable damage in which the maximum dislocations of the masonry wall occur)
C	Medium damage (presence of cracks in the masonry wall)
D	No damage (presence of spherical chipping of the mortar coating)

From Table 8 we see that in this article two distinct types of walls were treated, one with clay bricks and the other with airborne bricks. The analyzes made focus on the first type of wall because they are more similar to the project carried forward in the treatment. From the results obtained by Junguo Wang it is observed that in the first four tests carried out there are two cases of collapse, ie the wall has not resisted the force of the shock wave and was totally damaged and the second and third tests were intermediate damage, that is the wall following the explosion has reported damage with the formation of cracks and deflection of the reinforcement without reaching collapse.

We note that for each test the weight in kg of equivalent TNT is changed and the distance scaled giving results and for this reason they can not be compared to each other because they have different basic characteristics. Implementing the data present in the article on Matlab, it was possible to

determine the pressure-distance curve (Figure 43) obtained from the data reported by Junguo Wang. It is observed in the graph the distinct points are of different color, this to distinguish the characteristics and the behavior of the different walls. It is emphasized that tests 1 to 4 are made using clay brick walls, while the remaining ones are aereated brick walls. The graph also distinguishes the unreinforced walls marked with the empty symbol and reinforced marked with the filled symbol.

The field of our interest is the intermediate damage. This is because in the case of collapse or no damage to the structure it is not possible to analyze any type of behavior of the characteristics of the material in question. Precisely because we want to define the behavior of the structures, that is the wall characterized by different types of reinforcement, subject to a pressure wave generated by an IED explosive (*Improvised Explosive Device*).

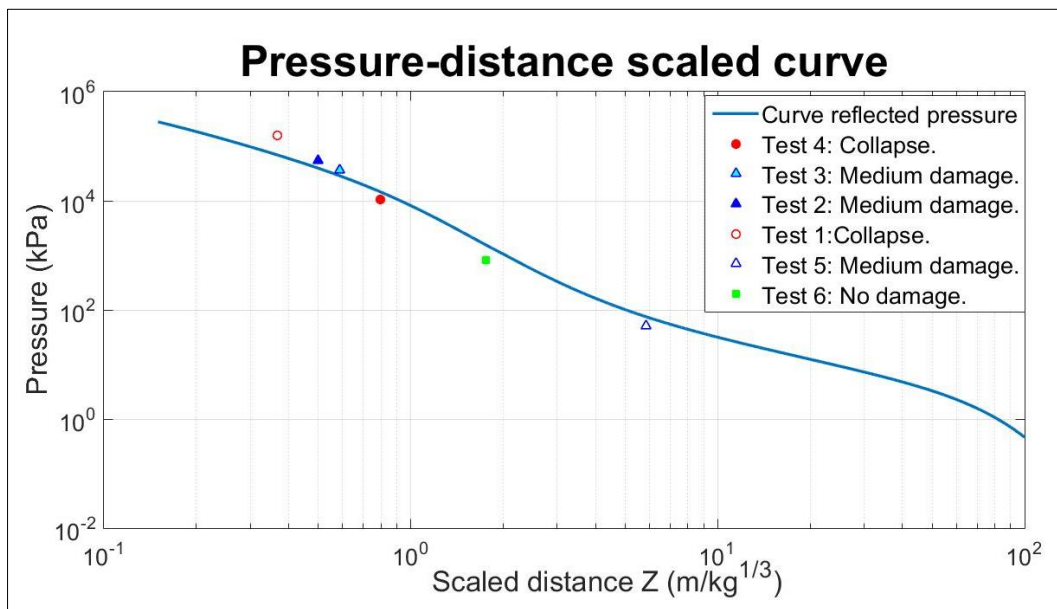


Figure 43. Pressure-distance scaled curve of Junguo Wang data

In this case, considering the clay brick in intermediate damage conditions it can be seen from Table 8 that the tests of our interest are number three and two. In these two cases the walls are characterized by the partial and total presence of the reinforcement, but by a very small scaled distance of 0.58  $m/kg^{1/3}$  and 0.50  $m/kg^{1/3}$ . The scaled distances present are too small to be considered comparable for our project because we want to study a case in which the distance of the charge from a structure is generally more representative of reality and also consider a distance that allows to study the incident pressure at the wall.

For example, references were made to the Xueying Wei [2010] experiment. In this case we studied the effect of explosives placed at a height (h) from the ground equal to 1.5 m and with a charge in kg equivalent of TNT (W) and a scaled distance (z) both variable. We take 17 walls as specimens characterized by two different types of thickness, from 230 mm or from 355 mm. As can be seen in Table 10, in addition to checking the previously mentioned data, there are the results due to the explosion effect in which the same symbology in Table 9 are divided into damage levels.

This case was of greater help in determining the distance climbed than the previous one due to the fact that the wall considered was masonry as in our case, moreover the walls of the Xueying Wei article are all without reinforcement and in the PICAEX project they are present in every prava control wall without reinforcements. As previously mentioned, the cases in intermediate damage condition in which they are interesting for the project are analyzed. It is noted that the cases to be taken into account are for a thickness of 230mm with the distances climbed between  $1.44 \text{ m/kg}^{1/3}$  to  $1.91 \text{ m/kg}^{1/3}$  and the test charge varies between 21.5 kg to 59.5 kg.

We went to compare these results found with other pre-existing results, for example from the article by Ahmad S. [2014] in which they considered masonry walls without reinforcement, a distance (d) from the walls to the charge of about 3-4 m in function of the test considered. Table 11 shows all the parameters obtained by the author and the effects obtained. It is always remembered that the symbology of the results of the effect of the walls are reported in Table 9. From the values obtained from Ahmad S. the graph present in Figure 44 was also realized in which the values of the pressures were reported with respect to the distance scaled for go to see graphically the line of the incident and reflected pressure. We note quickly in the graph that in the Ahmad S. tests the intermediate damage conditions occur in a distance range between  $2.07 \text{ m/kg}^{1/3}$  and  $2.2 \text{ m/kg}^{1/3}$ .

## Project PICAEX

Table 10. Characteristics of the tests performed by Xueying Wei, 2010

Test	Type renf.	Wall thickness	d	W	z	h	Result
-	-	mm	m	kg	m/kg <sup>1/3</sup>	m	-
1	brick masonry unreinforced	230	4	21.5	1.44	1.5	C
2	brick masonry unreinforced	230	7	49.5	1.91	1.5	C
3	brick masonry unreinforced	230	6	43.2	1.71	1.5	B
4	brick masonry unreinforced	230	5,5	50.6	1.59	1.5	A
5	brick masonry unreinforced	230	5,5	51.4	1.48	1.5	A
6	brick masonry unreinforced	230	5,5	50.8	1.49	1.5	A
7	brick masonry unreinforced	355	4,5	43.2	1.28	1.5	B
8	brick masonry unreinforced	355	5	43.2	1.42	1.5	D
9	brick masonry unreinforced	355	7	22.4	2.48	1.5	D
10	brick masonry unreinforced	355	5,5	22.4	1.95	1.5	D
11	brick masonry unreinforced	355	4	23.4	1.4	1.5	C
12	brick masonry unreinforced	355	3,75	49.5	1.02	1.5	A
13	brick masonry unreinforced	355	4,5	43.2	1.28	1.5	B
14	brick masonry unreinforced	355	3,75	50.6	1.02	1.5	A
15	brick masonry unreinforced	355	6	23.3	2.1	1.5	C
16	brick masonry unreinforced	355	3,75	50.5	1.01	1.5	A
17	brick masonry unreinforced	355	3,75	49.5	1.02	1.5	A

Tabele 11. Characteristics of the tests performed by Ahmad S., 2014

Test	Type renf.	Wall thickness	d	h	W	$W_{TNT}$	z	Result
-	-	mm	m	m	kg	kg	$m/kg^{1/3}$	-
1	brick masonry unreinforced	380	3	1	4	2.4	2.24	D
2	brick masonry unreinforced	380	3.5	1	6	3.6	2.28	D
3	brick masonry unreinforced	380	3.5	1	8	4.8	2.07	C
4	brick masonry unreinforced	380	4	1	10	6	2.2	C
5	brick masonry unreinforced	380	3.5	1	12	7.2	1.81	B
6	brick masonry unreinforced	380	3.5	1	14	8.4	1.72	A

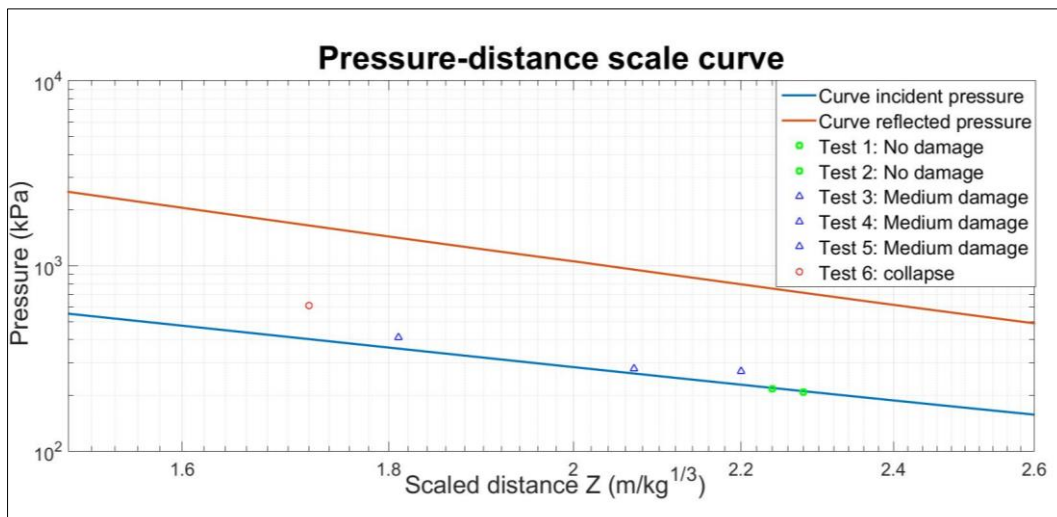


Figure 44. Pressure-distance scaled curves of Ahmad S., 2014

Furthermore, the information kept in mind includes those of Chen Li [2014] who always kept in mind a masonry wall with the characteristics shown in Table 12, generating only intermediate damage in two cases. Furthermore, taking into account the distance values of Ghaderi Masoud [2015] or, for example, the tests carried out by Alsayed Saleh H. we conclude that the distance we have to choose has a value between  $1.8 m/kg^{1/3}$  at  $2.2 m/kg^{1/3}$ . For each distance value scaled calculation at different distances the value of the charge in kg of TNT, as can be seen in Table 13.

Table 12. Characteristics of the tests performed by Chen Li, 2014

Test	Tipe ref.	Wall thickness	d	W <sub>TNT</sub>	z	Result
-	-	mm	m	kg	m/kg <sup>1/3</sup>	-
1	brick masonry unreinforced	90	5,85	0,2	10,00	D
2	brick masonry unreinforced	90	5,85	0,2	10,00	D
3	brick masonry unreinforced	90	5,85	3,9	3,72	D
4	brick masonry unreinforced	90	5,85	34,2	1,80	C
5	brick masonry unreinforced	90	5,85	21,2	2,11	B
6	brick masonry unreinforced	90	5,85	30	1,88	A

Table 13. TNT equivalent charge weight values for some of the distance values scaled in the range 1.8 m/kg<sup>1/3</sup>-2.2 m/kg<sup>1/3</sup>

d	W <sub>eq</sub> (z=1,81 m/kg <sup>1/3</sup> )	W <sub>eq</sub> (z=1,81 m/kg <sup>1/3</sup> )	W <sub>eq</sub> (z=1,91 m/kg <sup>1/3</sup> )	W <sub>eq</sub> (z=2,1 m/kg <sup>1/3</sup> )
m	kg	kg	kg	kg
3,5	8,57	7,2	6,15	4,63
3,7	10,13	8,5	7,27	5,47
3,9	11,86	10,0	8,51	6,41
4	12,8	10,8	9,19	6,91
4,1	13,78	11,6	9,89	7,44
4,3	15,90	13,4	11,41	8,59
4,5	18,22	15,4	13,08	9,84
4,7	20,76	17,5	14,90	11,21
4,9	23,52	19,8	16,88	12,70
5	24,99	21,1	17,94	13,50
5,1	26,54	22,4	19,04	14,32
5,3	29,77	25,1	21,37	16,08

In the project under examination it is established that the distance between the walls and the explosive charge is 5 m. By using the distance and the scaled distance, the weight of equivalent TNT of the charge is obtained, as shown by the formula 21. As shown in Table 14 in this project we will consider three different explosive charges of 18 kg, 22 kg and 25 kg.

$$W_{eq} = \left(\frac{d}{z}\right)^3 \quad (21)$$

Table 14. Distance values ( $d$ ), distance scaled ( $z$ ) and weight in kg of equivalent TNT ( $W$ )

<b>d</b>	<b>z</b>	<b><math>W_{eq}</math></b>
<b>m</b>	<b><math>m/kg^{1/3}</math></b>	<b>kg</b>
5	1,91	18
5	1,78	22
5	1,71	25

## 2.4.2 - Determination of the triple point

During the explosion, the wave propagates radially from the center of the charge and affects the surface of the ground before reaching the structure. The shock wave continues to propagate radially and at a certain distance interacts with the reflected wave from the ground generating the Mach face (Figure 19). It is necessary to define the triple point, as explained in the previous section, in order to simplify and consider that the wall under examination is subjected to a uniform pressure.

The project in question is characterized by masonry walls with a height of 2.5 m. For this reason we will have to find a suitable solution to obtain that the triple point has a height greater than that of the wall considering a distance of 5 m and a equivalent charge value of TNT equal to 18 kg. To do this we will have to modify the heights in which the explosive charge is located in order to keep the previously obtained distance distance unchanged.

Using the Unified Facilities Criteria (UFC, 2008) you can go to determinate the triple point height value as seen in Table 15, using the horizontal distance values scaled with respect to the weight in kg of equivalent TNT and the height values scaling of the charge that correspond to the values of the graph curves Figure 20.

Table 15. Values for calculating the height of the triple point ( $H_T$ ) by means of the value of the height scaled (Curve) and of the horizontal distance from the charge ( $R$ ) with  $W_{eq}$  equal to 18kg

<b>Curve</b>	<b>R</b>	<b><math>R/(W^{1/3})</math></b>	<b><math>H_T</math></b>
<b><math>ft/lb^{1/3}</math></b>	<b>m</b>	<b><math>m/kg^{1/3}</math></b>	<b>m</b>
0.5	5	1.91	3.9
1	5	1.91	2.85
1.5	5	1.91	1.51

In our case we obtain that for a height of one meter of charge from the ground the value of the triple point  $H_T$  is satisfactory because it is a value greater than the height of the wall. Note that as soon as you ascend with a charge height of 1.5 m the triple point value is no longer suitable and you can no longer simplify the wave as a plane wave and that the pressure acts evenly.

The same calculation also occurred considering an equivalent charge value of TNT equal to 22 kg and 25 kg as can be seen in Table 16-17.

Table 16. Values for calculating the height of the triple point ( $H_T$ ) by means of the value of the height scaled (Curve) and of the horizontal distance from the charge (R) with  $W_{eq}$  equal to 22 kg

Curva	R	$R/(W^{1/3})$	$H_T$
ft/lb <sup>1/3</sup>	m	m/kg <sup>1/3</sup>	m
0,5	5	2,32	3,5
1	5	2,32	2,60

Table 17. Values for calculating the height of the triple point ( $H_T$ ) by means of the value of the height scaled (Curve) and of the horizontal distance from the charge (R) with  $W_{eq}$  equal to 25 kg

Curva	R	$R/(W^{1/3})$	$H_T$
ft/lb <sup>1/3</sup>	m	m/kg <sup>1/3</sup>	m
0,5	5	1,91	3,41
1	5	1,91	2,08

From the values of the heights of the triple point, it is noted that maintaining the same height of charge with respect to the ground but varying the value of the equivalent weight of TNT of the charge, the values vary. Increasing the weight of the charge decreases the value of the height of the triple point at a distance of 5 m from the charge. For a charge of 25 kg equivalent TNT, a value of 2.08 m is produced, a height value of the lowest triple point at the height of the project wall. For this reason, the height of the charge and the distance of the wall with respect to the charge are not suitable for considering that the wall is subject to a uniform pressure value. On the other hand, by decreasing the charge values, it is assumed that the triple point rise values remain higher than the test wall height value. Subsequent to these analyzes, it was decided that the equivalent TNT charge in the project under study is 18 kg which allows to assume as a triple point height equal

to 2.7 m (Figure 45). For this reason the charge will be positioned at a height above the ground of 1 m.

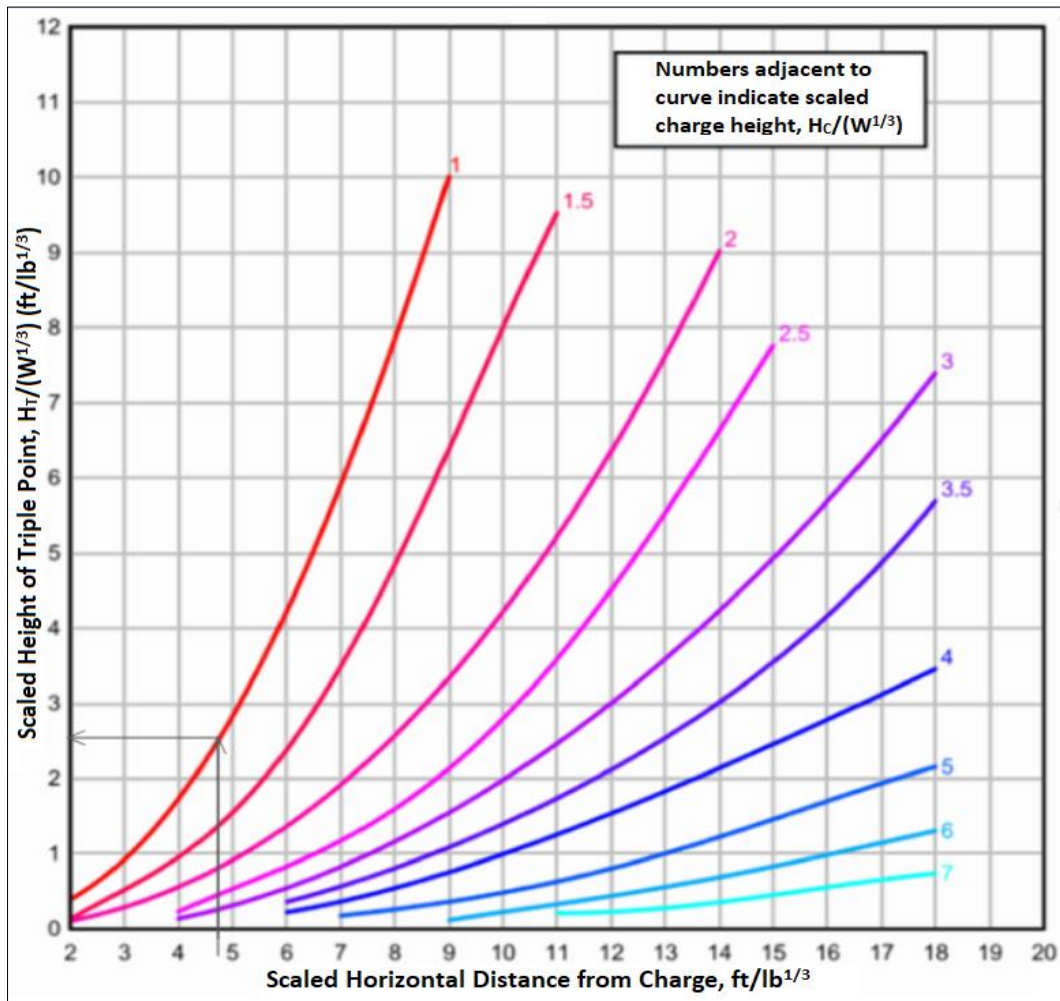


Figure 45. Characterization of the triple point height using UFC, 2008

### 2.4.3 – Parameters of shock wave

To learn more about the characteristics of the shock wave generated by the explosive charge, the Unified Facilities Criteria (UFC, 2008) was used in this project.

Using the graph in Figure 18 we can determine the values of the positive phase shock wave parameters for the explosion of hemispherical TNT on the surface of the sea level. From this graph, knowing the value of the distance scaled ( $z$ ) we can obtain the values of:

- $P_r$ , reflected pressure of first arrival;
- $P_{so}$ , first arrival peak overpressure;
- $i_r$ , reflex impulse;

- $i_r$ , impulses associated with the reflected pressure;
- $i_s$ , impulses associated with the first peak pressure incident pressure;
- $U$ , the speed of the wave;
- $t_0/W^{1/3}$ , duration of the positive phase scaled with respect to the weight of kg of equivalent TNT;
- $t_A/W^{1/3}$ , time of first arrive scaled with respect to the weight of kg of TNT equivalent.

In the case under examination with a scaled distance equal to  $1.91 \text{ m}/\text{kg}^{1/3}$ , the parameters in Table 18 are obtained. Furthermore, by means of the UFC, the two cases in which the charge is characterized by 22 kg have also been calculated. and 25 kg of TNT equivalent (Table 19-20).

Table 18. Parameters by means of the UFC related to 18 kg of equivalent TNT

$P_r$	$P_{so}$	$i_r$	$i_s$	$U$	$t_0$	$t_a$
<b>PSI</b> 175.9	<b>PSI</b> 45.9	<b>Pa s</b> 1010.30	<b>Pa s</b> 368.89	<b>m/s</b> 0.65	<b>ms</b> 5.37	<b>ms</b> 4.04
<b>KPa</b> 1213.04	<b>KPa</b> 316.5					

Tabella 19. Parametri mediante dall'UFC relativi a 22 kg di TNT equivalente

$P_r$	$P_{so}$	$i_r$	$i_s$	$U$	$t_0$	$t_a$
<b>PSI</b> 214.61	<b>PSI</b> 53.56	<b>Pa s</b> 1173.25	<b>Pa s</b> 420.71	<b>m/s</b> 0.69	<b>ms</b> 5.75	<b>ms</b> 3.83
<b>KPa</b> 1479.74	<b>KPa</b> 369.31					

Table 20. Parameters by means of the CFU for 25 kg of equivalent TNT

$P_r$	$P_{so}$	$i_r$	$i_s$	$U$	$t_0$	$t_a$
<b>PSI</b> 244.10	<b>PSI</b> 59.11	<b>Pa s</b> 1291.00	<b>Pa s</b> 475.55	<b>m/s</b> 0.71	<b>ms</b> 6.04	<b>ms</b> 3.69
<b>KPa</b> 1683.09	<b>KPa</b> 407.60					

These parameters were compared by empirical formulas in the literature such as for example for the determination of peak pressure the Henrych formulas are used [J. Henrych, 1979]:

$$p_s = \frac{14.072}{z} + \frac{5.54}{z^2} + \frac{0.0062}{z^3} \quad \text{for } 0.005 \leq z \leq 0.3 \quad (22)$$

$$p_s = \frac{6.194}{z} + \frac{0.326}{z^2} + \frac{2.132}{z^3} \quad \text{for } 0.03 \leq z \leq 1 \quad (23)$$

$$p_s = \frac{0.662}{z} + \frac{4.05}{z^2} + \frac{3.288}{z^3} \quad \text{for } 1 \leq z \leq 10 \quad (24)$$

Furthermore, the Wei and Dharani [J.R.Florek, 2007] formulas can be used:

$$p_s = p_0 \cdot \left( \frac{0.696}{z} + \frac{2.1}{z^2} + \frac{4.13}{z^3} \right) \quad (25)$$

The empirical formula for the determination of Sadovski [Gelfand Boris, 2004] peak apressioene is also widely used:

$$p_s = \frac{0.81}{z} + \frac{2.8}{z^2} + \frac{7.07}{z^3} \quad (26)$$

Where  $p_s$  is the peak pressure,  $z$  is the escalated distance at which the explosive charge will be placed with respect to the test wall and finally  $p_0$  corresponds to the atmospheric pressure.

Using the analytical formulas we can also calculate the value of the arrival time which is considered as the interval of time that elapses between the moment of initialization of the detonation, at the moment of arrival of the front at the distance of the wall of interest. The only expression [Iqbal, 2009] empirical for this parameter is:

$$t_a = 0.4 \cdot R^{1.2} \cdot W^{-0.2} / a_0 \quad (27)$$

Where  $R$  represents the charge distance,  $W$  the weight of the explosive charge and is the speed of sound in the air at sea level of 343 m/s.

In Table 21 we can see the results obtained in empirical form of the pressure peaks and we can see that the values obtained correspond and are close to the peak pressure value determined with the UFC. In addition, the value of the arrival time is also reported, which is very similar to that of the UFC values.

Table 21. Values obtained from the empirical formulas of Henrych, Wei and Dharani, Sadovski and Iqbal

$p_{s, Henrych}$	$p_{s, Wei \& Dharani}$	$p_{s, Sadovski}$	$t_a$
bar	bar	bar	s
3.4	2.9	3.5	0.0045

Next, to analyze the pressure trend with the passing of time, the values of the decay coefficients are obtained, as explained previously in the previous

---

section. From the Formulas 3-4-5 described in the previous chapter we obtain the values of the decay coefficients (Table 22) all according to the distance to be removed. Each value of the decay coefficients allows us to go and plot the value of pressure at the beginning of time.

Table 22. Decay coefficients by Friedlander, Friedlander modified and Wei and Dharani formulas

$b_{\text{Friedlander}}$	$b_{\text{Friedlander-Mod}}$	$b_{\text{Wei\&Dharani}}$
-	-	-
2.45	0.78	1.11

By the first value of decay coefficient, formulated by Friedlander, calculated taking into account the impulse associated with the positive phase. The trend observed using this methodology is plotted in Figure 46 and does not take into account the phase of depression that follows the displacement of air caused by the shock front.

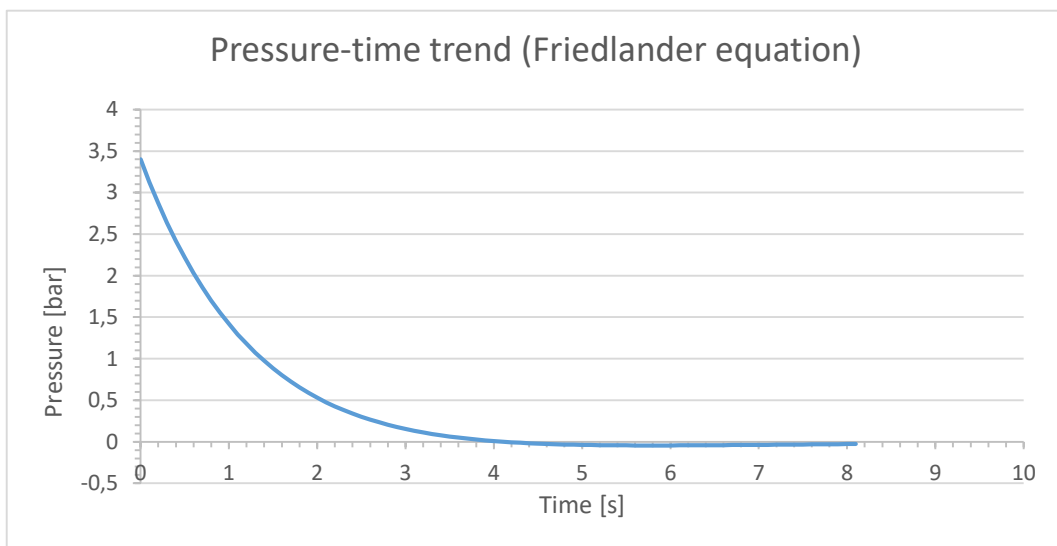


Figure 46. Pressure-time trend with the decay coefficient deriving from the Friedlander equation

From the second coefficient of decay, deriving from the modified Friedlander formula going to consider the ratio between the minimum and maximum pressure we are going to obtain a trend that also takes into account the negative phase of the pressure trend (Figure 47).

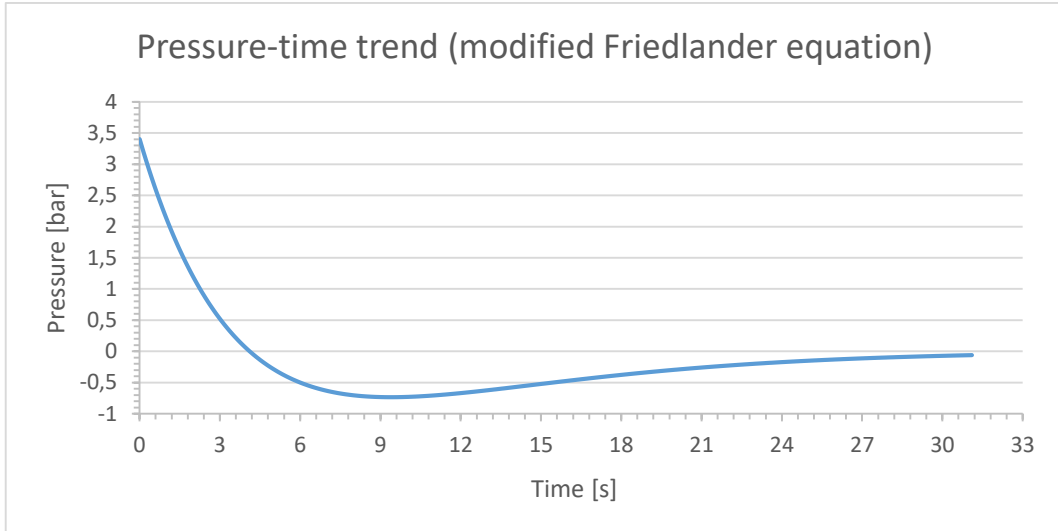


Figure 47. Pressure-time trend with the decay coefficient deriving from the modified Friedlander equation ( $p_{s,min} / p_{s,max}$ )

Finally, through the last coefficient of decay calculated using the empirical formula of Wei and Dharani, which also takes into account both the negative phase and the positive phase of the pressure trend over time (Figure 48).

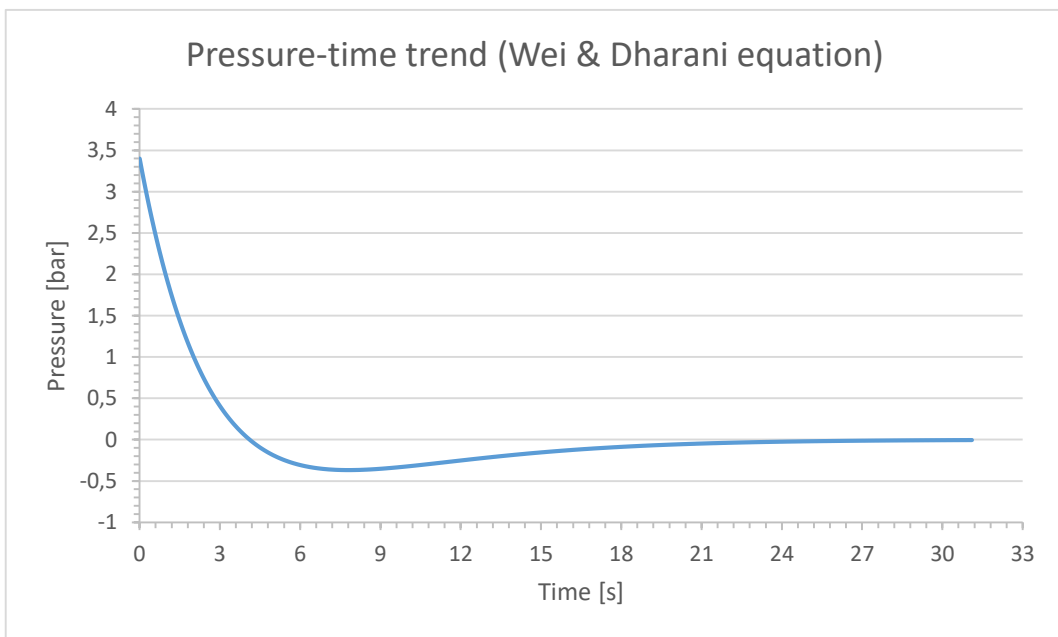


Figure 48. Pressure-time trend with the decay coefficient deriving from the Wei & Dharani equation

It is noted that even if both the trends of the Figures 47 and 48 take into account the negative phase, we note a pattern distinct from each other. The Figure 47 with respect to the Figure 48 shows a peak of depression and a longer duration, due to the fact that the decay coefficient is lower than the

ratio of the minimum pressure with respect to the maximum. In the case in which the distance value is changed with values up to 0.5 bar, it is noted that the pressure-time diagram calculated by the decay coefficient of Wei and Dharani undergoes distortions that are unsuitable for the shape of the curve that was assumed to be assumed. It is necessary to note that the coefficient to be taken into account, considering a blast load generated by a spherical charge detonated to a height of 1 m above the ground, is best suited to that obtained from the minimum and maximum peak pressure ratio.

#### 2.4.4 - Determination of the charge used in the test

From the theoretical analyzes made it is possible to define the charge that will be used in the project. Knowing that the weight of TNT equivalent explodes the effects of the different explosive charges depending on the amount of TNT needed to produce an expanding wave that has the same properties as the explosive to be characterized.

To do this we must go to choose the most suitable explosive that goes to make an explosive effect identical to what is expected through 18 kg of TNT equivalent. In considering the weight of an explosive charge it is necessary to introduce the *equivalence coefficient* which allows to derive the weight of the explosive charge used in the experimental tests. This coefficient is determined by mediating the ratio between the specific explosion heat  $Q_w$  of the explosive materials as seen in the following formula:

$$q = \frac{Q_{EXP}}{Q_{TNT}} \quad (28)$$

The determination of the coefficient of equivalence defines the explosive weight required for the experimental tests by means of the following formula [UFC 3-340-02,]:

$$W_{TNT} = q \cdot W_{EXP} \quad (29)$$

Where:

- $q$  represents the equivalence coefficient;
- $W_{TNT}$  represents the equivalent weight of TNT;
- $W_{EXP}$  represents the weight of the explosive in question;
- $Q_{EXP}$  represents the heat of detonation of the explosive in question;

- $Q_{TNT}$  represents the heat of detonation of the TNT.

The explosion is an exothermic phenomenon, that is, triggered the charge generates a reaction in which a quantity of heat is released equal to the relationship of the enthalpy of formation of the products generated by the explosion and the entanglement of formation of the explosive itself. For this reason it is important the explosion heat defined as the amount of thermal energy that is freed, under adiabatic conditions by one kilogram of explosive and which is exploded in Kcal/kg o in KJ/kg.

In the case in question, the explosive charge chosen consists of a civil explosive, the Dynamite. Considering this type of explosive, the value of the equivalence coefficient has been the subject of research for multiple projects. From the theoretical values found we will go to consider that the value of the coefficient of equivalence of the Dynamite is equal to 0.79. Through this value it was possible to derive the dynamite weight related to the different values of equivalent TNT, as shown in Table 23.

Table 23. Determination of the weight values of Dynamite used in the test

<b>z</b>	<b>d</b>	<b>W<sub>eq_TNT</sub></b>	<b>q</b>	<b>W<sub>Dynamite</sub></b>
<b>m/kg<sup>1/3</sup></b>	<b>m</b>	<b>kg</b>	<b>-</b>	<b>kg</b>
1.91	5	18	0.79	22.8
1.78	5	22	0.79	27.8
1,71	5	25	0.79	31.6

As we can see in Table 23, the analysis is concentrated in three different charge values. As the TNT equivalent weight of the charge increases, the kilograms of dynamite that will be used will increase.

### **Fireball**

In general, static models consider that the fireball reaches the maximum diameter instantaneously and maintains that size for the duration of the fireball. Static methods consider that the determination of the diameter of the charge is connected to the mass of the explosive coinvote as seen from the following formula:

$$D = k \cdot M^n \tag{30}$$

Where D is the diameter of the fire wing, M is the mass of the explosive in kg, k and n are two constants. In the models present in the network, the

---

constant  $k$  assumes a value ranging from 2.97 to 6.48 and the constant  $n$  is generally considered equal to  $1/3$ .

From the formulations of Roberts A. F. [1981] it is assumed that the evaluation of the diameter of the fireball is given by the equation:

$$D = 5.8 \cdot M^{1/3} \quad (31)$$

From the mass values in kilograms of equivalent TNT we can determine the three different diameter values as shown in Table 24.

Table 24. Determination of diameter values ( $D$ ) of the fireball

<b>z</b>	<b>W<sub>eq_TNT</sub> = M</b>	<b>D</b>
<b>m/kg<sup>1/3</sup></b>	<b>kg</b>	<b>m</b>
1.91	18	15.20
1.78	22	16.25
1,71	25	16.95

In addition, you can also calculate the duration of the fireball using a formula that correlates the duration of the fireball in seconds ( $t_d$ ) with the mass ( $M$ ) of the explosive in kilograms.

$$t_d = k \cdot M^n \quad (32)$$

Where  $k$  and  $n$  are always constant, in which the theory the constant  $k$  varies between a range of 0.23-2.61 and the  $n$  varies between values between 0.0966 and 0.333.

As we can see in the treatises of IChemE [1989] we get that the formula in the case is:

$$t_d = 0.45 \cdot M^{1/3} \quad (33)$$

The Table 25 shows calculated values.

Table 25. Determination of the time values of the duration ( $t_d$ ) of the fireball

<b>z</b>	<b>W<sub>eq_TNT</sub> = M</b>	<b>t<sub>d</sub></b>
<b>m/kg<sup>1/3</sup></b>	<b>kg</b>	<b>s</b>
1.91	18	1.17
1.78	22	1.26
1,71	25	1.31

## 2.5 – Fragmentation analyses

To get an estimate of the theoretical secondary fragmentation we went to use the formulas in the Unified Facilities Criteria [UFC 3-340-02, 2008]. The main interest in this project is the behavior of the structure and therefore the secondary fragmentation, that is the one generated by the shock wave interaction with the structures close to the explosive charge. The pressure of the explosive wave causes, as previously mentioned, a damage to the structure subject to the explosion generating fragments similar to projectiles, very rapid and small that can go to threaten human life. Think of the people in a house, as a result of an explosion the plaster or the tiles that line the walls of the houses can be transformed into dangerous projectiles for people who are present in its trajectory. Precisely for this reason, in this discussion it is of greater importance to consider the analysis of secondary fragmentation with respect to primary fragmentation. As shown in Table 26, the values of the velocities will be determined taking into account the size of the target, mediating the Formula 13.

Table 26. Values for the calculation of the initial velocity  $V_0$

Area	Volume	Mass	$i_s$	$\beta$	$V_0$
m <sup>2</sup>	m <sup>3</sup>	kg	psi-ms	-	m/s
6.25	1.625	2700	53.49	1	71.15

In which we remember that  $i_s$  is the specific impulse acquired,  $\beta$  is the form factor obtained from Figure 27 and  $V_0$  is the initial velocity to be considered. For the estimation of the final speed of the structure, reference should be made to the figures in the section. We will see how fragmentation evolves in the conclusions that will follow the discussion by comparing the theoretical results with those observed in the test.

In the test it is hypothesized to find the fragmentation along the perpendicular to the two facades, based on the combination of reinforcing materials on the facades.

## 2.6 – Tools used

### 2.6.1 – Schmidt's hammer (sclerometer)

The Hammer of Schmidt, or also called Sclerometer, is an instrument based on the measurement of the rebound of an elastic mass that depends on the hardness of the surface on which it impacts. We note that resistance and hardness are two factors connected to each other. This instrument is characterized by a hinged steel mass, driven by a spring and a metal percussion rod resting directly on the wall, as can be seen in Figure 49.

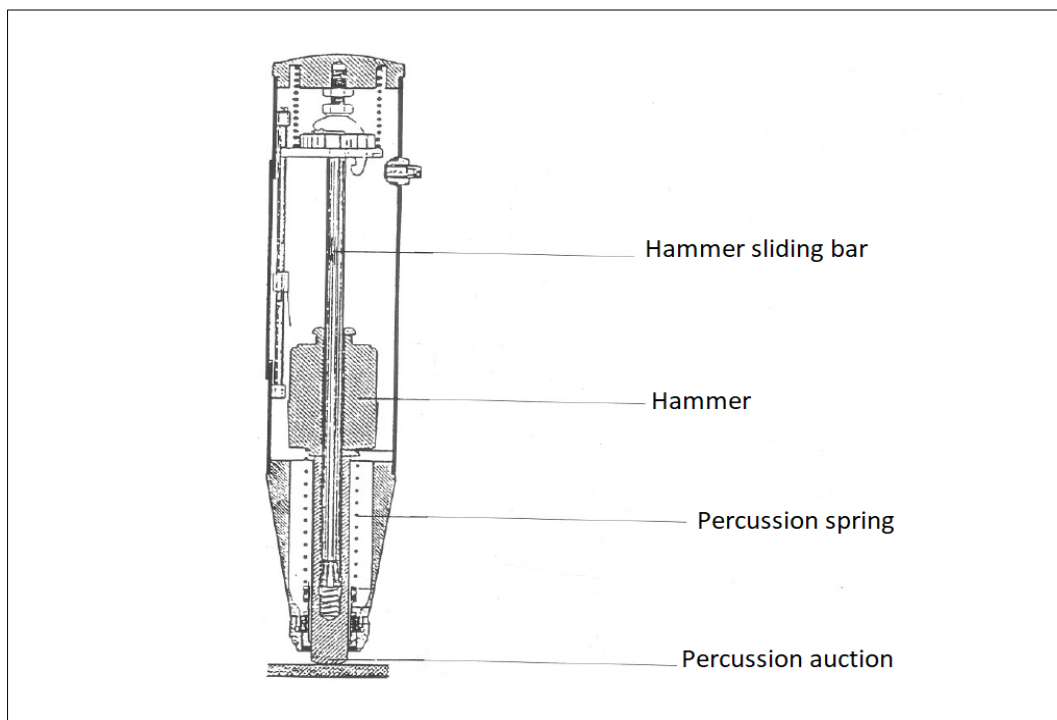


Figure 49. Hammer of Schmidt structure

The impact energy is partly absorbed by the material in which it impacts in the form of permanent inelastic deformations and partly returned to the mobile mass of the rebounding sclerometer. In general, the rebound height is greater the more the material is resistant and the permanent deformations are less.

The sclerometer is a very simple tool to use. To use this tool, press the percussion rod on the surface to be analyzed until it stops. In this way the mass inside the instrument is loaded by the presence of the spring of a fixed quantity of energy. Subsequently, the mass in which it strikes against the

striker, still in contact with the surface, is released and it rebounds. The amount of the rebound is measured by an index.

In general, the rebound value is a parameter in which it is a function of the stop angle which gives an indication of the resistance of the material on which the test was carried out. However, traditional sclerometers are instruments that measure the R value, that is the mechanical stroke or the rebound of the mass. These types of instruments are subject to errors caused by mass friction, the influence of gravity and the relative velocity between the unit and the sample to be measured. In fact, in our case the test would be distorted for positioning not completely orthogonal to the wall to be examined. Precisely for this reason we use the factor Q, a parameter that allows you to obtain a result independent from the inclination, so it should not be more correct according to the direction of impact. Furthermore, this factor allows measurements to be made within a wider range than traditional methods.

In the project of the following discussion, is used *SilverSchmidt model of type L*, characterized by the measurement of the Q index. This instrument is used to delimit areas of poor quality of deteriorated concrete structures. The European Standard (EN 12504-2: 2012) requires that for the use of the Schmidt Hammer the concrete wall must have a minimum thickness of 100 mm and must be fixed to a structure. The measurement is made by trying to avoid areas where there is an irregular, wrinkled surface and the presence of cracks and by looking for theoretical calculations to take place inside the wide brick avoiding the mortar. Instrumentalization is used in the case of temperatures between 0 °C to 50 °C.

### **Number of shots for each test wall**

As previously mentioned, in the case of the PICAEX project the SilverSchmidt test hammer was used as a Hammer of test, an instrument suitable for walls and with a lower impact energy than those traditionally used for rocks in order to avoid damage to the wall due to the instrument. For the analysis of the walls different measures are carried out.

Through analysis made from the presence of pre-existing tests, it was decided to carry out measurements on a number of 40 points for each wall. 20 measurements are made for each face of the wall, where each point is characterized by a template defined by 12 measuring points (Figure 50). Thus, in each face of the wall there are 20 points, in which each of them is characterized by a 12-point shape where 6 measurements will be made

using the sclerometer before the test and the remaining 6 which will be carried out after the test.

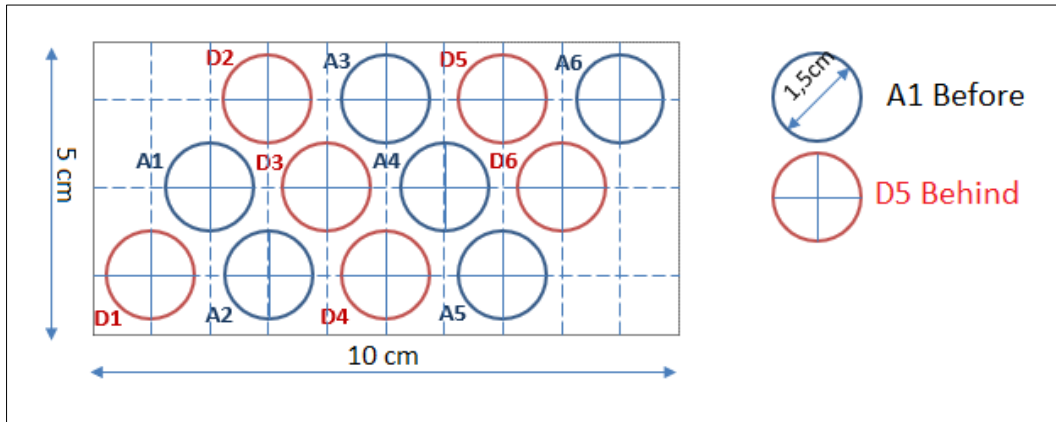


Figure 50. Template of the 12 points, each of them corresponding to a measurement with the sclerometer

The most suitable template chosen is the one in Figure 50 in which there are blue points that represent the measurement points that will occur before the test and the red points that represent the measurements by means of the sclerometer that will occur after the charge starts.

### Verification of the measuring point

The main problem encountered with the use of Schmidt's Hammer is the positioning of the measuring point on the facade of the wall.

All the walls of the project, as mentioned above, are masonry. As can be seen in Figure 51, the facades of the walls are characterized by some rows in which the bricks are positioned with the longer side parallel to the façade of the wall, these bricks are called *long bricks*, and the rows in which the bricks are arranged perpendicularly, called *short bricks*.

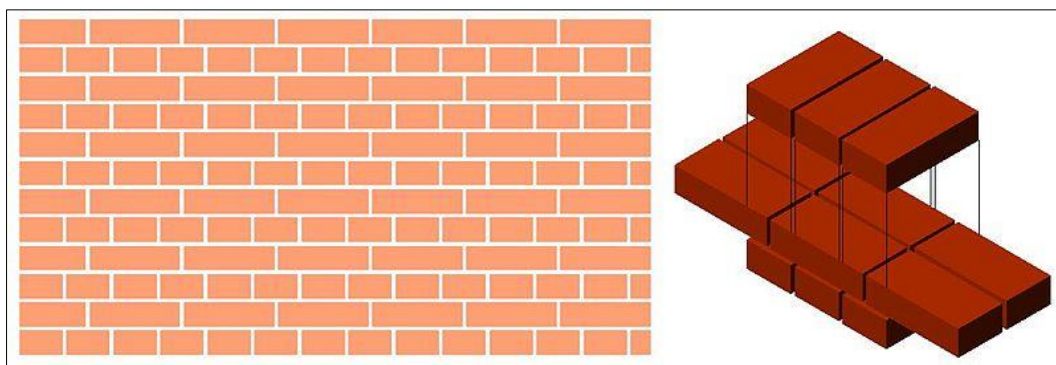


Figure 51. Positioning of the bricks that make up the wall

The problem that has arisen is whether the measurements made in the short bricks gave the same results as the measurements made on the long bricks. To verify that the two different measurements were comparable to each other, they were made by testing small walls 1 m by 1 m in size. The small test wall was constructed in the same way as the control walls used for testing (Figure 52). 16 measurements were made each of which were characterized by the test pattern of Figure 50. Knowing the position of each brick and their arrangement, 8 measurements were made in the long bricks that were compared with the 8 measurements made in the short bricks.

In order to verify that the calculated values are comparable, the average of the six shape values obtained by means of the Schmidt hammer and contrasted with the value of the average of the value of the short brick has been realized for each point of the long brick. The values were compared using the T.TEST function in Excel which returns the probability associated with the Student's t test. Going to use t of Student allows us to determine if two samples can derive from the same two populations having the same mean. Let's see Table 27 the values obtained from the tests going to refer to the different measurements numbered in Figure 52.

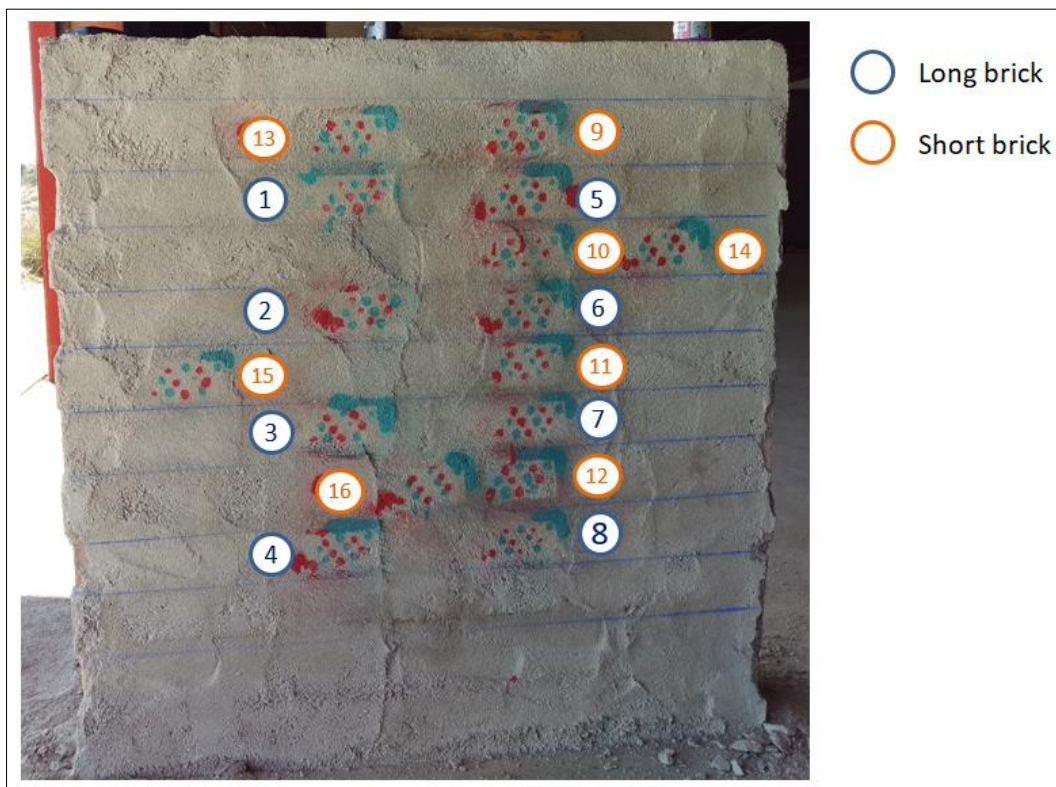


Figure 52. Wall of 1x1 m size of test

Table 27. Values of the mean and of the t di Student test relative to the measurement points of Figure 52

Average of the values to be compared: 1 with 9		T-Test	Average of the values to be compared: 5 with 13		T-Test
Short brick	21,3	0,29	Short brick	20,0	0,24
Long brick	18,8		Long brick	21,1	
Average of the values to be compared: 2 with 10		T-Test	Average of the values to be compared: 6 with 14		T-Test
Short brick	20,0	0,11	Short brick	18,2	0,01
Long brick	21,0		Long brick	20,0	
Average of the values to be compared: 3 with 11		T-Test	Average of the values to be compared: 7 with 15		T-Test
Short brick	22,4	0,36	Short brick	21,3	0,25
Long brick	22,0		Long brick	21,8	
Average of the values to be compared: 4 with 12		T-Test	Average of the values to be compared: 8 with 16		T-Test
Short brick	23,4	0,14	Short brick	18,2	6,1E-06
Long brick	24,8		Long brick	24,4	

Moreover the values obtained can also be compared graphically as shown in Figure 53.

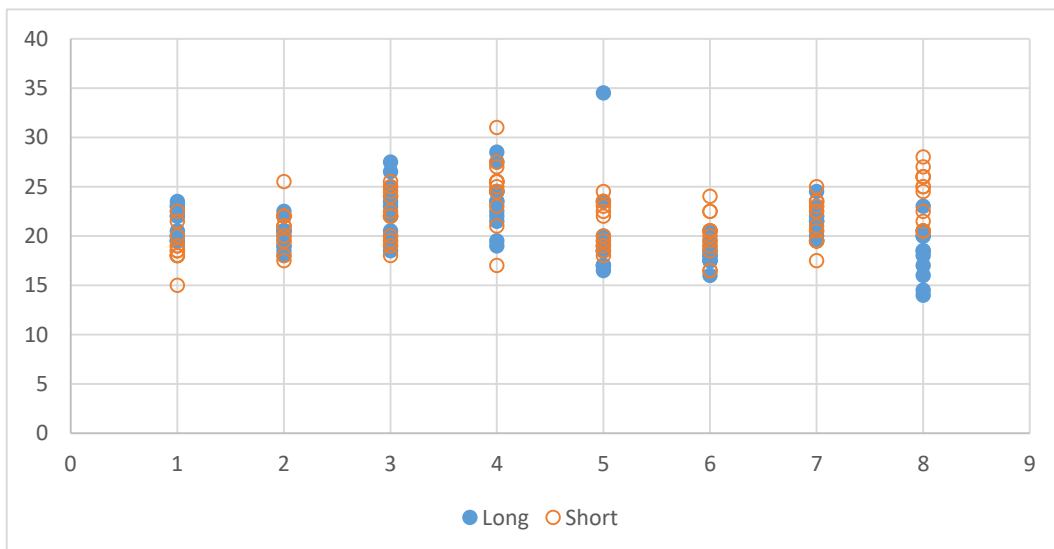


Figure 53 Values of the different bricks compared

As can be seen in Table 27 and from Figure 53 the values measured in the long and short bricks are quite similar but in some cases the two samples can not be assimilated to the same populations with the same mean. For example, in the case of the comparison of the bricks 7-14 and 8-16 in which

the value of the  $t$  of Student is too small a value and therefore not comparable. Precisely for this reason the measurements that will take place during the test will always take place in the long bricks with positioning for each side of the wall as shown in Figure 54. In this figure are placed the 20 points in which the shape of Figure 50 is drawn with the 12 points of measurement. For the study of the wall behavior, before the test, evaluations of the  $Q$  value are carried out, using the sclerometer, in the 6 blue points of the template. Subsequently these values will be compared with the 6 red points of the template which are measured subsequently the ignition of the explosive charge. This system allows us to compare in each of the 20 points the behavior of the wall in the face of an explosion of a charge placed at a distance of 5 m.

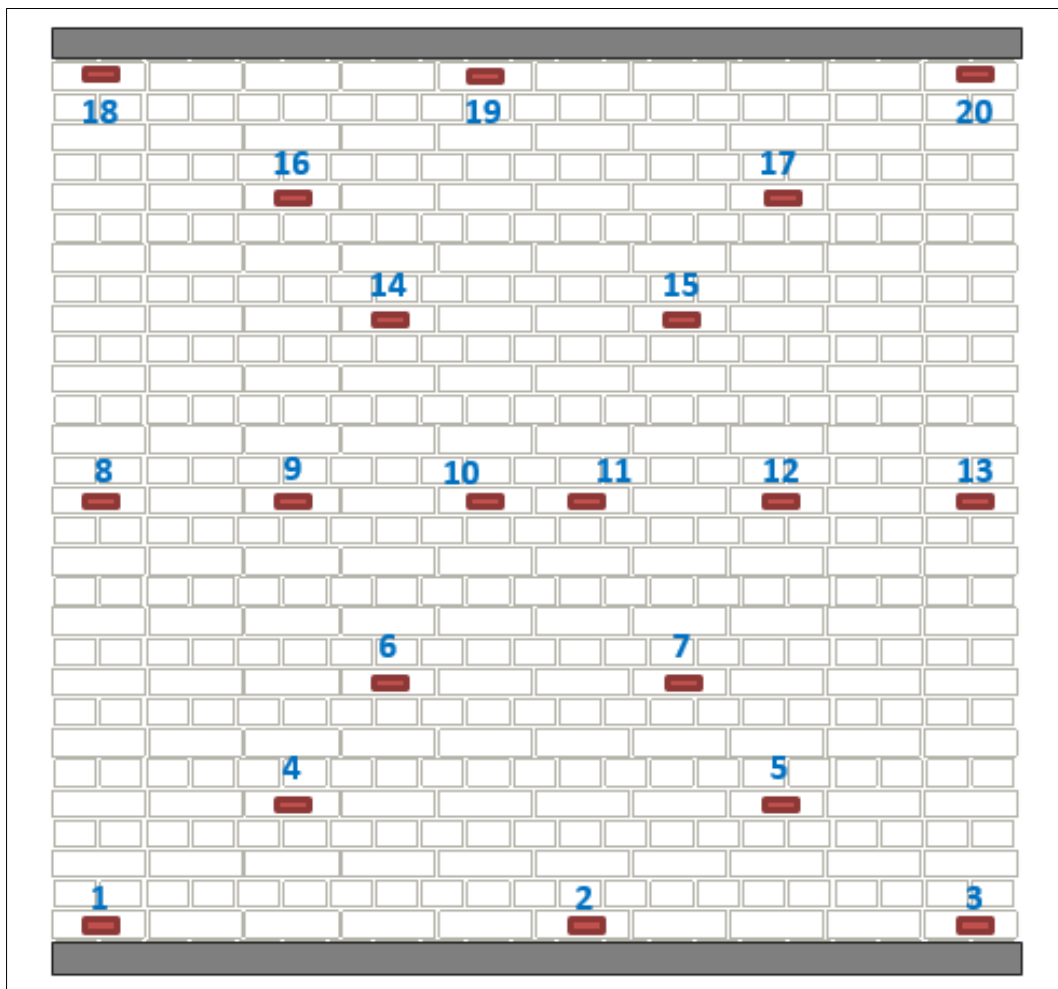


Figure 54. Points where the template is placed for measurements using the sclerometer

## 2.6.2 – Accelerometer

The accelerometer is a tool used to measure the wavefront acceleration resulting from the explosion of the explosive charge. It is based on the force measured with respect to the mass of the object (force per unit of mass).

In our case, the accelerometer will be placed on the outer face of the wall. In order to insert this instrument on the external facade of the parades, a steel solid consisting of a cylinder of dimensions equal to those of Figure 55 will be used.

The accelerometer is characterized by the standard American male screw end ( $\frac{1}{4}$ -28, UNF-3A), with measurements equal to those visible in Figure 56. The related assembly instructions are shown in Attached C.

In the project under examination, an accelerometer is used for each positioned wall, as previously mentioned on the outer face of the wall, so that the fireball does not damage the instrumentation. It is placed at a height from the ground of 1.25 m and the inner side of the wall of 0.10 m.

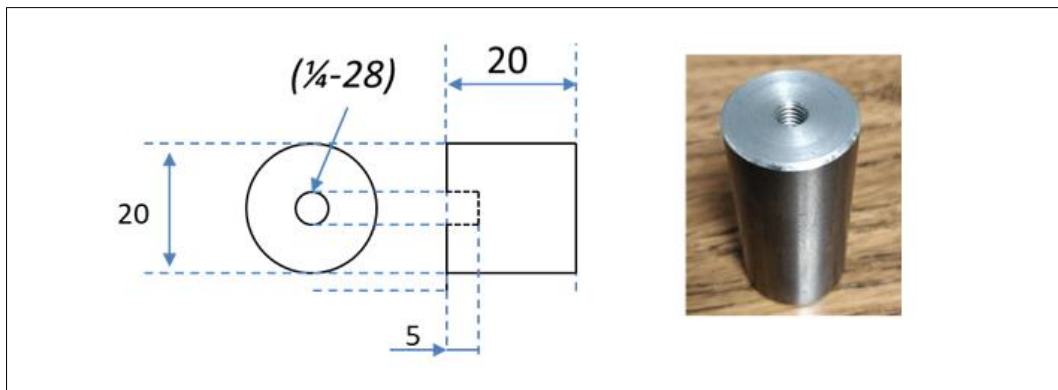


Figure 55. Cylinder inserted on the external side of the wall where the accelerometer will be placed

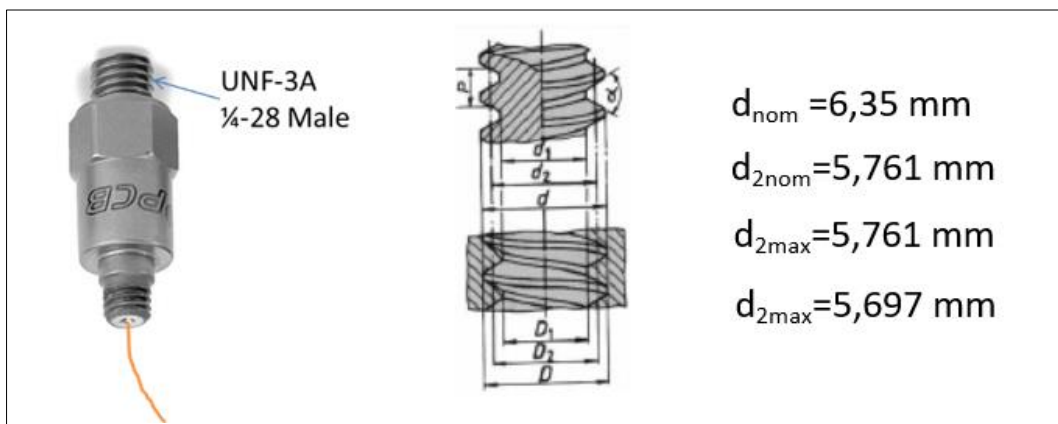


Figure 56. Accelerometer and relative measures of the head

### 2.6.3 – Pressure gauge

Three pressure sensors are used in the project, instruments that convert the incident pressure into an analog electric signal. This conversion of the pressure into an electrical signal is obtained by the physical deformation of the strain gauges connected to the pressure transducer membrane and calibrated in a Wheatstone bridge configuration. The pressure applied to the pressure gauge produces a bending of the diaphragm which in turn leads to the de-forming of the strain gauges. So the deformation will produce a change in electrical resistance proportional to the incident pressure that arrives. The pressure gauges or sensors were located inside a metal cup that was almost buried to the ground level, as we can see in Figure 57.



Figure 57. Details of the metal cup with the sensor of pressure and cable



Figure 58. Connect the pressure sensor with the data acquisition system before burying it

The three boxes containing the transducers will be placed at a distance of 5 m from the point where the explosive charge is positioned. This distance is the same distance from the walls with the explosive, precisely for this reason these transducers allow to measure the incident pressure to which the project walls are subjected. Figure 58 shows the connection between the pressure sensor, the motor on the metal cup cap, and the wire that connects it to the data acquisition system.

## **2.6.4 – High speed camera**

In the project a high-speed camera was used, model Photron FASTCAM SA3-120k (Figure 59) because it is an instrument suitable for the realization of high precision digital video. In fact, the most common use of this high-speed camera is in the field of research and analysis in various fields and automotive safety tests.

The FASTCAM SA3 camera features remote control via user-selectable camera controls on the rear panel, Gigabit Ethernet communications or an optional RS422 keyboard with a built-in 5" LCD display [web, FASTCAM SA3] characterized by a high sensitivity to light, image quality and color fidelity meditate a 12-bit ADC, through a larger recording time thanks to the 8-bit recording mode.

Two FASTCAM SA3 high-speed cameras, one of 60K and the other of 120K, are commercially available. The video camera used in this project, as previously mentioned, is a FASTCAM SA3-120K. This camera model is characterized by a resolution of 1024 x 1024 pixels with frame rates of up to 2,000 fps and a reduced resolution of up to 120,000 fps. This camera is placed at a certain distance so that you can take the whole test very well. Precisely because of its proximity to the site (Figure 60) of the test is placed behind a protective bariera (Figure 59) to protect it from the fragmentation that causes an explosion. Attached D shows the technical specifications of the FASTCAM SA3-120k high-speed chamber.



Figure 59. FASTCAM SA3-120k high-speed camera and fragment protection structure



Figure 60. Position of the high-speed camera at a distance from the test point and positioning within the protective structure

## 2.6.5 - Data acquisition system

In this project there is a need to record acceleration and pressure in difficult external conditions. To do this we use DataTrap II, MREL (Figure 61), which is the only robust recorder able to record the dynamic effort and the detonation speed of the explosives. This tool is also used many times to determine the delay times between the shots.

The DataTrap II is characterized by a large circular memory consisting of 64 million, 128 million or 256 million data points depending on the memory option that is installed. It is a robust and portable data acquisition system

with 8 channels. The high recording speed per channel can be for example 10 MHz with a resolution of 14 bits. Using the software, as described in the DAS (Data Acquisition Suite) manual, select the number of tests to be recorded, the number of channels and the recording speed. The exact amount of memory allocated to a particular channel for a particular test can be adjusted. This tool allows us to record wave pressure and near-field burst vibrations using uniaxial and triaxial accelerometers.



Figure 61. DataTrap II acquisition system, MREL

### 2.6.6 – Scanner

In the project it was necessary to have a precise long-range scanning tool for the 3D geometry analysis of the test site, before and after the initiation of the explosive charge. Precisely for this reason, the ScanStation P30 / P40 laser (Figure 62) of the Leica Geosystems was used. The ScanStation P30 / P40 [Web, Leica Geosystems] laser allows you to derive 3D images and HDR images of the highest quality with realistic clarity and an extremely

fast scanning speed of 1 million points per second reaching distances up to 270 m. This instrument is resistant to harsh environmental conditions, for example, at temperatures ranging from -20°C to +50°C and resistant to dust and rain.

In the project this tool has the role of going to analyze the displacement of walls so that to go to identify how the walls behave after the explosion. So it goes to detect the different deformations of the walls and structures around following the test. The different technical features of the P30/P40 Laser ScanStation are listed in Attached E.



*Figure 62. Laser ScanStation P30 /P40 from Leica Geosystems*

## 2.7 – Tests

The project in consideration is characterized from a total of four tests but in this treatise only the first three will be explained because the last test could not be carried out in the time established due to the unfavorable weather conditions for the test. Each test is characterized, as previously mentioned, by four masonry walls in which three are reinforced by additives procured by Mapei, an Italian company, and a wall remains without reinforcement and is called a control wall. In all three tests, the walls are transported out of the building where a forklift truck has been built. As was theoretically designed at the beginning of the project, the walls had to be transported out of the building by a forklift truck. The wall was placed on a sheet of polystyrene placed between the wall and the metal parts of the machine and fixed by ropes and hooks as shown in Figure 38. Afterwards each wall was loaded on a crane truck and surrounded by sandbags to prevent damage during the move. This transport process was modified during the displacement. The walls are always transported out of the building by means of a forklift but they were fixed by means of ropes to the structure of the forklift truck. Moreover, between the metallic structure and the bricks, wooden boards are inserted to isolate the walls (Figure 63).



*Figure 63. Forklift to transport the walls to the outside of the building*

Subsequently outside the building, the wall is attached to the crane truck which loads the four walls together into the container of the transport vehicle as shown in Figure 64. As can be seen from the figure, the four walls are fixed in the carriage in a position tilted the vertical. This increases stability and avoids the risk of damage that may occur during the irregular journey that must be taken to reach the site where the test takes place.



Figure 64. Transporting the walls on the crane truck to the test site

At the test site the walls are mounted on the auxiliary structures already attached to the concrete base as shown in Figure 65. It should be noted that each test is characterized by a distinct combination that will be explained in detail in the treatment of the individual tests.

Subsequently, before the test takes place, as previously mentioned, the measurements must be made by mediating the sclerometer for each wall façade and positioning the accelerometers, the manometers, the DataTrap and the high-speed camera. Remember that two data acquisition systems are used, that is, two DataTrap II. The DT2 recognition system is connected to the accelerometer A1 and A2 and to the monometer P1 and P2, the DT1 system is connected to the accelerometer A3 and A4 and to the monometer P3 as shown in Figure 66. These connections can be initiated to the test.



Figure 65. Positioning of the walls

## - Test number 1

The first trial is held on Wednesday, February 21st. As a first test the walls that characterize the test are arranged according to the diagram of Figure 66. In the location number 1 (U1) the reinforced wall is placed in the external façade, ie the one that is not positioned directly to the fire bubble of the explicative charge , from the Mapewrap EQ Net with Adhesive and the first accelerometer (A1) is positioned in the external façade. In the second location (U2), the wall with the external façade reinforced by Planitop Intonaco Armato is inserted and it is the wall associated with the accelerometer A2. The wall with the reinforcement on the external façade with the Mapegrid C170 with Mapewrap 31 T is located in position U3 and the accelerometer is always positioned on the external façade. Finally, the control wall, without reinforcement, is placed in position U4, as shown in Figure 66, and the accelerometer A4 is associated with this wall.

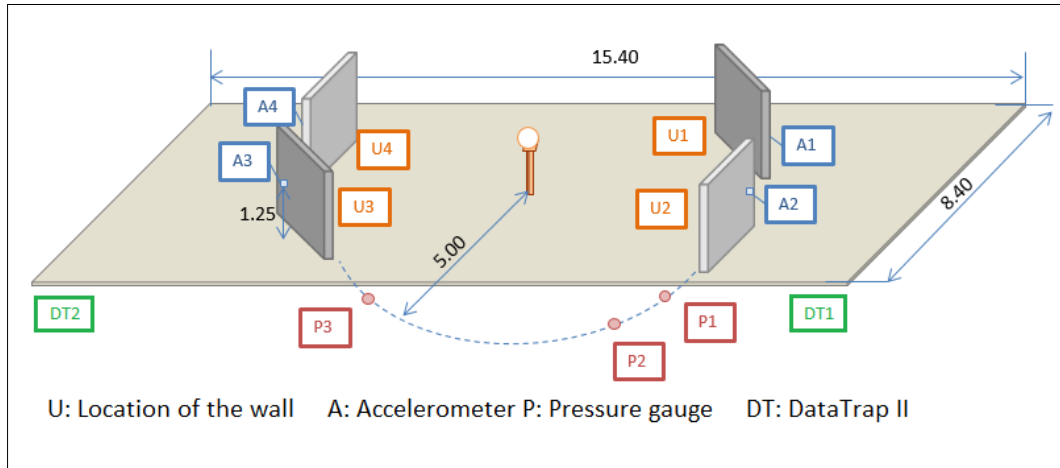


Figure 66. Order of wall locations and measurement sensors

In this first test a charge of 18 kg of equivalent TNT is used which corresponds to 22.8 kg of Dynamite. As can be seen in Figure 67, the charge must be a certain height, considering the center of the dynamite charge. By analyzing the calculation of the triple point in Table 15, choose to proceed to a height of 0.5 m above the ground. The dynamite charge will be placed in the center of the test yard, at a distance of 5 m from the walls fixed to the ground and on a mount created with polyester as shown in Figure 67. Once the explosive charge is positioned, the electric detonator is inserted in the upper part of the charge which allows the ignition. The detonator is connected to the trigger (Figure 68), that is an electrical system, which allows to assume as zero time the moment in which the activation occurs. The trigger is connected to the data acquisition system, so you can record the start time of the explosion called zero time.



*Figure 67. Positioning of the explosive charge in the first test*



*Figure 68. Union of trigger with the detonator*

## - Test number 2

The second trial is held on 22 February. The walls were fixed the day before always following the diagram of Figure 66. In this case the position of the walls is the same as in the previous case but all the reinforcements are positioned on the inside face of the wall. Precisely for this reason, in this case, the reinforcements placed in direct contact with the fireball generated by the explosive. In this case the amount of the tax has changed. In this case a charge of 25 kg of equivalent TNT is considered, which corresponds to 31.6 kg of dynamite. Furthermore, the height at which the charge is positioned also varies. It goes from a height of 0.5 m to 0.7 m, always considering the center of the charge as seen from Figure 69. Subsequently, as explained above, after the position of the explosive charge the trigger is combined with the detonator (Figure 68).



*Figure 69. Positioning of the explosive charge in the second test*

### - Test number 3

In the last test that we will analyze in this discussion, which took place on February 23rd, we will consider the same explosive charge as test 2, that is a charge of 25 kg of equivalent TNT which corresponds to 31.6 kg of dynamite. In this case the reinforcements are all applied to the facade of the outer wall as the first case. In this test the position pattern of the walls is different. Referring again to Figure 66, the control parity without reinforcement is positioned at the location U1 and is associated with the accelerometer A1. In the second location the wall with the reinforcement of Planitop Intonaco Armato is positioned and with the accelerometer A2 positioned always in the external facade. The wall with the reinforcement of Mapegrid C170 with Mapewrap 31 T is fixed in position U3 in which the accelerometer A3 is associated. Finally in position U4 is located the wall with the reinforcement of Mapewrap EQ Net and Adhesive, in which the accelerometer A4 is placed. We see in Figure 70 the arrangement of the walls and the explosive charge before the start.

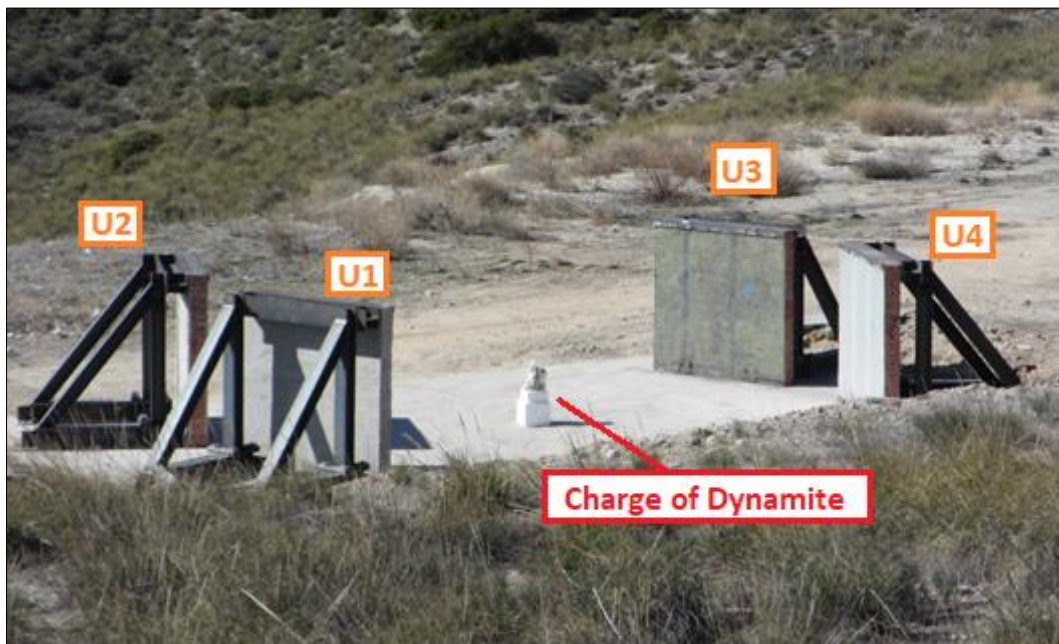


Figure 70. Moment before the charge starts

## 2.8 – Results

Following are the values found by the three tests carried out.

### - Test number 1

As mentioned above, the first test is characterized by an explosive of 18 kg of equivalent TNT which corresponds to 22.8 kg of dynamite, placed at a height of 0.5 m above the ground. From the literature we went to get the parameters that characterize the wavefront that were calculated mediated by the UFC as can be seen in Table 18. The sensors present in the test were three pressure meters and four accelerometers. In the first test, DataTrap II was able to record all the values obtained from the three pressure sensors and only two signals between the four accelerometers. The values of the accelerometers A1 and A4, as shown in Figure 66, belong to the wall characterized by the reinforcement of the Mapewrap EQ Net with adhesive and to the control wall. As shown in Figure 71, the accelerometers are inserted into the walls and connected by a cable to the acquisition system. During the test, the DataTrap II was unable to record any signal of the accelerometers A1 and A4. The pressure wave investing the sensors disconnected the cables that joined the accelerometers. For this reason the values were not recorded and stored. An example can be expressed from Figure 71 of the accelerometer A1 positioned in the wall with the reinforcement of Mapewrap EQ Net and Adhesive. In the figure we see how the accelerometer is connected to the cable before the test and how it is detected after the test with the cable disconnected.

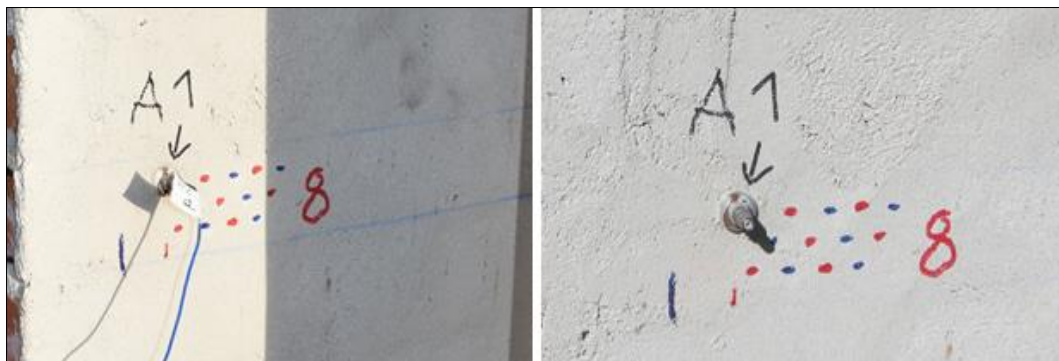


Figure 71. Status of accelerometer status before (left) and after (right) of the test

The Table 28 shows the values that detected the accelerometers and the pressure monometers. Furthermore, the values of the pressures detected by the three pressure sensors that can be compared to those studied theoretically have been reported in Figure 72-73-74.

Table 28. Values obtained from the registration of the test 1

Channel	Measure	ID	Estimated UFC of Pressure (PSI)	Experimental estimate of the peak value
DT1-1	Acceleration	A3	-	1209,56 g
DT1-2	Acceleration	A4	-	-
DT1-3	Pressure	P3	45,88	64,23 PSI
DT2-1	Acceleration	A1	-	-
DT2-2	Acceleration	A2	-	1042,55 g
DT2-3	Pressure	P1	45,88	46,35 PSI
DT2-4	Pressure	P2	45,88	50,97 PSI

We note from the curves, of the successive figures, which are quite uniform to what was expected by comparing the values of literature. From the values derived from the theory (Table 18) we can see that the peak value of the arrival times vary from reality. In fact, for the UFC the receipt time is 4.04 ms and in the recordings the time varies between 3.2 and 3.5 ms. We will also see that the calculated peak pressure value also deviates from the experimental values. The theoretical value of the peak pressure calculated at 18 kg of TNT is 45.88 PSI but in the test the value varies between 46.35 and 64.23 PSI. This can be explained by the fact that the explosive used is dynamite and this is not a military but civil exhibit that can very well behave with equal effects to charge higher TNT.

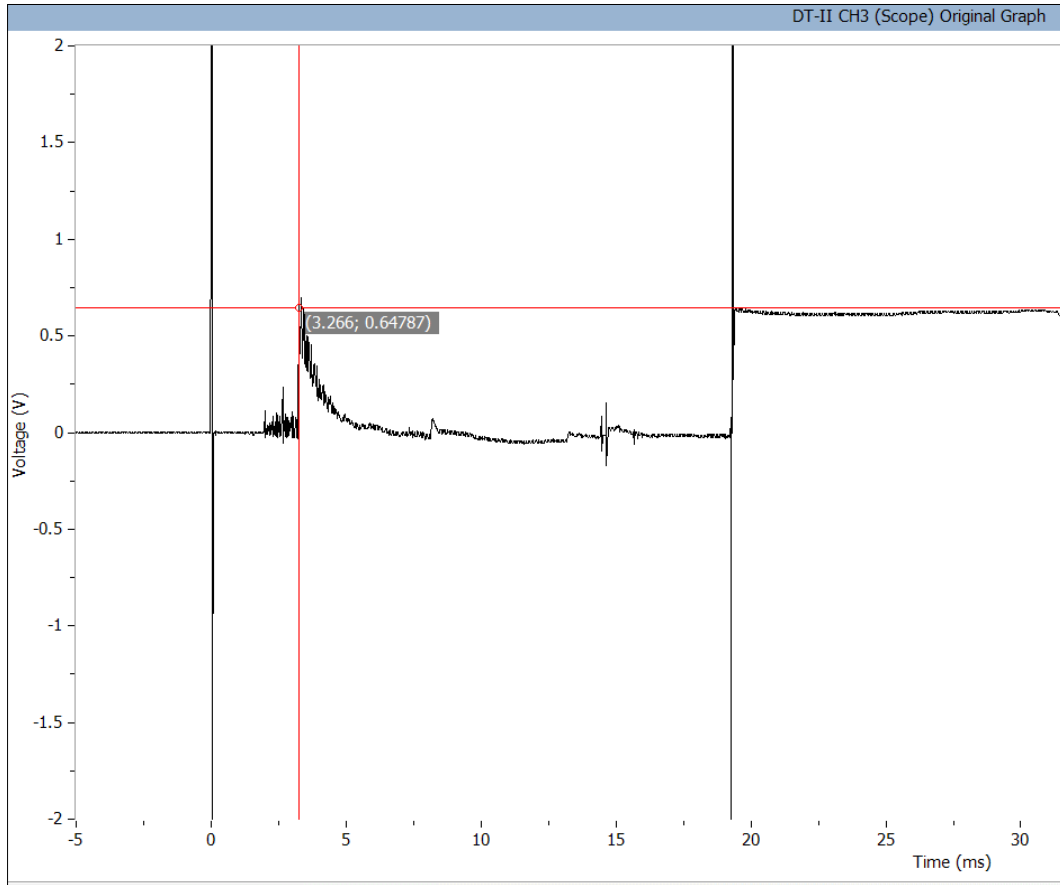


Figure 72. Signal of the monometer P3

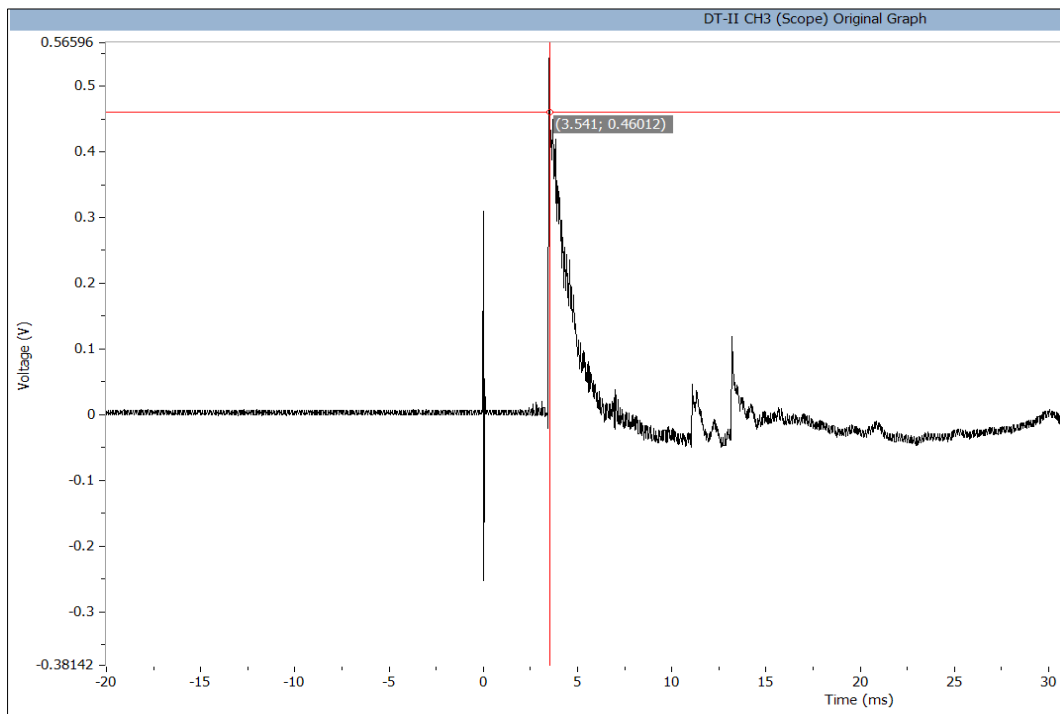


Figure 73. Signal of the monometer P1

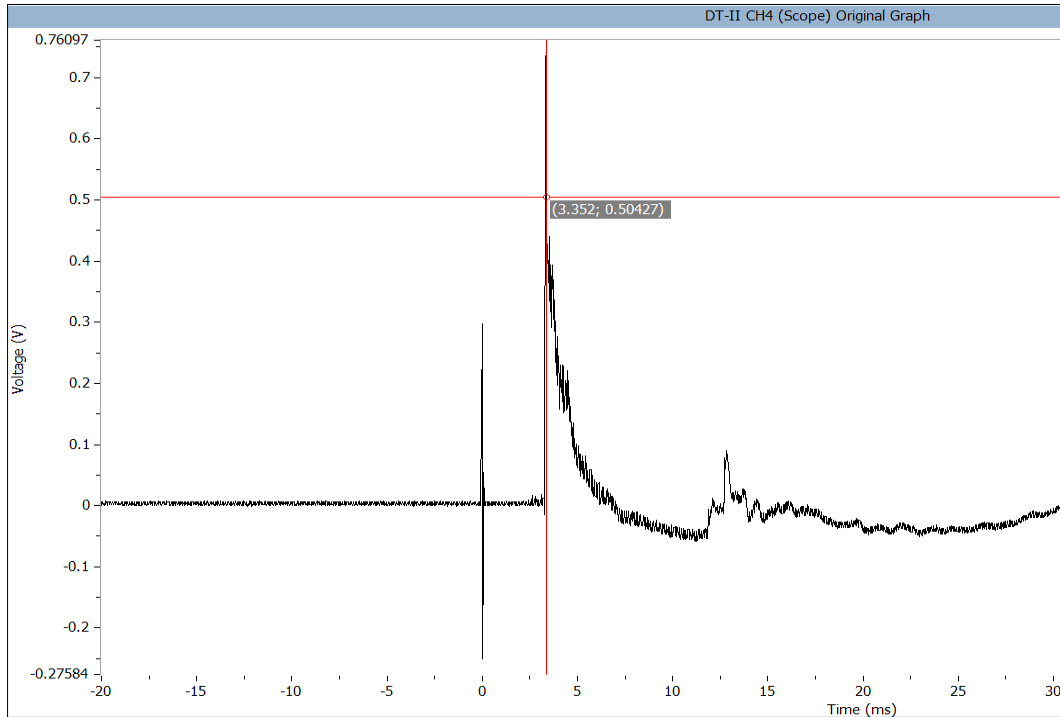


Figure 74. Signal of the monometer P3

From the obtained results of the test and reported in Figure 75-76-77-78 we can see the different fractures that are generated in the face of the explosion. It is emphasized that such a test does not cause fragmentation both along the back face and along the front face.



Figure 75. Control wall after the explosion in position U4



Figure 76. Mapegrid C170 and Mapewrap 31 T reinforcing wall in position U3

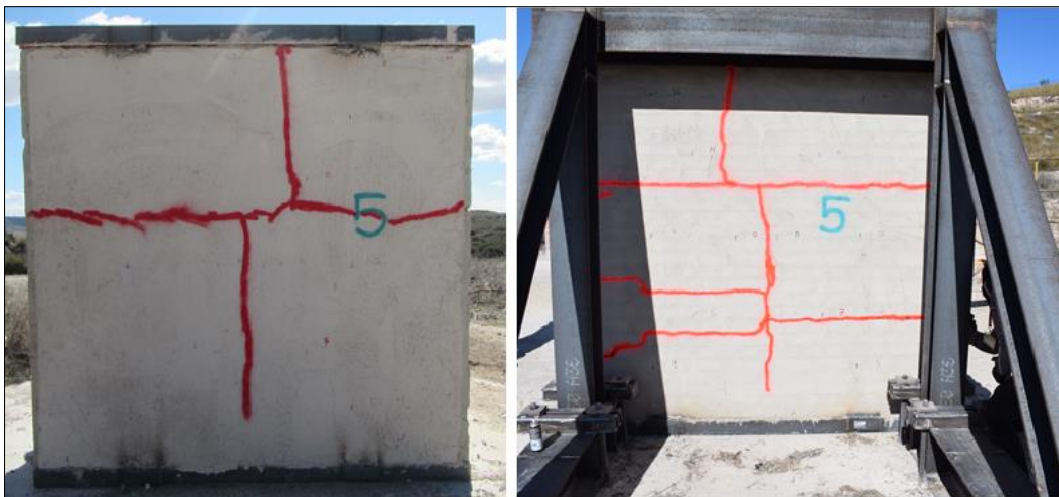


Figure 77. Planitop Armored Plaster reinforcement wall in U2 position



Figure 78. Mapewrap EQ Net reamer wall with Adhesive in position U1

After the explosive activated, the value of the damage to the walls is analyzed by means of the values obtained from the sclerometer before and after the test. The damage values went to study by *t* of Student. As previously mentioned, the 6 points before and after the test are measured using the sclerometer. Every six points is averaged and the *t* of Student value is calculated and then the damage value is calculated using the formula:

$$D = 1 - \frac{Q_{m,before}}{Q_{m,behind}} \quad (34)$$

Where  $Q_{m,before}$  is the value obtained by means of the sclerometer before the test takes place and  $Q_{m,behind}$  is the value taken later by the test.

The value of the damage can arise if the value obtained from the student's *t*-analysis is less than 0.05. When this condition does not occur, the damage is null. If the damage is high and it was not possible to make the measurements with the Hammer Schimdt after the explosion, the damage value of 100% is assumed.

Furthermore, in some cases the calculated damage is negative. These cases are called false negatives because they are points where the value by means of the Hammer of Schimdt provides a value greater than that found before the test. These negative values are caused (we think, but are being analyzed at the Universidad Politecnica de Madrid) by the conformity of the metal structure and the positioning of the reinforcement. Following are shown in Table 29-30-31-32 the values of the damage found for each wall. It is emphasized that only in Table 29, as an example, are the parameters  $Q_{m,before}$ ,  $Q_{m,behind}$  and the values of the Student *t* obtained. Recall that the points in the tables are those associated with Figure 54 on page 86.

Table 29. Damage of the control wall

External wall facade				
Points	$Q_{m,before}$	$Q_{m,behind}$	t of Student	Damage
11	25,5	24,08	0,047	6%
13	28,33	24	0,015	15%
Interior wall facade				
Measurment points	Average of the values before the test	Average values after the test	t of Student	Damage
4	21,58	27,33	0,021	-27%
12	24,17	26,42	0,0036	-9%
16	25,17	27,33	0,021	-9%
17	26,5	28,33	0,0193	-7%

Table 30. Damage of the wall with reinforcement in the inside facade Mapegrid C170 and Mapewrap 31 T

External wall facade	
Measurement points	Damage
1	6%
2	14%
5	23%
6	54%
7	56%
9	13%
12	21%
13	10%
14	12%
17	12%
Interior wall facade	
Measurement points	Damage
7	16%

Table 31. Damage of the wall with reinforcement in the internal facade with Mapewrap EQ Net with Adhesive

External wall facade	
Measurement points	Damage
14	15%
15	35%
Interior wall facade	
Measurement points	Damage
4	-13%
5	-23%
6	-7%
8	-9%
9	-24%
10	-17%
12	-16%
16	-7%
17	-17%

Table 32. Damage of the wall with reinforcement in the internal facade with Planitop Intonaco Armato

External wall facade	
Measurement points	Damage
6	16%
7	15%
Interior wall facade	
Measurement points	Damage
2	11%
9	-10%
17	-11%

The damage that occurs through the previously imposed conditions, characterized by an explosive of 18 kg of equivalent TNT, suffers a damage of type C (Table 9) that corrects to an intermediate damage. In fact, the walls are found with high fractures especially in the facades where there is no reinforcement. In fact, the façades in which the Mapewrap EQ Net reinforcement is present with Adhesive and the one with Mapegrid C170 and Mapewrap 31 T we can see that they are not characterized by superficial cracks and the walls are intact. However, in these walls in the exterior facade there are high fractures, especially in the case of the Mapewrap EQ Net with Adhesive. In the case of the Planitop Intonaco Armato reinforcing wall, we note that fractures are present on both sides. It is noted that in this case, a long façade in which reinforcement is not present, there is a greater fracture density than the façade in which reinforcement is present. Even the wall without reinforcement is characterized by cracks in both facades. In this case we note that the values of the fractures obtained are intermediate values and for this reason we can say that by analyzing the video generated by the high-speed video camera I can say that the explosive worked well without any problem. Moreover, from the percentage damage values that have been reported in the tables, it is noted that negative values occur only on the internal façade, that in direct contact with the explosive charge. In this case we can give the cause to the metallic structure. The auxiliary structure is fixed to the wall only in the upper end but the pressure wave striking the wall causes a displacement of the base. From the high-speed camera one can clearly see the displacement that the wall undergoes. Proprop for this reason the internal façade is subject to compression producing a value greater than the parameter Q. In the following tests to avoid this displacement of the lower base of the wall it was decided to

attach behind the base of the wooden planks that fill the gap between the UPE profile and the metal structure.

## - Test number 2

In the second test it was decided to increase the explosive charge by a value of 18 kg of TNT equivalent to a value of 25 kg of equivalent TNT. This value generates a value of 31.6 kg of Dynamite and leads to an altitude value of 0.70 m. The values found in the test are shown in Table 33. We note that in this case the values that were able to record are those of the sensors A3, A2, P3 and P1. We see that for the other sensors there are no recorded values due to the fact that the pressure wave investing the sensors and their components have disconnected the cables that connected them to the data acquisition system.

Table 33. Values obtained from the registration of the test 2

Channel	Measure	ID	Estimated UFC of Pressure (PSI)	Experimental estimate of the peak value
DT1-1	Acceleration	A3	-	659.9 g
DT1-2	Acceleration	A4	-	-
DT1-3	Pressure	P3	59.12	80 PSI
DT2-1	Acceleration	A1	-	-
DT2-2	Acceleration	A2	-	1170.2 g
DT2-3	Pressure	P1	59.12	82.6 PSI
DT2-4	Pressure	P2	59.12	-

Also shown in **Figure 79-80** are signals of the pressures that were recorded during the test. Observing the values of the pressure peaks in the signal we can see that the values of the sagnale vary from 80 PSI to 82.6 PSI. In the literature, using the UFC a value of about 60 PSI has been obtained. This big difference can be caused by the fact that Dynamite is a civil and non-military explosive. In general, the effects calculated using the equivalent TNT can be reported to the effects of a military explosive but may be lower than those of a civilian explosive. Precisely for this reason we can explain the difference between the values found experimentally and theoretically.

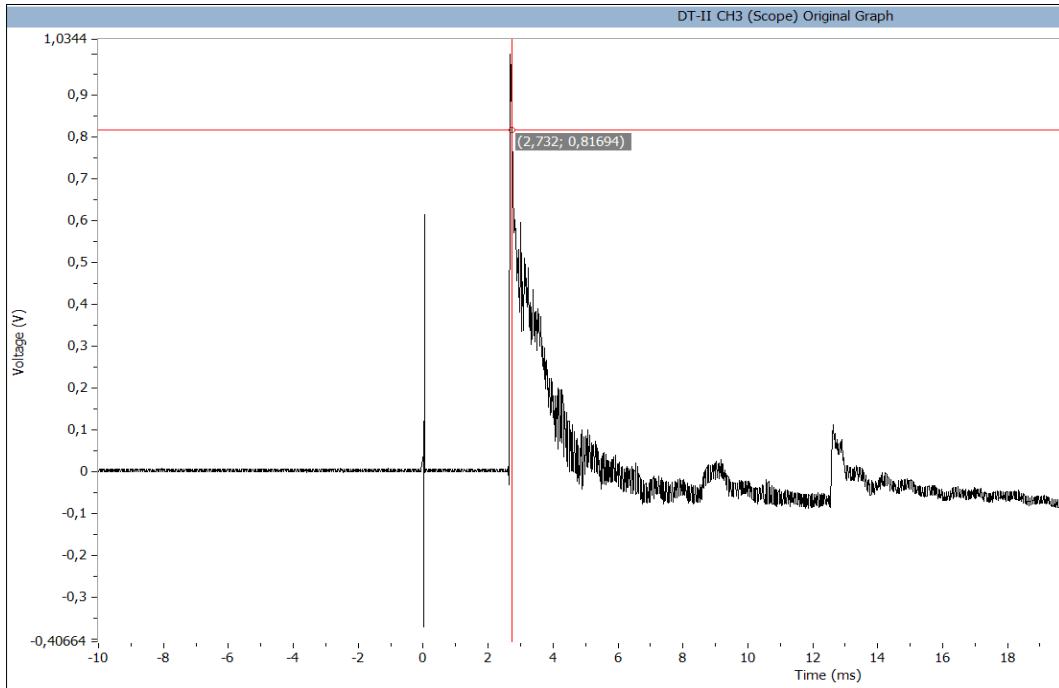


Figure 79. Signal of the monometer P1

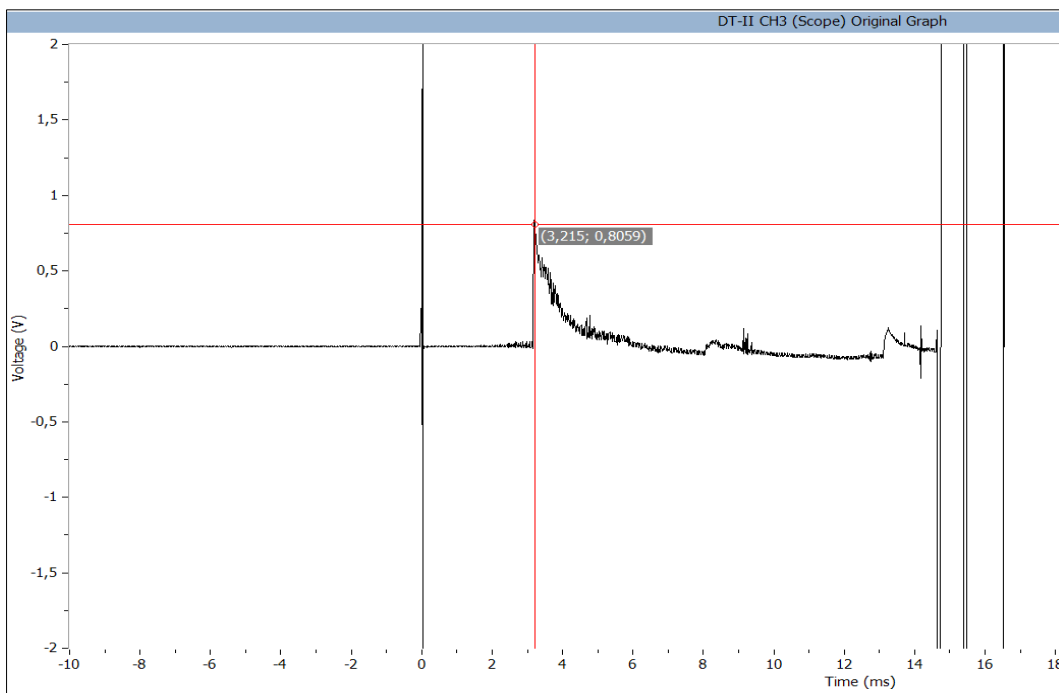


Figure 80. Signal of the monometer P1

The effects observed after the start of the 31.6 kg charge of Dynamite are reported in the following Figures 81-82-83-84.



Figure 81. Control wall after the explosion in position U4

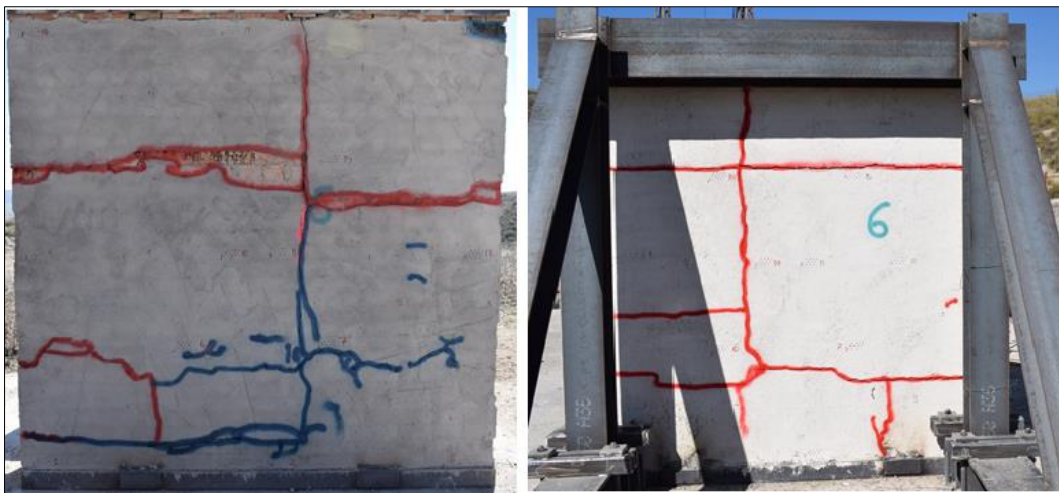


Figure 82. Damage of the wall with reinforcement in the external facade with Planitop Armored Plaster in position U2



Figure 83. Damage of the wall with reinforcement in the external facade with Mapegrid C170 and Mapewrap 31 T in position U3



Figure 84. Damage of the wall with reinforcement in the external facade with Mapewrap EQ Net with Adhesive in position U1

As can be seen from the preceding figures, there has been the generation of fragmentation in the internal façade, that is to say, positioned in direct contact with the explosive charge. It is noted that in this case the most damaged walls are the walls with Mapewrap EQ Net and Adhesive reinforcement, in fact, as shown in Figure 84, the adhesive is also torn, and the control wall. The wall with less damage is reinforced with Mapegrid C170 and Mapewrap 31 T. We can recognize the walls with greater damage by calculating the areas in which the coating is no longer present as shown in Table 29.

Table 39. Value of damaged areas of walls using AutoCad

Total areas of the damage			
Control wall	Mapewrap EQ Net and Adhesive	Planitop Intonaco Armato	Mapegrid C170 and Mapewrap 31 T
m <sup>2</sup>	m <sup>2</sup>	m <sup>2</sup>	m <sup>2</sup>
0.46	0.52	0.21	0.09

Furthermore, for each wall the percentage damage was calculated as in the previous test by the Student's t method and the Formula 34. Subsequently in the Tables 40-41-42-43 the values of the wall damage are always reported relative to the points schematized in Figure 54.

Project PICAEX

Table 40. Damage of the control wall

External wall facade			
Measurement points	Damage	Measurement points	Damage
2	13%	13	11%
4	100%	14	12%
7	12%	16	13%
8	11%	17	39%
9	10%	19	20%
Interior wall facade			
Measurement points		Damage	
5		8%	
10		8%	
11		17%	
16		17%	
17		35%	

Table 41. Damage of wall with Planitop Intonaco Armato

External wall facade			
Measurement points	Damage	Measurement points	Damage
1	22%	10	9%
2	39%	11	9%
3	14%	12	10%
5	13%	14	100%
6	22%	15	41%
7	40%	16	6%
8	7%	20	100%
9	10%		

Table 42. Wall damage with Mapegrid C170 and Mapewrap 31 T

External wall facade			
Measurement points	Damage	Measurement points	Damage
1	19%	10	11%
2	22%	11	10%
3	23%	12	9%
Interior wall facade			
Measurement points	Damage	Measurement points	Damage
6	10%	13	21%

8	15%	14	9%
9	28%	15	12%
10	26%	16	5%
11	31%	17	11%
12	17%		

Table 43. Damage to the wall with Mapewrap EQ Net with Adhesive

External wall facade			
Measurement points	Damage	Measurement points	Damage
2	14%	10	40%
3	55%	11	52%
6	29%	12	56%
7	26%	13	100%
8	100%	15	6%
9	49%	18	7%
Interior wall facade			
Measurement points	Damage	Measurement points	Damage
2	13%	10	14%
4	17%	11	15%
5	7%	12	16%
8	10%		

We note that in this test in many cases the damage reaches the Maximum (100%). These are the points where the fragment part of the fragment has been shattered and that the shape of the points to be measured has not remained.

### - Test number 3

In the third and final test the charge of 31.6 kg of Dynamite is always used at a height of 0.70 m above the ground. In this case the internal facade, in direct contact with the charge, is the one in which reinforcement is present. The recorded data are shown in Table 44.

# Project PICAEX

Table 44. Values obtained from the registration of the test 3

Channel	Measure	ID	Estimated UFC of Pressure (PSI)	Experimental estimate of the peak value
DT1-1	Acceleration	A3	-	1351.1 g
DT1-2	Acceleration	A4	-	1493.7 g
DT1-3	Pressure	P3	59.12	-
DT2-1	Acceleration	A1	-	1241.7 g
DT2-2	Acceleration	A2	-	1329.8 g
DT2-3	Pressure	P1	59.12	87
DT2-4	Pressure	P2	59.12	97.1

The Figures 85-86-87-88 shows photos of the wall conditions after the test has started.



Figure 85. Control wall after the explosion in position U1



Figure 86. Damage of the wall with reinforcement in the internal facade with Wallewrap EQ Net with Adhesive in position U4



Figure 87. Damage of the wall with reinforcement in the internal facade with Planitop Armored Plaster in position U2



Figure 88. Damage of the wall with reinforcement in the internal facade with Mapegrid C170 and Mapewrap 31 T in position U3

As can be seen from the photographs in this test fragmentation does not occur. The walls after the priming of the wall are characterized by fractures. The wall in which Mapegrid C170 and Mapewrap 31 T is present is the one characterized by less damage. Fractures are only present on the façade where reinforcement is not present. In the other walls the breakages are present in both the facades but there is no presence of fragmentation as is found in the previous case. Table 45-46-47-48 shows the different values of the damage characterized by the formula 34 previously present.

Table 45. Damage of the control wall

External wall facade			
Measurement points	Damage	Measurement points	Damage
2	33%	11	46%
4	27%	12	48%
6	63%	13	63%
7	55%	14	10%
8	100%	15	15%
9	36%	17	6%
10	19%		
Interior wall facade			
Measurement points		Damage	
6		21%	
8		10%	
11		18%	

Table 46. Damage of the wall with Mapewrap EQ Net with Adhesive

External wall facade			
Measurement points	Damage	Measurement points	Damage
1	9%	12	-5%
2	24%	14	38%
4	40%	17	-6%
5	14%	18	13%
7	-5%	20	-7%
Interior wall facade			
Measurement points	Damage	Measurement points	Damage
2	8%	11	5%
5	10%	12	9%

Table 47. Damage of wall with Planitop Intonaco Armato

External wall facade			
Measurement points	Damage	Measurement points	Damage
5	100%	13	36%
7	-13%	14	24%
8	25%	15	14%
9	17%		
Interior wall facade			
Measurement points	Damage	Measurement points	Damage
5	14%	12	-10%
11	-8%	14	-15%

Table 48. Wall damage with Mapegrid C170 and Mapewrap 31 T

External wall facade			
Measurement points	Damage	Measurement points	Damage
3	10%	12	21%
4	38%	13	46%
5	38%	16	45%
6	20%	17	43%
7	15%	18	14%
11	23%		
Interior wall facade			
Measurement points	Damage	Measurement points	Damage
2	18%	12	11%
4	18%	14	16%
6	16%	17	15%
11	13%		

As can be seen in the percentage damage tables, here too there are negative values that will be studied in greater detail in the following months, but that we can attribute to the type of reinforcement and to the auxiliary structure that supports the walls.

---

---

## 3 - Conclusions and future developments

In this master thesis, the behaviors of different constructive solutions were analyzed following an explosion. Three tests were performed characterized by an explosive amount of 22.8 kg or 31.6 kg of Dynamite and four walls for each of it.

In the first period of work, the explosive was studied and designed to be used in the experimental phase. At this stage, it is worked by referring to a charge in kilograms of TNT, as it is the explosive that has more documentation and, once finished the initial analysis, it is converted into a charge of dynamite which produces the same effects produced by the Trinitrotoluene.

To determine the weight value of equivalent TNT, we proceeded to define that the distance between charge and wall is equal to 5 m. Subsequently, the distance value was searched for with respect to the weight of equivalent TNT which provided an intermediate damage to the walls. This was done taking into account a range of possible scaled distances obtained from pre-existing items.

Furthermore, to consider that a uniform pressure acts on the walls, it is necessary to consider a height of the triple point, where the incident and the reflected waves generated by the explosive charge are encountered, is greater than the height of the wall (2.5 m). For this reason, to obtain a triple point greater than 2.5 m, it was calculated that the explosive charge is placed at a height of 0.50 m above ground in the case of 18 kg of TNT and 0.70 m in the case of 25 kg of TNT and in both cases the explosive was positioned at a distance of 5 m.

The masonry test walls were characterized by a wall, called a *control wall*, without reinforcement and three consisting of a reinforcement placed on the façade in direct contact with the explosive charge or on the opposite side. The types of reinforcements were of three types:

- Planitop Intonaco Armato, a fluid cement mortar;
- Mapegrid C170 recycled grid impregnated with Mapewrap 31T semi-fluid epoxy adhesive;
- the combination of a MapeWrap EQ Net, the glass fibre reinforcement used in combination with MapeWrap EQ Adhesive.

### 3 - Conclusions and future developments

---

From the three tests performed, the pressure trends were obtained that were compared with the values extracted by the UFC. It should be noted that from the recordings of the pressure in the tests, it is stated that the explosive has worked well even if it is noted that the experimental values are higher than the theoretical values obtained from the literature. This is explained by the fact that the initial calculations were made on an explosive consisting of a value in kilograms of TNT. Subsequently by means of coefficients, the value in kilograms of the explosive charge that will actually be used in the test is determined. In this case Dynamite, a civil explosive, is used. Precisely for this reason the values obtained by the UFC considering the explosive in TNT equivalents can give less results than those obtained experimentally from a civil explosive. In the case of a military explosive, it would be safer to obtain a value more similar to the theoretical one.

The tests generated different effects. In the first test, in which the reinforcements are positioned on the facade of the innermost wall, where an explosive of 22.8 kg of dynamite was used at a height of 0.50 m, intermediate damage of type C was caused (Table 9). Increasing the charge to 31.6 kg of Dynamite in the following cases we obtain that in the second test the fragmentation of a portion of the internal facade of the wall without reinforcement is obtained. In the third test, in which the reinforcements were positioned on the internal facade, with a 31.6 kg charge of dynamite, there were no fragmentation values but only cracks in the wall. In the second and third tests, damage values of intermediate type of category B are generated (Table 9).

For the evaluation of the damage, reference is made to the comparison of the values measured by the Schmidt Hammer before and after the start of the explosive charge, by means of statistical analyzes.

In particular, in accordance with the forecasts made in the dimensioning of the explosive for the determination of the intermediate damage, comparing the behavior of the walls of the second and third tests, both characterized by the charge of 31.6 kg of dynamite placed at a distance of 5m and raised from the ground by 0.70 m by means of a polyester block, there are evident differences.

In the second test the reinforcements were placed on the façade of the outer wall, not in direct contact with the explosive, and in the third test to the contrary. It was found that the biggest difference is fragmentation. In the second test the spalling phenomenon does not occur only in the case of Mapegrid C170 with Mapewrap 31T in which only fractures are found. In the third test, where all the reinforcements are positioned on the façade in

direct contact with the explosive, no fragmentation is generated in any reinforced wall and the best result obtained from the statistical analysis would seem to be the wall with the Planitop Intonaco Armato.

Based on the results deduced from the analyzes, the percentage of the damage, and considering the cases of fragmentation, in first approximation we consider that: the Mapewrap 31T and MapeWrap EQ Net does not work very well because in both tests the reinforcement fabric is torn. In fact, in the second test does not avoid fragmentation and does not remain glued to the wall. Instead the walls with Planitop Intonaco Armato work quite well. In conditions of reinforcement placed on the façade in direct contact with the explosive, fracturing formation is obtained that is lower than that obtained from the other walls, but it works poorly with the reinforcement on the opposite side, in fact it generates fragmentation. Finally, the Mapegrid C170 with Mapewrap 31T works well. In both cases the phenomenon of chipping does not occur. You notice that it reacts worse when it is placed in direct contact with the explosive, but in general it seems the best of all three products.

This thesis is part, as mentioned earlier, of a first phase of the PICAEX project, which will then be better analyzed by a pure 3D lagrangic approach using LS-DYNA. For this reason also the statistical analysis on the damage from the values obtained from the measurements by means of the Hammer of Schmidt, which have been reported in this final thesis, will be examined in greater detail in the following months with the continuation of the project.

---

---

## References

Ahmad, S., et al. "Experimental study of masonry wall exposed to blast loading." *Materiales de Construcción* 64.313 (2014): 007.

Alsayed, S. H., Elsanadedy, H. M., Al-Zaheri, Z. M., Al-Salloum, Y. A., & Abbas, H. (2016). Blast response of GFRP-strengthened infill masonry walls. *Construction and Building Materials*, 115, 438-451.

Centro para el desarrollo Tecnològico Industrial, *Protección de Infraestructuras Críticas frente a Explosiones: PICAEX MEMORIA TÉCNICA, PROYECTO EN COOPERACIÓN DE I+D*, 2017.

Chen, Li, et al. "Responses of masonry infill walls retrofitted with CFRP, steel wire mesh and laminated bars to blast loadings." *Advances in Structural Engineering* 17.6 (2014): 817-836.

FASTCAM SA3, High-G High Speed Video System ([http://www.highspeedimaging.com/media/photron\\_datasheets/FASTCAM\\_SA3.pdf](http://www.highspeedimaging.com/media/photron_datasheets/FASTCAM_SA3.pdf)) consulted on 27/02/2018 at 11:20.

Florek, Jason R. *Study of simplified models of aircraft structures subjected to generalized explosive loading*. Rutgers The State University of New Jersey-New Brunswick, 2007.

Gelfand, Boris, and M. Silnikov. Translation from Russian to English the Book "Blast Effects Caused by Explosions" Authored by B. Gelfand and M. Silnikov, 2004.

GHADERI, Masoud, Vahid A. MALEKI, and Keyvan ANDALIBI. "Retrofitting of unreinforced masonry walls under blast loading by FRP and spray on polyurea." *Cumhuriyet Science Journal* 36.4 (2015): 462-477.

Henrych, Josef, and Rudolf Major. *The dynamics of explosion and its use*. Vol. 569. Amsterdam: Elsevier, 1979.

## References

---

Hopkinson, B. "British ordnance board minutes 13565." *The National Archives, Kew, UK (1915): 11.*

IChemE (1989), Thermal Radiation Monograph; Calculation of the Intensity of Thermal Radiation from Large Fires. Institution of Chemical Engineers.

Iqbal, J. A. V. E. D., and DR SAEED AHMAD. Effects of an External explosion on a Concrete Structure. Diss. Ph. D. Thesis, Faculty of Civil and Environmental Engineering, Taxila University of Engineering and Technology, Pakistan, 2009.

Karlos, Vasilis, George Solomos, and Martin Larcher. "Analysis of the blast wave decay coefficient using the Kingery-Bulmash data." *International Journal of Protective Structures* 7.3 (2016): 409-429.

Kernicky, Timothy P., et al. "Structural identification and damage characterization of a masonry infill wall in a full-scale building subjected to internal blast load." *Journal of Structural Engineering* 141.1 (2014): D4014013.

Kingery, Charles N., and Gerald Bulmash. *Airblast parameters from TNT spherical air burst and hemispherical surface burst*. US Army Armament and Development Center, Ballistic Research Laboratory, 1984.

Lam, Nelson, Priyan Mendis, and Tuan Ngo. "Response spectrum solutions for blast loading." *Electronic Journal of Structural Engineering* 4.4 (2004): 28-44.

Leica Geosystems, ScanStation laser P30/P40 ([https://geoinn.com/wp-content/uploads/2017/12/Leica\\_ScanStation\\_P30-P40\\_Civil\\_DS\\_es.pdf](https://geoinn.com/wp-content/uploads/2017/12/Leica_ScanStation_P30-P40_Civil_DS_es.pdf)) consulted on 20/02/18 at 13:07.

López L M, Segarra P, Castedo R, Sanchidrián J A, Navarro J, Santos A P and Chiquito M. *Performance of different constructive solutions against explosions in full-scale masonry walls*, 2015.

Mancini, Renato, and Marilena Cardu. Libro: *Scavi in roccia-gli esplosivi*. 2001.

## References

---

- MAPEI, adesivi, sigillanti, prodotti chimici per l'edilizia (<http://www.mapei.com/it/it/prodotti-soluzioni/prodotti/dettaglio/planitop-sr>), consulted on 23/01/2018 at 15:50.
- MAPEI, adesivi, sigillanti, prodotti chimici per l'edilizia (<http://www.mapei.com/docs/librariesprovider2/products-documents/1025mapegridc170it.pdf?sfvrsn=14e84aba0>) consulted on 24/01/2018 at 11:50.
- MAPEI, adesivi, sigillanti, prodotti chimici per l'edilizia (<http://www.mapei.com/docs/librariesprovider2/products-documents/317-mapegrou tt60itfa7aa07179c562e49128ff01007028e9.pdf?sfvrsn=d0d9c9530>) consulted on 24/01/2018 at 12:30.
- MAPEI, adesivi, sigillanti, prodotti chimici per l'edilizia ([http://www.mapei.com/docs/librariesprovider2/products-documents/1019mapewrap\\_eq\\_adhesive\\_it2af4a37179c562e49128ff01007028e9.pdf?sfvrsn=d71c6bc3\\_0](http://www.mapei.com/docs/librariesprovider2/products-documents/1019mapewrap_eq_adhesive_it2af4a37179c562e49128ff01007028e9.pdf?sfvrsn=d71c6bc3_0)) consulted on 07/02/18 at 12:09.
- MAPEI, adesivi, sigillanti, prodotti chimici per l'edilizia ([http://www.mapei.com/docs/librariesprovider2/products-documents/1018\\_mapewrap\\_eq\\_net\\_itb7f4a37179c562e49128ff01007028e9.pdf?sfvrsn=e060de12\\_0](http://www.mapei.com/docs/librariesprovider2/products-documents/1018_mapewrap_eq_net_itb7f4a37179c562e49128ff01007028e9.pdf?sfvrsn=e060de12_0)) consulted on 07/02/18 at 12:09.
- Roberts, A. F. (1981). Thermal radiation hazards from releases of LPG from pressurised storage. *Fire Safety Journal*, 4(3), 197-212.
- Sochet, Isabelle. "Blast effects of external explosions." Eighth International Symposium on Hazards, Prevention, and Mitigation of Industrial Explosions. 2010.
- Swisdak Jr, Michael M. *Simplified Kingery airblast calculations*. NAVAL SURFACE WARFARE CENTER INDIAN HEAD DIV MD, 1994.
- UFC 3-340-02, "Structures to resist the Effects of accidental Explosion", Department of Defense, United States of America, 5 December 2008.
- Wang, Junguo, et al. "Blast response of polymer-retrofitted masonry unit walls." *Composites Part B: Engineering*, 2016.

## References

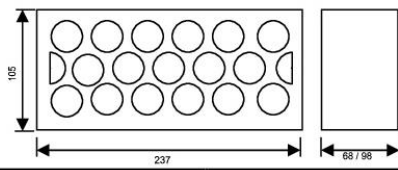
---

Wei, Xueying, and Mark G. Stewart. "Model validation and parametric study on the blast response of unreinforced brick masonry walls." *International journal of impact engineering* 37.11 (2010): 1150-1159.

Zukas, Jonas A., William Walters, and William P. Walters, eds. *Explosive effects and applications*. Springer Science & Business Media, 2002.

# Attachments

## Attachment A: Main characteristics of bricks

FICHA DE INFORMACION PARA EL MARCADO CE				
Nº FICHA TECNICA: ELU/LD237.107.98_68/A/MR		28/03/2012		
FABRICA: CERAMICA ELU S.L.				
LOCALIDAD: Pantoja (Toledo)				
CROQUIS				
		Dimensiones en mm		 07
MODELO	Pieza de arcilla cocida aligerada LD R-10 de 237 x 105 x 98-68 CATEGORÍA I UNE EN 771-1			
DESIGNACION COMERCIAL	Ladrillo cerámico NO VISTO			
DIMENSIONES(mm)	237 x 107 x 98/68			
CARACTERISTICAS TECNICAS EN 771-1:2011			PROPIEDADES GARANTIZADAS	
EXFOLIACIONES / LAMINACIONES			UD	Ninguna Pieza
PIEZAS FISURADAS			UD	≤ 2 Piezas
PIEZAS DESCONCHADAS			UD (7 < d < 15 mm)	≤ 1 Pieza
			UD (d > 15 mm)	Ninguna
TOLERANCIAS DIMENSIONALES		VALOR MEDIO		T1
		RECORRIDO		R1
ESPESOR DE PARED		CARA EXTERIOR NO VISTA		≥ 5 mm
		INTERIORES		≥ 3 mm
PARALELISMO DE LAS CARAS (Ortogonalidad)			mm	Parámetro no exigido
PLANEIDAD DE LAS CARAS		DIAGONAL	L > 300 mm	≤ 4 mm
			300 ≥ L ≥ 250	≤ 4 mm
			L ≤ 250mm	≤ 4 mm
PORCENTAJE DE HUECOS			(%)	≤ 60%
VOLUMEN DEL HUECO MAYOR (% del bruto)			%	≤ 12.5
EXPESOR COMBINADO DE TABIQUILLOS (%)			(%)	≥ 20
ABSORCION			(%)	Parámetro no exigido
SUCCION			( Kg/(m²xmin) )	≤ 0.8
RESISTENCIA A COMPRESION			( N / mm² )	≥ 10
MASA	GRUESO	98 mm 68 mm	(g)	≥ 2000 g ≥ 1400 g
DENSIDAD			ABSOLUTA (Kg/m³)	1900
			APARENTE (Kg/m³)	900
			TOLERANCIA (%)	≤ 10%
DURABILIDAD (HELADICIDAD)				F0. Parámetro no exigido
PROPIEDADES TÉRMICAS (Método)			Valor tabulado Catálogo Elementos Constructivos	
λ <sub>piezas</sub> (W/m x K )			Catálogo CTE	0,350
R <sub>muro</sub> h <sub>1</sub> (m² x K/W)				0.23 fábrica de medio pie (100)
R <sub>muro</sub> h <sub>2</sub> (m² x K/W)				0.21 fábrica de medio pie (68)
PERMEABILIDAD AL VAPOR DE AGUA			Catálogo CTE	μ
				10
CONTENIDO EN SALES SOLUBLES				S0 Sin Necesidad de Ensayo
REACCION AL FUEGO				A1 Sin Necesidad de Ensayo
EXPANSIÓN POR HUMEDAD			mm/m	0.7
ADHERENCIA			(N/mm²)	0.15 (Morteros de Uso General)
OBSERVACIONES:				

## Attachment B: Mapei products

### Attachment B1: Product 1 called PLANITOP INTONACO ARMATO

DATI TECNICI (valori tipici)	
DATI IDENTIFICATIVI DEL PRODOTTO	
Comp. A	
Aspetto:	polvere
Colore:	chiaro
Massa volumica apparente (kg/m <sup>3</sup> ):	1.400
Diametro massimo aggregato (mm) (UNI EN 1015-1):	1,5
Contenuti di doruri (EN 1015-17) (%):	< 0,05
Comp. B	
Aspetto:	liquido fluido
Colore:	bianco
Massa volumica apparente (g/cm <sup>3</sup> ):	1,02
Residuo solido (%):	10
Contenuti di doruri (EN 1015-17) (%):	< 0,05
DATI APPLICATIVI	
Rapporto dell'impasto:	1 sacco da 25 kg di componente A con 1 tanica di componente B
Consistenza dell'impasto:	fluida-spatolabile
Massa volumica dell'impasto (UNI EN 1015-6) (kg/m <sup>3</sup> ):	1.900

## Attachments

<b>Spessore di applicazione (mm):</b>	da 3 a 10 mm per mano			
<b>Temperatura di applicazione permessa:</b>	da +5°C a +35°C			
<b>Durata dell'impasto:</b>	ca. 1 h			
<b>Tempo di presa (inizio-fine):</b>	10 h / 20 h			
<b>PRESTAZIONI FINALI</b>				
Caratteristica prestazionale	Metodo di prova	Requisiti in accordo alla EN 998-1	Requisiti in accordo alla EN 998-2	Prestazione prodotto
<b>Resistenza a compressione a 28 gg (N/mm<sup>2</sup>):</b>	EN 1015-11	CS I (da 0,4 a 2,5)	da Classe M 1 (> 1 N/mm <sup>2</sup> ) a Classe M d (> 25 N/mm <sup>2</sup> )	> 15 (Categoria CS IV) (Classe M 15)
		CS II (da 1,5 a 5,0)		
		CS III (da 3,5 a 7,5)		
		CS IV (≥ 6)		
<b>Adesione al supporto (laterizio) (N/mm<sup>2</sup>):</b>	EN 1015-12	valore dichiarato emodo di rottura (FP)	non richiesto	≥ 0,8 Modo di rottura (FP) = B
<b>Resistenza iniziale a taglio (f<sub>vd</sub>) (N/mm<sup>2</sup>):</b>	EN 1052-3	non richiesto	valore tabulato	0,15
<b>Modulo elastico a compressione (GPa):</b>	UN EN 13412	non richiesto	non richiesto	8,000
<b>Assorbimento d'acqua per capillarità [kg/(m<sup>2</sup>·min<sup>-0,5</sup>):</b>	EN 1015-18	da Categoria W 0 a Categoria W 2	valore dichiarato	Categoria W 2 ≤ 0,2
<b>Coefficiente di permeabilità al vapore acqueo (μ)</b>	EN 1015-19	valore dichiarato	valore tabulato	≤ 60
<b>Conducibilità termica (λ<sub>10,div</sub>) (W/m·K):</b>	EN 1745	valore tabulato	0,75	P - 50°C
<b>Reazione al fuoco (Euroclasse):</b>	EN 13501-1	valore dichiarato dal produttore	valore dichiarato dal produttore	Classe E

**Attachment B2.1: Product 2.1 called MAPEGRID C170**

<b>TECHNICAL DATA (typical values)</b>	
<b>PRODUCT IDENTITY</b>	
Type of fibre:	high-strength carbon
Weight (g/m <sup>2</sup> ):	≥ 170 (fibres only)
Mesh size (mm):	10 x 10
Density of fibre (g/cm <sup>3</sup> ):	1.83
<b>APPLICATION DATA</b>	
Tensile strength (kN/m):	>240
Modulus of elasticity (GPa):	252 ± 2%
Load-resistant area per unit of width (mm <sup>2</sup> /m):	48.00
Equivalent thickness of dry fabric (mm):	0.048
Elongation at failure (%):	2

**Attachment B2.2: Product 2.2 called MAPEWRAP 31 T**

<b>TECHNICAL DATA (typical values)</b>		
<b>PRODUCT IDENTITY</b>		
	<b>component A</b>	<b>component B</b>
<b>Consistency:</b>	paste	paste
<b>Colour:</b>	yellow	white
<b>Specific gravity (g/cm<sup>3</sup>):</b>	1.34	1.25
<b>Brookfield viscosity (mPa·s):</b>	200,000 (rotor 6 - 5 revs)	20,000 (rotor 5 - 10 revs)
<b>APPLICATION DATA (after 7 days at +23°C - 50% R.H.)</b>		
<b>Mix ratio:</b>	component A : component B = 4 : 1	
<b>Mix consistency:</b>	thixotropic paste	
<b>Colour of mix:</b>	yellow	
<b>Specific gravity of the mix (g/cm<sup>3</sup>):</b>	1.30	
<b>Brookfield viscosity (mPa·s):</b>	70,000 (rotor 6 - 10 revs)	
<b>Workability time:</b> – at +23°C:	50 mins.	
<b>Setting time:</b> – at +23°C:	4 hours	
<b>Application temperature:</b>	from +5°C to +30°C	
<b>FINAL PERFORMANCES</b>		
<b>Adhesion to concrete (N/mm<sup>2</sup>):</b>	> 3 (after 7 days - failure of concrete)	
<b>Tensile strength* (ASTM D 638) (N/mm<sup>2</sup>):</b>	≥ 20	
<b>Tensile strain* (ASTM D 638) (%):</b> – after 28 days:	1.0	
<b>Compressive strength (ASTM D 695) (N/mm<sup>2</sup>):</b>	≥ 70	
<b>Flexural strength* (ISO 178) (N/mm<sup>2</sup>):</b>	≥ 25	

\* Results obtained from tests carried out on 5 samples (+23°C (+73°F) - 50% R.H.)

## Attachment B3.1: Product 3.1 called MAPEWRAP EQ NET

TECHNICAL DATA (typical values)	
<b>PRODUCT IDENTITY</b>	
Type of fibre:	E (primed) type glass fibres
Weight (g/m <sup>2</sup> ):	286
Appearance:	balanced bi-directional fabric
Equivalent thickness of dry fabric (mm <sup>2</sup> /m):	57.00
Tensile strength (N/mm <sup>2</sup> ):	> 1,620
Tensile modulus of elasticity (GPa):	42
Width (cm):	100
Elongation at failure (%):	4
<b>APPLICATION DATA</b>	
Tensile strength (N/5 cm):	> 4,600
Elongation at failure (%):	4

## Attachment B3.2: Product 3.2 called MAPEWRAP EQ ADHESIVE

TECHNICAL DATA (typical values)	
<b>PRODUCT IDENTITY</b>	
Consistency:	gel
Colour:	milky white
Density (g/cm <sup>3</sup> ):	1.10
Dry solids content (%):	35
EMICODE:	EC1 Plus - very low emission
<b>APPLICATION DATA (at +23°C - 50% R.H.)</b>	
Brookfield viscosity (mPa s):	200,000 (rotor 3 - 1 rpm)
Application temperature range:	from +5°C to +30°C
Tensile strength (DIN 53504) (N/mm <sup>2</sup> ):	5.25
Tensile modulus of elasticity (DIN 53504) (N/mm <sup>2</sup> ):	0.55
Maximum tensile elongation (DIN 53504) (%):	1,200
Peel strength (brickwork) (EN 1348) (N/mm):	1.1
Peel strength (concrete) (EN 1348) (N/mm):	2.1

# Attachment C: Accelerometer mounting instructions

APPLICATION			REVISIONS				
NEXT ASSY	USED ON	VAR	REV	DESCRIPTION	ECN	DATE	APP'D

10943

PCB Piezotronics Inc. claims proprietary rights in the information disclosed herein. Neither it nor any reproduction thereof will be disclosed to others without written consent of PCB Piezotronics Inc.

10-32 COAXIAL CONNECTOR

.375(9.52) HEX  $\triangle 3$

1.02(25.9)

.78(19.8)

.20(5.1)

1/4-28 UNF-3A

ø.37(ø9.4)

.02(.5)

**MOUNTING HOLE PREPARATION**

ø.213 (ø5.41)  $\triangle 1$

X .30 (7.6)  $\nabla$  MIN.  $\triangle 1$

TAP 1/4-28 UNF-3B

X .20 (5.1)  $\nabla$  MIN.

$\triangle 3$  RECOMENDED MOUNTING TORQUE ON .375 (9.52) HEX 2.4-4 FOOT POUNDS (2.8-3.4 NEWTON METERS).

$\triangle 2$  MOUNTING SURFACE SHOULD BE FLAT TO WITHIN .001 (0.03) TIR OVER ø.375 (ø9.53) WITH A MAXIMUM 63 $\sqrt{}$  (1.6 $\sqrt{}$ ) FINISH FOR BEST RESULTS.

$\triangle 1$  DRILL PERPENDICULAR TO MOUNTING SURFACE TO WITHIN  $\pm .1^\circ$ .

UNLESS SPECIFIED TOLERANCES		DRAWN	MFG	DATE	<p>3425 WALDEN AVE. DEPEW, NY 14043 (716) 684-0001 EMAIL: SALES@PCB.COM</p>	
DIMENSIONS IN INCHES	DIMENSIONS IN MILLIMETERS (IN PARENTHESIS)	DKM	JL	5-4-19		CODE IDENT. NO. 52681 DWG. NO. 10943
DECIMALS XX $\pm$ .01 XXX $\pm$ .005 ANGLES $\pm$ 2 DEGREES	DECIMALS XX $\pm$ 0.3 XXX $\pm$ 0.13 ANGLES $\pm$ 2 DEGREES	CHK'D EM 5/5/19	ENGR APC 5-4-19	SALES CSA 5-4-19	TITLE INSTALLATION DRAWING MODEL 350B03 AND 350B04 ACCELEROMETER	
FILLETS AND RADII .003 - .005	FILLETS AND RADII (0.07 - 0.13)	DD011 REV. B 03/13/98				SCALE: 3 X

# Attachment D: High-speed camera specifications

## FASTCAM SA3

HIGH SPEED VIDEO SYSTEM

**TARGET APPLICATIONS:**

- Onboard vehicle impact testing
- Military test ranges where a scaled unit is beneficial
- Particle Image Velocimetry (PIV)
- Digital Image Correlation (DIC)
- Biomechanics

---

Specifications: Frame Rate / Resolution Table

FRAME RATE (fps)	MAXIMUM RESOLUTION				RECORD DURATION (12-BIT)													
	Model 60K		Model 120K		TIME (Sec.)						FRAMES							
	Horizontal	Vertical	Horizontal	Vertical	Model 60K		Model 120K		Model 60K		Model 120K		Model 60K		Model 120K			
	2GB	4GB	8GB	2GB	4GB	8GB	2GB	4GB	8GB	2GB	4GB	8GB	2GB	4GB	8GB	2GB	4GB	8GB
1,000	1,024	1,024	1,024	1,024	1.36	2.72	5.45	1.36	2.72	5.45	1.361	2,726	5,457	1,361	2,726	5,457		
1,500	896	736	1,024	1,024	1.44	2.89	5.78	0.90	1.81	3.63	2,164	4,335	8,677	1,361	2,726	5,457		
2,000	768	608	1,024	1,024	1.52	3.06	6.12	0.68	1.36	2.72	3,057	6,123	12,255	1,361	2,726	5,457		
2,500	640	544	896	896	1.64	3.28	6.57	0.71	1.42	2.85	4,100	8,212	16,436	1,778	3,561	7,127		
3,000	512	512	896	736	1.81	3.63	7.27	0.72	1.44	2.89	5,445	10,906	21,829	2,164	4,335	8,677		
5,000	384	352	640	544	2.11	4.23	8.46	0.82	1.64	3.28	10,560	21,152	42,335	4,100	8,212	16,436		
6,000	384	288	512	512	2.15	4.30	8.62	0.90	1.81	3.63	12,907	25,852	51,743	5,445	10,906	21,829		
7,500	384	224	512	416	2.21	4.43	8.87	0.89	1.78	3.58	16,595	33,239	66,527	6,701	13,423	26,866		
10,000	256	192	384	352	2.90	5.81	11.64	1.05	2.11	4.23	29,041	58,168	116,423	10,560	21,152	42,335		
15,000	256	112	384	224	3.31	6.64	13.30	1.10	2.21	4.43	49,785	99,718	199,582	16,595	33,239	66,527		
20,000	256	80	256	192	3.48	6.98	13.97	1.45	2.90	5.82	69,700	139,605	279,415	29,041	58,168	116,423		
25,000	256	64	256	144	3.48	6.98	13.97	1.54	3.10	6.20	87,125	174,506	349,269	38,722	77,558	155,230		
30,000	256	48	256	112	3.87	7.75	15.52	1.65	3.32	6.65	116,167	232,675	465,692	49,785	99,718	199,582		
50,000	384	16	256	64	4.64	9.30	18.62	1.74	3.49	6.98	232,334	465,351	931,384	87,125	174,506	349,269		
60,000	128	16	256	48	11.61	23.26	46.56	1.93	3.87	7.76	697,002	1,396,053	2,794,154	116,167	232,675	465,692		
75,000	-	-	256	32	-	-	-	2.32	4.65	9.31	-	-	-	174,506	349,013	698,538		
100,000	-	-	384	16	-	-	-	2.32	4.65	9.31	-	-	-	232,334	465,351	931,384		
120,000	-	-	128	16	-	-	-	5.80	11.63	23.28	-	-	-	697,002	1,396,053	2,794,154		

<b>Sensor</b>	12-bit ADC (Bayer system color, single sensor) with 17µm pixel size	<b>Event Markers</b>	Ten user entered event markers mark specific events within the image sequence in real time. Immediately accessible through software
<b>Shutter</b>	Global electronic shutter from 16.7ms to 2µs independent of frame rate	<b>Variable Framerate/Resolution</b>	User selectable Variable Framerate/Resolution function adjustable in 128 x 16 pixel steps
<b>Lens Mount</b>	Interchangeable F-mount and C-mount using supplied adapters (Optional High-G block mount available)	<b>Selectable Recording Bit Depth</b>	User selectable 12-bit (high-dynamic range) or 8-bit (50% frame increase) recording mode
<b>Extended Dynamic Range</b>	Selectable in twenty steps (0 to 95% in 5% increments) to prevent pixel over-exposure	<b>Trigger Modes</b>	Start, End, Center, Manual, Random, Random Reset
<b>Memory</b>	2GB (standard), 4GB (optional) and 8GB (optional)	<b>Saved Image Formats</b>	JPEG, AVI, TIFF, BMP, RAW, PNG, MOV, and FTIF. Images can be saved with or without image or comment data
<b>Video Outputs</b>	NTSC/PAL composite VBS (BNC). Ability to zoom, pan and scroll within image via keypad (option). Live video during recording	<b>Data Display</b>	Frame Rate, Shutter Speed, Trigger Mode, Date or Time, Status (Playback/Record), Real Time, Frame Count, Resolution and LUT
<b>Camera Control</b>	Through optional keypad with integrated viewfinder and Gigabit Ethernet or RS-422	<b>Partitioning</b>	Up to 8 memory partitions may be set by the user
<b>User Preset Switch</b>	User selectable camera function control mounted on the camera's rear panel	<b>High-G</b>	Tested to 100G, 10ms, six-axis
<b>Low Light Mode</b>	Low light mode for simple camera adjustment when working in low ambient light, high frame rate or short exposure modes	<b>Operating Temperature</b>	0-40 degrees C (32-104 degree F)
<b>Triggering</b>	Selectable positive or negative TTL 5Vp-p or switch closure	<b>Mounting</b>	1 x 1/4-20 UNC, 6 x M5 on all four sides
<b>Trigger Delay</b>	Programmable delay on selected input and output triggers, 100ns resolution	<b>Dimensions</b>	120mm (4.72")H x 120mm (4.72")W x 21.58mm (8.50")D *excluding protrusions
<b>Timing</b>	Internal clock or external source	<b>Weight</b>	9.48 lbs (4.3kg)
<b>IRIG Time Code</b>	IRIG/GPS timing is recorded in real time on every frame	<b>Power Requirements</b>	100V-240V AC ~ 1.5A, 50-60Hz optional DC operation 22-32VDC, 60VA

Specifications subject to change without notice

<b>PHOTRON USA, INC</b> 9520 Padgett Street, Suite 110 San Diego, CA 92126-4446 USA Tel: 858.684.3555 or 800.585.2129 Fax: 858.684.3558 Email: image@photron.com www.photron.com	<b>PHOTRON (EUROPE) LIMITED</b> The Barn, Bottom Road West Wycombe, Bucks, HP14 4BS United Kingdom Tel: +44 (0) 1494 481011 Fax: +44 (0) 1494 487011 Email: image@photron.com www.photron.com	<b>PHOTRON LIMITED</b> Fujimi 1-1-8 Chiyoda-Ku, Tokyo 102-0071 Japan Tel: +81 (0) 3 3238 2107 Fax: +81 (0) 3 3238 2109 Email: image@photron.co.jp www.photron.co.jp
---	--	--

SLOW MOTION IMAGING SOLUTIONS